Summer 8-15-2018

Viral MHC Class I Evasion Affects Anti-viral T Cell Development and Responses

Elvin James Lauron
Washington University in St. Louis

WASHINGTON UNIVERSITY IN ST. LOUIS

Division of Biology and Biomedical Sciences
Molecular Microbiology and Microbial Pathogenesis

Dissertation Examination Committee:
Wayne M. Yokoyama, Chair
Adrianus C. M. Boon
Brian T. Edelson
Haina Shin
L. David Sibley

Viral MHC Class I Evasion Affects Anti-viral T Cell Development and Responses

by
Elvin J. Lauron

A dissertation presented to the
Graduate School
of Washington University in
partial fulfillment of the
requirements for the degree
of Doctor of Philosophy

August 2018
St. Louis, Missouri

Table of Contents

List of Figures

List of Tables

Acknowledgments

Over the past four years I have received tremendous support and encouragement from a number of awesome individuals. Dr. Wayne Yokoyama, who never seems to get angry and displays an infinite amount of patience, provided me the opportunity to freely exercise my creativity and to pursue basic questions that were of great interest to me. My thesis committee members offered encouragement at times when I desperately needed it and pushed me to excel in my scientific thinking. In particular, Dr. Adrianus Boon has drilled the importance of rationale deep into all aspects of my mind (i.e. conscious, subconscious, and even unconscious). I am indebted to Liping Yang for her assistance with experiments and training on various biomethods. The other members of the Yokoyama laboratory also provided helpful discussions on science and life in general. Finally, I could not have accomplished this work without the support of my family and my amazing wife Jamielynn, a hard working mother who also did the lion's share of raising our two beautiful daughters during our stay in St. Louis. My daughters kept me grounded and were a major source of motivation for me to keep on in my PhD journey.

Elvin J. Lauron

Washington University in St. Louis

August 2018

Dedicated to my parents, my siblings, my wife, and my two strong daughters.

Abstract of the Dissertation

Viral MHC Class I Evasion Affects Anti-viral T Cell Development and Responses

Elvin J. Lauron

Doctor of Philosophy in Biology and Biomedical Sciences

Molecular Microbiology and Microbial Pathogenesis

Washington University in St. Louis, 2018

Professor Wayne M. Yokoyama, Chair

Cytotoxic $CD8^+$ T cells (CTLs) play a critical role in protective immunity against viruses, which is underscored by the evolution of viral CTL evasion mechanisms. For instance, many viruses commonly target the major histocompatibility complex class I (MHCI) antigen presentation pathway to prevent CTLs from recognizing infected cells. A striking example of this is cowpox virus (CPXV), which interferes with MHCI antigen presentation through two distinct mechanisms. One mechanism of CPXV-mediated MHCI inhibition is to retain MHCI molecules in the endoplasmic reticulum (ER). The second mechanism is to prevent antigen peptide loading onto MHCI molecules. These mechanisms when combined result in potent inhibition of MHCI antigen presentation and effective evasion of CPXV-specific CTL responses *in vivo*. However, it is unclear how viral MHCI inhibition affects the CTL repertoire and the subsequent development of memory $CD8^+$ T cells. Furthermore, the effects of viral MHCI inhibition on local memory $CD8^+$ T cell responses during peripheral CPXV infection has not been examined.

To explore these issues, I used the CPXV murine infection model to compare $CD8^+$ T cell responses against CPXV and a recombinant CPXV mutant that is incapable of inhibiting

MHCI antigen presentation. Here, I demonstrate that viral MHCI inhibition affects the local CTL and memory $CD8^+$ T cell repertoire in specific niches. Primary anti-CPXV responses and memory responses were shaped by antigen abundance and $CD8^+$ T cell cross-competition for viral peptide-MHCI complexes on the cell surface of antigen presenting cells (APCs), respectively. Additionally, I show that the overall quality and quantity of CTL and memory $CD8^+$ T cells is unaffected by viral MHCI inhibition following CPXV infection. Finally, I determined that viral MHCI inhibition contributes to evasion of local memory $CD8^+$ T cell responses. Collectively, the results of these studies provide insight on determinants that influence the anti-viral $CD8^+$ T cell repertoire, local memory formation, and local memory responses.

Chapter 1:

Introduction

Introduction to orthopoxviruses

Orthopoxviruses are large DNA viruses capable of causing devastating disease in humans and a wide range of animal hosts. This broad host range is a feature of zoonotic orthopoxviruses, such as cowpox virus (CPXV) and monkeypox virus (MPXV). Moreover, human MPXV incidence has increased over 20-fold since cessation of vaccinia virus (VACV) smallpox vaccination[1], which previously provided cross-protection against MPXV, CPXV, and related orthopoxviruses. The capacity of orthopoxviruses to infect a wide range of hosts is attributed to their large genomes that encode a plethora of immunomodulatory proteins. Accordingly, some of these immunoevasin proteins exhibit broad host-specificity. Here I highlight the interplay between orthopoxvirus immunoevasins and the host immune response and discuss open questions in regards to the effects of viral immune evasion.

Innate immunity against orthopoxvirus infection

The innate immune response can be triggered when conserved structures on pathogens, known as pathogen associated molecular patterns (PAMPs), are detected. PAMPs are detected by pattern recognition receptors (PRRs), which can induce signaling cascades that ultimately converge to activate the interferon regulatory factor 3 (IRF3) and nuclear factor kappa-light-chain enhancer of activated B cells (Nf-κB)[2]. These transcription factors promote the expression of proinflammatory cytokines and type I interferons (IFNs), resulting in a potent antiviral state. This antiviral state can be initiated at several early points during orthopoxvirus infection. At the earliest stage of infection, orthopoxviruses can be sensed when extracellular virions come in contact with cells via toll-like receptor (TLR) 4, a cell surface PRR. TLR4 signaling restricts viral replication and protects mice against VACV infection, as mice that are TLR4-deficient are more susceptible to infection with VACV[3].

VACV is also recognized at the stage of viral entry by several endosomal PRRs that recognize pathogen-derived nucleic acids, including TLR3, 7, 8, and 9[4–7]. Mice that are deficient in TLR9 are also highly susceptible to orthopoxvirus infection[7], while mice infected with lethal orthopoxvirus survive when TLR9 is activated. Conversely, TLR3 signaling plays a negative role during orthopoxvirus infection, as mice lacking TLR3 are less susceptible to VACV infection, presumably due to excessive inflammation caused by TLR3 signaling. VACV DNA can also activate TLR7[5], yet VACV infected cells do not produce IFN-α or the proinflammatory cytokine tumor necrosis factor (TNF) through TLR7 signaling. The antiviral defense mechanisms remain unclear for TLR7 signaling, whereas TLR4, 8, and 9-mediated innate immunity is known to activate Nf-κB and IRF3 to induce proinflammatory cytokine and type I IFN production. However, the production of IFN and proinflamatory cytokines is not completely dependent on TLRs during orthopoxvirus infection[3,7,8].

Orthopoxviruses can induce expression of antiviral cytokines through retinoic acid-inducible gene 1 (RIG-I)-like receptors (RLRs) and cytosolic double- stranded DNA (dsDNA) sensors (CDSs), which are cytosolic PRRs of RNA and DNA respectively. More recently, the cytosolic sensors activating cyclic guanosine monophosphate-adenosine monophosphate synthase (cGAS) was identified as a cytosolic DNA sensor with strong antiviral effects against orthopoxviruses[9,10]. The importance of cGAS in antiviral innate immunity against orthopoxviruses was similarly demonstrated with infections in mice that lack cGAS[10]. The protective effects of cGAS are likewise mediated by Nf-κB, IRF3, and type I IFN. These important factors are linked to RLR-mediated innate immunity against orthopoxviruses as well. Important RLRs involved in controlling orthopoxvirus infections include RIG-I, melanoma differentiation-associated protein 5 (MDA5), and laboratory of genetics and physiology 2

(LGp2)[11–13]. Protein kinase RNA-activated (PKR), although not an RLR, also plays an important role in inducing type I IFN production upon sensing orthopoxvirus-derived RNA. PKR is particularly important since activated PKR can elicit additional antiviral defense mechanisms, such as apoptosis[12].

Nonetheless, orthopoxviruses have evolved mechanisms to efficiently target the signaling pathways of these PRRs and the activation of Nf-κB and IRF3, highlighting the importance of these factors in the orthopoxvirus-induced innate immune response.

Orthopoxvirus evasion of innate immune responses

The central role for IRF3 and Nf-κB in innate immunity applies strong evolutionary pressure for orthopoxviruses to evolve mechanisms of IRF3 and Nf-κB antagonism. Indeed, orthopoxvirus immunoevasins can target the activation of IRF3 and Nf-κB directly or target activating signaling pathways proximally. For example, the VACV proteins A46 and A52 can disrupt TLR-mediated activation of Nf-κB by inhibiting the proximal signal transducers TNF receptor-associated factor 6 (TRAF6) and Myd88 adapter-like (Mal) respectively. The receptor-proximal adaptor proteins MyD88 and Mal initiate signal cascades when TLRs are stimulated. MyD88 and Mal activate the IL-1 receptor-associated kinase (IRAK) or IRAK2, which in turn recruits TRAF6[14]. TRAF6 is essential to activate TGF-β-activated kinase 1 (TAK1) and TAK1 binding protein 1 (TAB1) dependent phosphorylation of IκB kinase (IKK)[15], which is normally in complex with Nf-κB. Phosphorylated IKK results in activated Nf-κB. The VACV protein N1 inhibits Nf-κB from being activated by associating with IKK[16]. The VACV protein B14 and C4 also inhibits activated IKK[16,17]. Importantly, C4, B14, A46, and A52 are virulence factors as VACV mutants that lack these factors are attenuated *in vivo*[17–20]. The VACV mutant VV811 lacks 55 open reading frames (ORFs) and is missing all the known Nf-κB inhibitors.

Intriguingly, VV811 can still inhibit Nf-κB[21], suggesting that other Nf-κB inhibitors likely remain to be identified.

Additional poxvirus-encoded inhibitors include secreted soluble proteins that bind to cytokines capable of inducing Nf-κB activity, thereby blocking cytokine-receptor interactions and Nf-κB signaling. One commonly targeted cytokine is TNF, which can be intercepted by the T2 protein from shope fibroma virus (SFV) and myxoma virus (MYXV) [22,23]. T2 plays a critical role in MYXV pathogenesis since the absence of T2 attenuates MYXV *in vivo*[23]. Similarly, TNF binding proteins encoded by CPXV, known as cytokine response modifier (Crm) B, C, D and E, have been shown to neutralize TNF[23–25] and contribute to CPXV pathogenesis[27]. Crm B orthologues are present in the genomes of multiple orthopoxviruses, including MPXV, ectromelia virus (ECTV), and VARV[28]; as emphasized by the conservation of these orthopoxvirus TNF inhibitors, orthopoxvirus fitness largely impinges on inhibiting the function of TNF. TNF can also synergistically induce Nf-κB activity in combination with other cytokines such as IFN-γ[29]. CONCLUSION?

IFN-γ is a proinflammatory cytokine that is critical in mediating anti-orthopoxvirus immunity[30–32] and is also a target of orthopoxvirus-encoded cytokine inhibitors. The secreted IFN-γ binding protein B8 can neutralize rat, rabbit, bovine, human, equine and mouse IFN-γ and is conserved among orthopoxviruses[33,34]. Deletion of B8R from the genome of ECTV significantly attenuates ECTV pathogenesis in an IFN-γ dependent manner[35]. In contrast, deletion of B8R does not have any effects on VACV and CPXV pathogenesis in mice[33,36]. This may be explained by the fact that B8 from VACV and CPXV does not bind to mouse IFN-γ, yet it is possible that VACV/CPXV B8 has alternative cytokine targets or redundant immunomodulatory functions in mice. Interestingly, B8 also contains a conserved epitope that

elicits a strong immunodominant $CD8^+$ T cell response in orthopoxvirus-infected mice bearing the major histocompatibility complex class I (MHCI) haplotype $H2^{b}$[31,35–37]. ←MAYBE BETTER TO BRING UP LATER?

CONCLUSION?

OVERALL CONCLUSION FOR SECTION?

Adaptive immunity against orthopoxvirus infection

$CD8^+$ T cells are an important arm of the adaptive immune response and play a critical role in controlling orthopoxvirus infections. Before gaining anti-viral effector functions, $CD8^+$ T cells must be primed by antigen presenting cells (APCs) that present endogenous pathogen-derived epitopes via MHCI molecules, a process known as direct presentation. Exogenous antigens can also be processed through the MHCI antigen presentation pathway and presented by APCs through a process known as cross-presentation. Upon encountering cognate antigen epitopes presented by APCs, $CD8^+$ T cells differentiate into cytotoxic $CD8^+$ T cells (CTLs) and mediate viral resistance directly by killing infected cells through secretion of the effector molecules perforin and granzyme B or indirectly by producing IFN-γ[38]. In the later stages of infection, the majority of CTLs die and a small proportion become long-lived memory $CD8^+$ T cells. SAY SOMETHING ABOUT NEEDING TO EXPAND A SMALL NUMBER OF VIRUS-SPECIFIC CTLS DURING PRIMING. DO YOU WANT TO INTRODUCE THE IMMUNODOMINANT ANTIGEN IDEAS HERE?

Intriguingly, $CD8^+$ T cells alone appear to provide incomplete protection against some orthopoxviruses and the role of $CD8^+$ T cells in orthopoxvirus immunity was somewhat controversial. For instance, survival following ECTV challenge was demonstrated to be completely dependent on $CD8^+$ T cells as $CD8^+$ T cell depletion resulted in 100% mortality in

comparison to $CD8^+$ T cell non-depleted controls[39]. Conversely, depletion of $CD8^+$ T cells during lethal CPXV infection had no effects on mortality[31,36]. Similarly, depletion of $CD8^+$ T cells during VACV infection had modest effects on viral clearance[40,41], and instead $CD4^+$ T cells and B cells largely mediated protection[40]. Nevertheless, $CD8^+$ T cells were important for controlling VACV infection in the absence of $CD4^+$ T cells and B cells[40].

B cells contribute to viral immunity through the production of protective antibodies. The surface antibodies on B cells serve as the B cell antigen receptor (BCR). Upon encountering antigen, the BCR delivers the antigen for processing through the MHCII pathway. The antigen peptide-MHC class II (pMHCII) complexes can then be presented to and recognized by $CD4^+$ T cells sharing the same antigen specificity[42]. $CD4^+$ T cell-B cell interactions stimulates the production of molecules that differentiate B cells into antibody-secreting plasma cells[43]. The elicited antibodies can then limit the spread of virus by blocking virion attachment to cells. Virions or infected cells bound by antibodies can also be opsonized by the complement system, resulting in phagocytosis or killing of infected cells and virions[44]. Studies using ECTV and VACV demonstrate a critical role for B cells and $CD4^+$ T cells, where deficiencies in either cell types results in death following viral challenge[40,45,46], despite the mounting of a normal $CD8^+$ T cell response. $CD8^+$ T cell responses can however complement $CD4^+$ T cell and B cell responses during orthopoxvirus infection[40,45].

Orthopoxvirus evasion of adaptive immunity

Given the importance of T and B cells in immunity against orthopoxviruses, it is no surprise that orthopoxviruses have evolved mechanisms to thwart the function of these adaptive immune cells. One such mechanism is to prevent the complement system from activating. VACV encodes a complement binding protein called vaccinia complement-control protein

(VCP). VCP prevents complement proteins from acting on antigen-bound antibodies[47]. Skin infection with VCP deficient VACV results in reduced lesion size in comparison to infection with VCP sufficient VACV[48]. Therefore, VCP is a virulence factor that indirectly inhibits antiviral antibodies produced by B cells.

Other mechanisms to evade B cell and $CD4^+$ T cell functions have been reported, yet the *in vivo* relevance remains to be determined. For instance, MPXV and CPXV encode an orthopoxvirus MHC class I-like protein (OMCP) that binds to an immunoregulatory receptor expressed on B cells. These findings strongly suggest a role for OMCP in evading B cell responses[49]. Additionally, B cell MHCII antigen presentation to $CD4^+$ T cells can be inhibited when B cells are infected with VACV[50], implying that VACV may also prevent $CD4^+$ T cell-B cell interactions *in vivo*. MPXV also encodes an immunoevasin that effectively suppresses both $CD4^+$ T cell and $CD8^+$ T cell stimulation, although MPXV does not inhibit MHCII and MHCI antigen presentation[51].

While many viruses target antigen processing and presentation through the MHCI pathway in order to evade anti-viral CTLs, CPXV is the only orthopoxvirus capable of doing so[31,36,52,53]. There are two CPXV encoded proteins that inhibit MHCI antigen presentation, CPXV203 and CPXV012. CPXV012 prevents MHCI molecules from being loaded with antigen by binding to transporter associated with antigen processing (TAP) molecules, whereas CPXV203 binds to and retains MHCI in the ER of infected cells[52,53]. The combined functions of CPXV203 and CPXV012 effectively prevent CPXV-specific CTLs from recognizing infected target cells, resulting in significant consequences *in vivo*.

Investigating the effects of viral MHCI evasion on $CD8^+$ T cell effector function and development.

CPXV-mediated MHCI inhibition effectively evades CPXV-specific CTL effector functions, but does not affect priming of naïve CPXV-specific CTL precursors. Direct priming is likely abrogated since CPXV-infected APCs are also subjected to CPXV-mediated MHCI inhibition[53]. However, following CPXV infection, $CD8\alpha^+/CD103^+$ dendritic cells ($BATF3^+$ DCs) prime naïve CTL precursors, suggesting that the induction of anti-CPXV CTL responses is dependent on cross-presenting $BATF3^+$ DCs subsets[31,36]. Although $BATF3^+$ DCs induce a strong anti-CPXV CTL response, CPXV-specific CTLs alone are ineffective at controlling CPXV infection and depletion of $CD8^+$ T cells has no effects on mortality or survival during lethal CPXV infection[31,36,52]. Strikingly, infection with a CPXV mutant lacking the endogenous viral MHCI inhibitors (Δ12Δ203) induces a CTL response that is also dependent on $BATF3^+$ DCs, but Δ12Δ203 is significantly attenuated *in vivo* in comparison to WT CPXV. In the absence of CPXV012 and CPXV203, CTLs are critical in viral clearance since mice depleted of $CD8^+$ T cells succumb to infection with Δ12Δ203. Furthermore, in the absence of $CD4^+$ T cells and B cells, CPXV-specific CTLs are sufficient in providing protection against Δ12Δ203, but not WT CPXV[31].

Interestingly, infection with both WT CPXV and Δ12Δ203 results in local CTL response dominated by the viral epitope $B8_{19\text{-}26}$, which is restricted to the $H\text{-}2K^b$ MHCI allomorph[31]. This phenomenon, known as immunodominance, has been investigated using VACV[54–57]. However, VACV does not inhibit MHCI antigen presentation[58]. Therefore, the determinants of immunodominance have not been thoroughly interrogated in a context where viral MHCI inhibition has significant consequences *in vivo*. Likewise, the effects of viral MHCI inhibition on

immunodominance within the memory $CD8^+$ T cell pool, memory $CD8^+$ T cell development in general, and memory $CD8^+$ T cell effector functions remain unclear.

To address these issues, I compared primary $CD8^+$ T cell and memory $CD8^+$ T cell responses against WT CPXV infection to the respective responses against Δ12Δ203 infection. In chapter 2, I present my study on $CD8^+$ T cell immunodominance during CPXV infection and discuss the factors that influence immunodominance in the presence of viral MHCI inhibition. I then present my study on memory $CD8^+$ T cell formation/responses following CPXV infection and discuss the effects of viral MHCI inhibition on these processes in chapter 3. Finally, in chapter 4, I discuss the implications of these findings and additional questions that stem from my studies.

Chapter 2:

Cross-priming induces immunodomination in the presence of viral MHC class I inhibition

This chapter was published as a research article in *PLOS Pathogens* (2018).

Authors: Elvin J. Lauron[1], Liping Yang[1], Jabari I. Elliott[2], Maria D. Gainey[3], Daved H. Fremont[2,4,5], Wayne M. Yokoyama[6,*]

[1]Department of Medicine, Washington University School of Medicine, St. Louis, Missouri, United States of America, [2]Department of Pathology and Immunology, Washington University School of Medicine, St. Louis, Missouri, United States of America, [3]Department of Biology, Western Carolina University, Cullowhee, North Carolina, United States of America, [4]Department of Biochemistry and Molecular Biophysics, Washington University School of Medicine, St. Louis, Missouri, United States of America, [5]Department of Molecular Microbiology, Washington University School of Medicine, St. Louis, Missouri, United States of America, [6]Division of Rheumatology, Washington University School of Medicine, St. Louis, Missouri, United States of America

Abstract

Viruses have evolved mechanisms of MHCI inhibition in order to evade recognition by cytotoxic $CD8^+$ T cells (CTLs), which is well-illustrated by our prior studies on cowpox virus (CPXV) that encodes potent MHCI inhibitors. Deletion of CPXV viral MHCI inhibitors markedly attenuated *in vivo* infection due to effects on CTL effector function, not priming. However, the CTL response to CPXV in C57BL/6 mice is dominated by a single peptide antigen presented by H-$2K^b$. Here we evaluated the effect of viral MHCI inhibition on immunodominant (IDE) and subdominant epitopes (SDE) as this has not been thoroughly examined. We found that cross-priming, but not cross-dressing, is the main mechanism driving IDE and SDE CTL responses following CPXV infection. Secretion of the immunodominant antigen was not required for immunodominance. Instead, immunodominance was caused by CTL interference, known as immunodomination. Both immunodomination and cross-priming of SDEs were not affected by MHCI inhibition. SDE-specific CTLs were also capable of exerting immunodomination during primary and secondary responses, which was in part dependent on antigen abundance. Furthermore, CTL responses directed solely against SDEs protected against lethal CPXV infection, but only in the absence of the CPXV MHCI inhibitors. Thus, both SDE and IDE responses can contribute to protective immunity against poxviruses, implying that these principles apply to poxvirus-based vaccines.

Introduction

Strategies to leverage strong $CD8^+$ cytotoxic T lymphocyte (CTL) responses to viral infections are of particular interest as CTLs play essential roles in controlling viral infections [31,52,59–61]. Before gaining effector functions, virus-specific CTL precursors must be primed by antigen presenting cells (APCs) that present pathogen-derived epitopes via major histocompatibility complex class I (MHCI) molecules on the cell surface. If the APC is infected and directly presents endogenously produced antigens, this is known as direct presentation. Alternatively, uninfected APCs may process and cross-present exogenous antigens from infected cells. Cross-presentation is mediated primarily by Batf3-dependent $CD103^+/CD8\alpha^+$ dendritic cells (DCs) [62–64], which we refer to as $BATF3^+$ DCs. Peptide-loaded MHCI molecules from infected cells may also be liberated by cell lysis or secreted in exosomes and then transferred onto cross-presenting APCs. When uninfected APCs acquire preformed peptide-MHCI complexes in this manner, they are termed cross-dressed and can drive expansion of $CD8^+$ T cells [65–67]. Induction of $CD8^+$ T cell responses by cross-dressing was previously demonstrated in studies using adoptive transfer of T cell receptor (TCR) transgenic (Tg) T cells [65–67] and also requires $BATF3^+$ DCs [67]. However, the relative contribution of these processes to non-TCR Tg CTL responses against viral antigens is largely unknown.

Upon recognizing cognate antigen on APCs, naïve CTLs are activated to undergo clonal expansion and traffic to the site of ongoing viral infection. There, virus-specific CTLs mediate host resistance by recognizing infected cells via surface MHCI molecules displaying processed viral antigens. Specific T cell recognition activates direct killing of infected cells and production of interferon-gamma (IFN-γ) and other cytokines that may have indirect effects. In the later

stages of the response, a proportion of CTLs become long-lived memory $CD8^+$ T cells that can provide rapid protection during secondary responses to the viral pathogens.

Many viruses display mechanisms that may contribute to evading CTL responses, such as inhibiting MHCI antigen presentation. The effects and mechanisms of MHCI inhibition on CTL responses have been well demonstrated *in vitro* with herpesviruses [68]. For instance, downregulation of MHCI by murine cytomegalovirus (MCMV) prevented MCMV-specific CTLs from killing infected cells, whereas cells infected with an MCMV mutant lacking the viral MHCI inhibitors were lysed by CTLs [69]. However, the *in vivo* relevance of viral MHCI inhibition in general was previously unclear since herpesvirus-mediated MHCI inhibition had few effects on *in vivo* CTL responses in murine and nonhuman primate infection models [70–72].

On the other hand, studies of cowpox virus (CPXV) by our lab and others indicated that CPXV, uniquely among the orthopoxviruses, mediated mouse and human MHCI inhibition by two open reading frames (ORFs), CPXV012 and CPXV203 [52,53,73]. CPXV203 retains MHCI molecules in the ER and CPXV012 inhibits peptide loading on MHCI molecules; when combined, these two evasion mechanisms allows CPXV to evade CTL responses. The deletion of intact CPXV012 and CPXV203 from the CPXV genome attenuated viral pathogenesis *in vivo* [31,52]. Furthermore, this attenuation was dependent on the anti-CPXV CTL response since depleting $CD8^+$ T cells restored the virulence of the Δ12Δ203 CPXV mutant, similar to wild type (WT) CPXV. Thus, these studies of CPXV established the *in vivo* importance of viral MHCI inhibition and its effects on antiviral CTL responses.

Interestingly, the virus-specific CTL response to CPXV in C57BL/6 mice is dominated by a single antigen (B8), displaying the immunological phenomenon known as immunodominance, that can impede the development of efficacious vaccines [74]. In theory,

removing the IDE(s) may circumvent immunity. However, for some viruses, subdominant epitopes (SDEs) may compensate and then dominate the immune response [35,75]. Such findings revealed that responses against an IDE(s) suppress immune responses to SDEs, which is a related yet distinct phenomenon coined immunodomination. $CD8^+$ T cell immunodomination also occurs during secondary responses whereby memory $CD8^+$ T cells can suppress naïve $CD8^+$ T cell responses [54]. $CD8^+$ T cell immunodomination is likely a mechanism that contributes to the immunodominance of the B8 antigen in CPXV infections [55], but has not been studied in the context of MHCI inhibition.

B8R is a highly conserved gene among orthopoxviruses and encodes the secreted soluble B8 protein that binds IFN-γ with broad species-specificity. B8 from ectromelia virus (ECTV) is a strong inhibitor of human, bovine, rat, and murine IFN-γ [34], but VACV and CPXV B8 does not neutralize murine IFN-γ [76]. These differences have been attributed to host-specificity. While the natural host of ECTV is not known, experimentally it is restricted to murine hosts, whereas VACV has a broad host-tropism with an unknown natural reservoir [77]. The natural reservoirs of CPXV are wild-rodent species, but CPXV also has broad host-tropism [78,79]. Despite these differences, B8 is the most dominant antigen identified in mice with the $H\text{-}2K^b$ MHCI allele, and the B8 $CD8^+$ T cell epitope sequence (TSYKFESV) is 100% conserved between ECTV, VACV, CPXV, and other orthopoxviruses [37]. However, it is not clear if B8 is an immunodominant antigen because it is a secreted soluble protein that may be efficiently cross-presented.

Previously, we showed that CPXV infection of *Batf3*$^{-/-}$ mice that selectively lack the main cross-presenting DC subsets ($CD103^+/CD8\alpha^+$ DCs) [80] display reduced priming of $B8_{19\text{-}26}$-specific $CD8^+$ T cells during CPXV infection [31], suggesting that cross-presentation is a major pathway used to induce CTLs. However, since *Batf3*$^{-/-}$ mice also lack the capability of cross-dressing, it is

also possible that cross-dressing is the main pathway to induce CPXV-specific CTLs. Moreover, it remained unclear whether other CPXV antigens (i.e., SDEs) are efficiently presented by BATF3$^+$ DCs because CPXV B8$_{19\text{-}26}$ immunodominates the primary CTL response [31]. Finally, due to the above limitations, it is not known if these processes could be affected by viral MHCI inhibition.

Here we studied if transmembrane anchoring of B8 affects its immunodominance, the role of MHCI inhibition in the generation of virus-specific CTLs to SDEs and for the first time, the relevance of cross-dressing in the induction of endogenous antiviral CTL responses.

Results

Secretion of the immunodominant antigen is not a determinant for immunodominance

The immunodominant CPXV B8 antigen is a secreted soluble protein [34], suggesting that its immunodominance may be due to its property as a secreted molecule, as shown for other antigens [81,82]. If this were true, we expect that altering the protein targeting of B8 so that it is no longer secreted from infected cells will affect the acquisition and availability of B8 for APCs, which in turn would affect priming of B8$_{19\text{-}26}$-specific CD8$^+$ T cells and its immunodominance. To test these hypotheses and detect subcellular location of B8, we produced a CPXV mutant expressing B8 fused to mCherry (B8mC) and another mutant (B8TMmC) expressing B8-mCherry fusion protein with a transmembrane domain (TMD) (Fig 2.1A).

We performed subcellular fractionation of infected HeLa cells and analyzed the cytoplasmic extract, membrane extract, and supernatant by Western blot to determine the subcellular location of the B8 variants and if they were secreted. The B8 variants were mainly

detected in the membrane extract of both B8TMmC- and B8mC-infected cells, indicating that the infected cells successfully expressed both B8 variants (Fig 2.1B). We note that the membrane fraction may contain proteins found within the mitochondria and endoplasmic reticulum, but not nuclear proteins, such that the secreted B8 variant detected in the membrane fraction is likely due to proteins localized within the ER and in transit through the secretory pathway. We also detected higher levels of the non-secreted B8 variant in the membrane fraction in comparison to the secreted variant, which is likely due to an accumulation of membrane-associated B8 within B8TMmC-infected cells. Most importantly, the B8 variant was detected in the supernatant of cells infected with B8mC, but not in the supernatant of cells infected with B8TMmC, demonstrating that the B8 variant remains cell-associated in cells infected with B8TMmC (Fig 2.1B). However, anchoring the B8 antigen did not negatively affect priming of $B8_{19\text{-}26}$-specific $CD8^+$ T cells and $B8_{19\text{-}26}$ maintained the highest position in the immunodominance hierarchy, as shown in mice infected intranasally (i.n.) with B8TMmC or B8mC (Fig 2.1C and 2.1D). These data show that secretion of the B8 antigen is not required for priming of $B8_{19\text{-}26}$-specific $CD8^+$ T cells or immunodominance during CPXV infection.

We also performed kinetic analyses of $B8_{19\text{-}26}$-specific $CD8^+$ T cells by staining with $H2K^b$ tetramers loaded with $B8_{19\text{-}26}$ peptide and found that priming by cell-associated B8 resulted in greater expansion of $B8_{19\text{-}26}$-specific $CD8^+$ T cells (Fig 2.1E). These results are consistent with previous findings that cell-associated antigens are cross-presented better than soluble antigens [83,84]. When we infected *Batf3*$^{-/-}$ mice with B8TMmC or B8TM, we found that priming of $B8_{19\text{-}26}$ -specific $CD8^+$ T cells was significantly reduced in *Batf3*$^{-/-}$ mice in comparison to B6 mice (Fig 2.1F), indicating that the introduced B8 mutations did not alter the dependence on cross-presentation (or cross-dressing) in the induction of $B8_{19\text{-}26}$-specific CTL

precursors. Since priming against the non-secreted B8 protein is still dependent on cross-presenting (or cross-dressed) $BATF3^+$ DCs, it is likely that antigens used for conventional cross-presentation by $BATF3^+$ DCs are acquired from infected apoptotic/necrotic donor cells or that $BATF3^+$ DCs are cross-dressed with peptide-loaded MHCI molecules.

Cross-presentation, but not cross-dressing of APCs, drives CTL responses during CPXV infection

While we previously reported that priming of $CD8^+$ T cell responses to CPXV is dependent on cross-presenting $BATF3^+$ DCs, others reported that direct priming is the main mechanism to induce CTL responses with VACV infection [85,86]. To directly compare these findings, we assessed the CTL response after systemic infection with WT CPXV, Δ12Δ203 (from here on referred to as ΔMHCIi) CPXV, or VACV in B6 and *Batf3*-deficient mice. At 8 days post-infection (dpi), the frequency of splenic $CD8^+$ T cells that produced IFN-γ in *ex vivo* stimulations with ΔMHCIi-infected DC2.4 cells was significantly reduced in WT CPXV- and ΔMHCIi-infected *Batf3*$^{-/-}$ mice (Fig 2.2A) in comparison to infected B6 mice, confirming the importance of cross-presentation (or cross-dressing) in inducing CPXV-specific CTLs, as we showed earlier [31]. Conversely, at 6 or 8 dpi, *ex vivo* stimulation with a set of 5 VACV/CPXV peptides (Fig 2.2B) or VACV-infected DC2.4 (Fig 2.2A) revealed no significant difference in the VACV-specific response between infected B6 and *Batf3*$^{-/-}$ mice. These results are consistent with the findings that ablation of XCR1-expressing ($CD103^+/CD8\alpha^+$) DCs does not completely abolish priming of $CD8^+$ T cells during VACV infection [87]. Thus, the *in vivo* responses to two highly related orthopoxviruses display distinct requirements for direct presentation (VACV) versus cross-presentation/cross-dressing (CPXV).

Given that priming of CPXV-specific CTL precursors and cross-dressing of APCs in other settings were both shown to require BATF3^{+} DCs [67], we sought to determine if cross-dressing could account for the source of antigen being presented to CD8^{+} T cells in CPXV infection. To do so, we transferred B6 bone marrow into lethally irradiated *Batf3*$^{-/-}$-F_1 (*Batf3*$^{-/-}$-B6 x *Batf3*$^{-/-}$-BALB/c) mice (Fig 2.3A). In B6→*Batf3*$^{-/-}$-F_1 chimeras, donor B6-derived (Batf3-dependent*)* APCs only express H-2^{b} MHCI molecules and should cross-prime CTL responses against H2^{b}-restricted epitopes (Fig 2.3A). However, priming by H-2^{d}-restricted epitopes would occur only if the H2^{b} APCs in these chimeric mice were cross-dressed with preformed peptide-loaded H-2^{d} class I molecules from the host parenchymal cells, which express both H-2^{b} and H-2^{d} class I molecules. We also produced BALB/c→*Batf3*$^{-/-}$-F_1 chimeras, to analyze the converse situation. The reconstituted mice were infected by i.n. administration with WT CPXV and CTL responses were determined against the immunodominant H-2K^{b}-restricted $B8_{19\text{-}26}$ and the H-2L^{d}-restricted $F2_{26\text{-}34}$ epitopes. As expected, we detected a $B8_{19\text{-}26}$ response in B6→*Batf3*$^{-/-}$-F_1 mice that was of similar magnitude to non-chimeric WT-F_1 (B6 x BALB/c) infected mice (Fig 2.3B). We also detected a small $B8_{19\text{-}26}$-specific response in BALB/c→*Batf3*$^{-/-}$-F_1, but the frequency of $B8_{19\text{-}26}$-specific CD8^{+} T cells was significantly lower (~12-fold) than in B6→*Batf3*$^{-/-}$-F_1 and WT-F_1 mice. A small, yet detectable response to $F2_{26\text{-}34}$ was also detected in the lungs of B6→*Batf3*$^{-/-}$-F_1-infected mice, but it was ~3 fold and ~8 fold lower in comparison to WT-F_1- and BALB/c→*Batf3*$^{-/-}$-F_1-infected mice respectively. Thus, these data suggest cross-dressing contributes minimally to priming against these peptide determinants.

It is possible that cross-dressing by H-2K^{b}- and H-2L^{d}-restricted epitopes other than $B8_{19\text{-}26}$ and $F2_{26\text{-}34}$, respectively, occurred in infected BMC mice, so we also performed *ex vivo* stimulations with ΔMHCIi-infected DC2.4 (H-2^{b}) and P815 (H-2^{d}) cells as these cells present a

broad array of naturally derived CPXV peptides (Fig 2.3B). The frequency of IFN-γ^+ $CD8^+$ T cells upon stimulation with ΔMHCIi-infected DC2.4 cells was significantly lower in BALB/c→*Batf3*$^{-/-}$-F_1 mice in comparison to B6→*Batf3*$^{-/-}$-F_1 and WT-F_1 mice. Similarly, the frequency of IFN-γ^+ $CD8^+$ T cells upon stimulation with ΔMHCIi-infected P815 cells was significantly lower in B6→*Batf3*$^{-/-}$-F_1 mice in comparison to BALB/c→*Batf3*$^{-/-}$-F_1 and ~10 fold lower in comparison WT-F_1 mice. The frequency of $CD8^+$ T cells that responded to ΔMHCIi-infected P815 cells was also significantly lower in WT-F_1 in comparison to BALB/c→*Batf3*$^{-/-}$-F_1. This was also seen in $F2_{26\text{-}34}$ responses (Fig 2.3B). These findings may be due to the additional epitope diversity from H-2^b as well as H-2^d expression in WT-F_1, which may compromise responses to H-2^d-restricted epitopes during the primary response. Regardless, these results suggest that cross-dressing from non-hematopoietic cells does not generate a vigorous response during primary CPXV responses.

We next assessed whether cross-dressing plays a role during secondary responses to CPXV infection since cross-dressed APCs are capable of stimulating memory $CD8^+$ T cells [65]. However, the secondary CPXV response in the B6→*Batf3*$^{-/-}$-F_1 and BALB/c→*Batf3*$^{-/-}$-F_1 mice were similar to what was observed in the primary CPXV response (Fig 2.3C). Thus, cross-dressing from non-hematopoietic cells also plays a minor role in activating endogenous memory $CD8^+$ T cells following CPXV infection.

To test if cross-dressed MHCI could be contributed by the hematopoietic compartment, we reconstituted lethally irradiated *Batf3*$^{-/-}$-F_1 mice with a 1:1 mixture of BALB/c-Thy1.1 and *Batf3*$^{-/-}$-F_1 bone marrow (S2.1A Fig). In these mice, cross-presentation should only be carried out by the donor BALB/c-Thy1.1-derived APCs (H-2^d). In contrast, cells that are of the donor *Batf3*$^{-/-}$-F_1 (H-2^b x H-2^d) origin will lack $BATF3^+$ DCs and should not carry out cross-presentation, but

may serve as a source of cross-dressing peptide-MHCI complexes. We systemically infected BALB/c-Thy1.1 + *Batf3*$^{-/-}$-F_1→*Batf3*$^{-/-}$-F_1 mice with WT CPXV and found that the H-2^d-restricted response was successfully reconstituted, whereas the H-2^b-restricted response was significantly lower than the response in WT-F_1 mice and was comparable to *Batf3*$^{-/-}$-F_1→*Batf3*$^{-/-}$-F_1 control mice (S2.1B Fig). These data indicate that APCs cross-dressed from other hematopoietic cells does not efficiently prime CD8$^+$ T cell responses in the setting of effective viral MHCI inhibition.

Taken together, these data suggest that antigens are predominantly cross-presented by BATF3$^+$ DCs during CPXV infection and that cross-dressing plays a minor role, if at all.

Cross-presentation of SDEs in the absence of the IDE induces a robust CD8$^+$ T cell response that is not affected by viral MHCI inhibition, revealing immunodomination

Insufficient cross-presentation of SDEs may explain the subdominance of other CPXV antigens. To test if cross-presentation of CPXV SDEs alone is capable of inducing a strong CTL response, we mutated the $B8_{19\text{-}26}$ epitope anchor residues required for binding to H-2K^b peptide-binding groove, postulating that this will prevent the $B8_{19\text{-}26}$ epitope from being presented by H-2K^b. According to the peptide-binding motif of H-2K^b, the $B8_{19\text{-}26}$ epitope contains a primary anchor residue (phenylalanine at position P5) and an auxiliary anchor residue (tyrosine at position P3) [88]. To determine whether mutating the primary anchor residue is sufficient to eliminate binding to H-2K^b or if both anchor residues should be mutated, peptide-binding assays were performed using the transporter associated with antigen processing 2 (TAP2)-deficient RMA-S cell line in which addition of peptides capable of binding H-2K^b stabilize its expression on the cell surface [89]. Alanine substitution of the primary anchor residue significantly reduced

binding of the $B8_{19\text{-}26}$ epitope peptide to H-$2K^b$ as compared to WT B8, but binding could be increased with increasing concentrations of peptide (S2.2A Fig). However, alanine substitutions of the primary and auxiliary anchor residues completely abrogated binding of the $B8_{19\text{-}26}$ epitope peptide to H-$2K^b$, even at higher peptide concentrations. Based on these findings, we introduced both substitutions into the WT and the ΔMHCIi CPXV genomes. The CPXV $B8_{19\text{-}26}$ epitope mutants B8Y3AF5A (referred to as $\Delta B8_{19\text{-}26}$) and a *B8R* deletion mutant (ΔB8R) that we generated did not exhibit defects in viral replication *in vitro* (S2.2B Fig). Surprisingly, they also did not show attenuated virulence *in vivo*, as measured by weight loss or lethality, as compared to WT CPXV (S2.2C Fig).

There was no detectable $B8_{19\text{-}26}$ response in $\Delta B8_{19\text{-}26}$- or ΔMHCIi$\Delta B8_{19\text{-}26}$-infected mice (Fig 2.4A and 2.4B, S2.3A and S2.3B Fig). However, infections with $\Delta B8_{19\text{-}26}$ or ΔMHCIi-$\Delta B8_{19\text{-}26}$ generated a robust SDE response. In contrast, as we previously reported [31], a large proportion of the CPXV-specific CTL response was directed against $B8_{19\text{-}26}$ in the lungs of WT- and ΔMHCIi-infected mice. Additionally, there were no significant differences between the overall CTL responses against WT, $\Delta B8_{19\text{-}26}$, ΔMHCIi, and ΔMHCIi$\Delta B8_{19\text{-}26}$ (Figs 2.4A and 2.4B), despite the loss of the $B8_{19\text{-}26}$-specific response. Therefore, the CTL response was completely compensated by SDEs in the absence of a $B8_{19\text{-}26}$ response.

It was possible that the $B8_{19\text{-}26}$ epitope mutation allows CPXV to replicate to higher titers in the lungs of infected mice resulting in higher antigen loads, which could explain the observed compensation. However, the $B8_{19\text{-}26}$ epitope mutations did not result in significantly increased viral titers in infected mice (Fig 2.4C), suggesting that the compensation is unlikely due to increased antigen loads.

Immunodomination and priming by SDEs were also not affected by CPXV-mediated MHCI inhibition since there were no significant difference in the SDE response against $\Delta B8_{19\text{-}26}$ and $\Delta MHCIi\Delta B8_{19\text{-}26}$, as measured by stimulation with ΔMHCIi- (used to estimate total response) or $\Delta MHCIi\Delta B8_{19\text{-}26}$- (used to estimate total SDE response) infected DC2.4 cells (Fig 2.4A and 2.4B). Additionally, there was no significant difference in the frequency of $CD8^+$ T cells that exhibited an effector T cell phenotype in infected mice (S2.3C and S2.3D Fig). Considering that the route of infection can alter antigen levels and immunodominance [55], we infected mice by intraperitoneal (i.p.) injections. Compensation by SDEs was also observed during systemic infection (Figs 2.4D and 2.4E), suggesting that compensation was not dependent on antigen levels or the route of infection. However, CTL responses against the panel of subdominant epitopes we tested were not significantly increased in the absence of $B8_{19\text{-}26}$, suggesting that other unidentified or cryptic subdominant epitopes compensated the CTL response. Interestingly, the response against $A42_{88\text{-}96}$ was significantly reduced in the absence of the $B8_{19\text{-}26}$-specific response (Fig 2.4D), suggesting that SDEs were up-ranked in the dominance hierarchy and were now themselves eliciting immunodomination. Furthermore, we found that priming of SDE-specific $CD8^+$ T cells was also dependent on $BATF3^+$ DCs (S2.3E Fig). These data suggest that the IDE-specific CTL response suppresses cross-priming of SDE-specific $CD8^+$ T cells during primary CPXV infections, indicating immunodomination, but this process was not affected by viral MHCI inhibition.

SDE-specific $CD8^+$ T cell are effective at immunodomination during primary and secondary CPXV infection

Memory $CD8^+$ T cells also have a capacity for immunodomination and can inhibit naïve $CD8^+$ T cell responses [54]. However, this is not the case for VACV since prior priming with individual SDEs does not alter the immunodominance hierarchy following VACV boost in SDE-primed mice [56]. Considering that the priming mechanisms are different during VACV and CPXV infection (Fig 2.2A), we tested whether CPXV-specific memory $CD8^+$ T cells can exert immunodomination. We primed mice with WT CPXV, boosted the mice with a low or high dose of $\Delta B8_{19\text{-}26}$ at 25 dpi, and assessed the $CD8^+$ T cell response in the lungs and spleens 8 days after boosting (Fig 2.5A). In this group, $B8_{19\text{-}26}$-specific memory $CD8^+$ T cells should be present pre- and post-boost, but will not undergo expansion following boost with $\Delta B8_{19\text{-}26}$. As expected, we detected $B8_{19\text{-}26}$-specific $CD8^+$ T cells in the lungs and spleens of WT CPXV-primed mice after boosting with $\Delta B8_{19\text{-}26}$ (Fig 2.5B and 2.5C) and before boosting (Fig 2.5D). Additionally, we found that WT and ΔMHCIi infection resulted in a similar relative abundance of $B8_{19\text{-}26}$-specific $CD8^+$ T cells with a memory phenotype ($CD44^+CD62L^+KLRG1^-CD127^+$) at 25 dpi, suggesting that viral MHCI inhibition does not affect memory T cell development (Fig 2.S4). In a separate group, mice were primed with SDEs by $\Delta B8_{19\text{-}26}$ infection and boosted with WT CPXV. In this group, we would expect mice to mount a naïve $B8_{19\text{-}26}$ response after boosting with WT CPXV only in the absence of memory $CD8^+$ T cell immunodomination. However, the naïve $B8_{19\text{-}26}$ response was significantly inhibited following boost with both a low and high dose of WT CPXV, suggesting that the SDE-specific memory $CD8^+$ T cells immunodominate naïve $CD8^+$ T cells. Alternatively, neutralizing antibodies may have reduced the antigen levels and therefore limited the naïve $B8_{19\text{-}26}$ response following boost with CPXV.

To assess the potential role of host-protective antibodies, we repeated the above experiments, but this time we depleted $CD8^+$ T cells prior to challenging mice with CPXV

(S2.5A and S2.5B Fig) and then monitored the mice for survival. CPXV-immunized mice that received CD8-depleting or isotype control antibodies survived, whereas naïve mice succumbed to the challenge (S2.5C Fig). Although this was somewhat expected because CPXV evades CTLs, these results suggest that host-protective antibodies may contribute to protection in the absence of $CD8^+$ T cells during secondary exposure to CPXV. We thus repeated the prime and boost experiments and examined immunodomination in μmT mice, which lack mature B cells. Because CPXV evades CTLs *in vivo* and μmT mice should not mount a protective antibody response, it is likely that μmT mice are highly susceptible to WT CPXV infection. To avoid this issue, we infected μmT mice with ΔMHCIi CPXV strains as CTLs can effectively control these viruses in WT mice. We primed μmT mice by skin scarification (s.s.) infection, which resembles human immunizations with VACV. We then boosted the mice at 25 dpi by i.n. administration, and subsequently assessed the $CD8^+$ T cell response 7 days after boost. Mice primed with ΔMHCIi resulted in expansion of a $B8_{19\text{-}26}$-specific $CD8^+$ T cells following i.n. boost with ΔMHCIi (Fig 2.5E). Mice primed with ΔMHCIiΔ$B8_{19\text{-}26}$ also mounted a detectable response against $B8_{19\text{-}26}$ following i.n. boost with ΔMHCIi, yet this response was significantly reduced by ~9-fold in comparison to mice immunized with ΔMHCIi. Therefore, memory $CD8^+$ T cell immunodomination still occurred in the absence of neutralizing antibodies and viral MHCI inhibition, suggesting that immunodomination may be due to T cell interference.

Because memory $CD8^+$ T cells are present at higher frequencies than naïve antigen-specific $CD8^+$ T cells, it is likely that memory $CD8^+$ T cells have a competitive advantage in accessing APC resources [90–92]. For instance, downregulation of MHCI on infected cells may limit the level of antigen presented during CPXV infection, thereby contributing to T cell cross-competition for peptide-MHCI complexes in the secondary response. Indeed, T cell cross-

competition for peptide-MHCI complexes during secondary responses has been demonstrated using a heterologous prime-boost strategy [93], but to our knowledge this has only been directly tested between memory and naïve T cells specific for IDEs. To test if SDE-specific memory $CD8^+$ T cells can cross-compete with naïve $B8_{19\text{-}26}$-specific $CD8^+$ T cells, we performed a competition experiment in which we primed mice with $\Delta B8_{19\text{-}26}$, adoptively transferred peptide-pulsed BMDCs at 25 dpi, and then assessed the $CD8^+$ T cells responses 6 days after transfer. Transfer of $B8_{19\text{-}26}$-pulsed BMDCs into $\Delta B8_{19\text{-}26}$ -primed mice resulted in a robust $B8_{19\text{-}26}$ response (Fig 2.5F). Likewise, transfer of $K3_{6\text{-}15}$-pulsed BMDCs resulted in moderate expansion of $K3_{6\text{-}15}$-specific memory $CD8^+$ T cells. However, when BMDCs that were pulsed with $B8_{19\text{-}26}$ and $K3_{6\text{-}15}$ at the same time were transferred the $B8_{19\text{-}26}$ response was inhibited, further supporting the findings that memory $CD8^+$ T cells immunodominate naïve $CD8^+$ T cells. Conversely, $B8_{19\text{-}26}$-specific $CD8^+$ T cells dominated the response when BMDCs pulsed with $B8_{19\text{-}26}$ and $K3L_{6\text{-}15}$ at the same time were transferred into naïve mice (Fig 2.5G). If immunodomination is an effect of cross-competition, then providing BMDCs that exclusively present $K3_{6\text{-}15}$ and BMDCs that exclusively present $B8_{19\text{-}26}$ alone should overcome the effects of immunodomination. When $B8_{19\text{-}26}$-pulsed BMDCs were mixed with $K3_{6\text{-}15}$-pulsed BMDCs (pulsed separately) and transferred into $\Delta B8_{19\text{-}26}$-primed mice, the $B8_{19\text{-}26}$ response was significantly greater than in mice that received BMDCs pulsed with $B8_{19\text{-}26}$ and $K3L_{6\text{-}15}$ at the same time, suggesting that cross-competition plays a role in memory $CD8^+$ T cell immunodomination.

Interestingly, the $B8_{19\text{-}26}$ response in mice that received the 1:1 mixture of $K3L_{6\text{-}15}$-pulsed and $B8_{19\text{-}26}$-pulsed BMDCs was significantly lower than in mice that only received $B8_{19\text{-}26}$-pulsed BMDCs. Therefore, the partial rescue of the $B8_{19\text{-}26}$ response when the epitopes were

presented on different APCs suggest that additional factors contribute to immunodomination during secondary responses. In contrast to the secondary response, separating the $K3_{6\text{-}15}$ and $B8_{19\text{-}26}$ epitopes during primary responses had no effect on immunodomination of $B8_{19\text{-}26}$-specific $CD8^+$ T cells (Fig 2.5G), suggesting that cross-competition for peptide-MHCI complexes contributes to immunodomination mainly during secondary responses.

Having demonstrated that SDE-specific memory $CD8^+$ T cells have a capacity for immunodomination, we asked if SDE-specific $CD8^+$ T cells could exhibit immunodomination during primary responses. We reasoned that modulating the immunodominant and subdominant antigen levels may allow SDE-specific $CD8^+$ T cells to immunodominate. To test this, we performed co-infection experiments in which the level of WT and $\Delta B8_{19\text{-}26}$ input were varied while maintaining the overall viral dose. We first synchronized the infections to limit the variation in the dose by infecting freshly harvested splenocytes with either WT or $\Delta B8_{19\text{-}26}$ separately. We then mixed WT- and $\Delta B8_{19\text{-}26}$-infected splenocytes at a ratio of 1:0, 10:1, 1:10, or 0:1, inoculated mice i.v. with a total of 1×10^5 infected cells, and assessed the CTL response at 7 dpi (Fig 2.6A). A graded $B8_{19\text{-}26}$ response was observed with the concurrent increase of $\Delta B8_{19\text{-}26}$ input and decrease of WT input (Fig 2.6B), while the overall response as determined by stimulation with ΔMHCIi-infected DC2.4 cells remained roughly equal (Fig 2.6C). These data suggest that SDE-specific CTLs are capable of immunodominating the primary response when the relative abundance of subdominant antigens is increased, even in the presence of the IDE. To confirm that the graded response was not simply due to reduced WT input, we repeated the co-infection experiment using mixtures of WT- and mock-infected splenocytes. Injecting the varying mixtures of WT- and mock-infected splenocytes did not result in a gradation of the $B8_{19\text{-}}$

$_{26}$ response (Fig 2.6B), suggesting that the observed graded $B8_{19-26}$ response was dependent on the subdominant antigen levels.

SDE-primed $CD8^+$ T cells control lethal CPXV infection in the absence of the CPXV MHCI inhibitors

Thus far, our results indicate that CPXV-mediated MHCI inhibition does not affect priming of $CD8^+$ T cells by SDEs. However, we wondered whether SDE-specific CTL responses could provide protection against CPXV infection *in vivo*. To examine the physiological relevance of SDEs in protecting against CPXV infection, we performed adoptive transfer experiments with CTLs primed with $\Delta B8_{19-26}$ or MCMV as a control for antigen specificity (Fig 2.7A). Mice that received primed CTLs were then challenged by i.n. administration with a lethal dose of $\Delta B8_{19-26}$ or $\Delta MHCIi\Delta B8_{19-26}$. The majority of mice that received MCMV-primed CTLs died following infection with $\Delta B8_{19-26}$ or $\Delta MHCIi\Delta B8_{19-26}$ (Fig 2.7B and 2.7C). All mice that received $\Delta B8_{19-26}$-primed CTLs also died after challenge with $\Delta B8_{19-26}$, whereas all mice challenged with $\Delta MHCIi\Delta B8_{19-26}$ survived. Therefore, CTLs primed by SDEs are capable of recognizing and controlling CPXV only in the absence of CPXV-mediated MHCI inhibition, which is consistent with our previous findings regarding WT CPXV exposure that is dominated by the $B8_{19-26}$ response [31,52].

Discussion

Headings may be typed above or on the same line as the sections they label. Type the chapter number and section number before the section title. The font size for section headings

should be no larger than 18. Here we demonstrate that the secretion of an immunodominant CPXV antigen does not affect immunodominance or cross-priming by the IDE. Intriguingly, we found that the IDE and SDEs are differentially presented by APCs during infection with CPXV and VACV, despite being closely related genetically. We also show that $CD8^+$ T cell immunodomination is not affected by viral MHCI inhibition and can be elicited by SDEs during primary and secondary responses against CPXV infection. Additionally, we show that SDEs alone are entirely capable of generating protective CTL responses, which is dependent on cross-priming by $BATF3^+$ DCs.

Cross-priming of $CD8^+$ T cells is important for inducing antiviral CTL responses, especially in settings where direct-presentation is not possible (e.g., APCs are not susceptible to infection) or is evaded (e.g., impairing maturation of infected-APCs or inhibiting MHCI presentation). Consistent with this notion, herein we showed that the induction of antiviral CTL responses is dependent on cross-presentation in the presence of CPXV-mediated MHCI inhibition. Priming of $CD8^+$ T cell in the absence of viral MHCI inhibition during CPXV infection was also dependent on cross-presenting $BATF3^+$ DCs, albeit to a less extent. While we have not ruled out the possibility that ΔMHCIi-infected $BATF3^+$ DCs prime CTL precursors by direct presentation, CPXV-infected DCs have reduced expression of costimulatory molecules involved in T cell activation [94,95], suggesting that direct-presentation may be limited even in the absence of CPXV012 and CPXV203. Nonetheless, there are clearly factors other than MHCI inhibition that skew priming of T cells towards cross-priming and further study of CPXV ORFs in the context of ΔMHCIi provides an excellent opportunity to investigate such factors. In this study, we provide evidence that cross-priming is the main mechanism driving CPXV-specific CTL responses.

Our studies also indicate that cross-dressing plays no significant role in the T cell response to CPXV infections *in vivo*. Cross-dressing has been proposed as a mechanism by which APCs can rapidly acquire peptide epitopes for presentation to CTL precursors, thereby eliminating the time spent for antigen processing [65,66]. In support of this, DCs can be cross-dressed *in vitro* by peptide-MHCI complexes from epithelial cells [96], which are commonly targeted by viruses and thus may serve as a common source of preformed viral peptide-MHCI. Moreover, peptide-MHCI from parenchymal cells cross-dressed DCs in vesicular stomatitis virus (VSV)-infected mice and the cross-dressed DCs induced proliferation of memory $CD8^+$ T cells, but not naïve T cells. However, priming of naïve antigen-specific $CD8^+$ T cells by cross-dressed DCs can occur, as demonstrated using DNA vaccination and transfer of adenovirus infected DCs [66,67]. In contrast to these studies, we found that cross-dressing does not efficiently prime or drive expansion of endogenous antigen-specific naïve and memory $CD8^+$ T cells during CPXV infection.

While previous reports on cross-dressing provide compelling evidence that cross-dressing occurs *in vivo*, the transfer of TCR tg T cells in these studies may have resulted in non-physiological induction of $CD8^+$ T cells by cross-dressed DCs. Additionally, cross-dressing in these experimental settings may have been promoted due to a potential generation of supraphysiological levels of peptide-MHCI by DNA vaccination or by transfer of adenovirus infected DCs. These factors may explain the difference between previous studies and our results using CPXV infection. Because CPXV encodes an extensive arsenal of immunomodulatory proteins, the possibility that CPXV directly or indirectly inhibits cross-dressing may also explain these conflicting results. For example, downregulation of MHCI cell surface expression by CPXV012 and CPXV203 may prevent transfer of peptide-loaded MHCI molecules by

trogocytosis, a process in which intercellular exchange of intact membranes occurs during the formation of an immunological synapse [97–100]. If trogocytosis is required for cross-dressing of APCs *in vivo*, as been demonstrated *in vitro* [65], then cross-dressing dependent T cell responses are expected to be abrogated during CPXV infection. Ultimately, our results suggest that antigens are acquired from necrotic/apoptotic bodies or secreted viral proteins found in the extracellular milieu and are then predominantly cross-presented during CPXV infection.

Cross-presentation of peptide epitopes may also be influenced by the nature of the antigens and can affect the extent of $CD8^+$ T cell immunodominance [101–103]. For instance, the secreted immunodominant antigens of *M. tuberculosis* are likely processed through the cross-presentation pathway [104,105] and eliminating bacterial secretion prevents priming of IDE-specific $CD8^+$ T cells during *M. tuberculosis* infection [81]. Priming of naïve $CD8^+$ T cells against cell-associated subdominant SV40 large tumor antigen (T Ag) epitope V is also dependent on cross-presentation, but the response against the V epitope is limited because it is inefficiently cross-presented relative to the T Ag IDE [103]. Our findings suggest that cross-presented CPXV IDEs can be derived from cell-associated antigen since ablating B8 secretion did not negatively affect cross-priming dependent induction of $B8_{19\text{-}26}$-specific $CD8^+$ T cells. Moreover, cell-associated B8 elicited a greater $B8_{19\text{-}26}$-specific $CD8^+$ T cell response in comparison to secreted soluble B8, which is consistent with the preferential *in vivo* cross-presentation previously reported for cell-associated antigens [83,84]. However, the underlying mechanisms of immunodominance are complex and are often context dependent as we found that secretion of CPXV B8 is not required for immunodominance and that cross-presentation of CPXV SDEs in the absence of the immunodominant $B8_{19\text{-}26}$ epitope stimulated a robust CTL response. The fact that the CTL

response to SDEs compensated for the absence of $B8_{19-26}$ suggests that the SDE response is suppressed by the $B8_{19-26}$ response, supporting the concept of immunodomination.

In many cases immunodomination occurs as a consequence of T cell competition for limiting APC resources [90,92,106,107]. For instance, competition for peptide-MHCI complexes on APCs during primary CTL responses can occur as a result of antigen abundance [108]. In support of this, we showed that concurrently increasing subdominant antigen levels and reducing immunodominant antigen levels allow SDEs to gain dominance during the primary response to CPXV infection. Similarly, modulating the antigen abundance through different methods during influenza A virus and VACV infection has been shown to influence immunodomination [55,109]. In certain models, immunodomination can be overcome when APCs present different epitopes separately [91,100,107], indicating that $CD8^+$ T cells of different specificities can cross-compete for peptide-MHCI complexes on APCs. This has been convincingly demonstrated in models where immunodomination occurs when APCs co-present model antigen epitopes. However, epitope co-presentation by APCs does not always influence immunodomination, as we have shown here for primary responses, and the role of cross-competition in inducing antiviral CTL responses is controversial [110].

We found that cross-competition for peptide-MHCI complexes is relevant and that immunodomination occurs during secondary responses as a consequence. Alternatively, the suppressed $B8_{19-26}$ response in our cross-competition experiments may have resulted from $K3_{6-15}$-specific memory $CD8^+$ T cells killing the BMDCs that were pulsed with $B8_{19-26}$ and $K3L_{6-15}$ at the same time. Nevertheless, we observed partial rescue of the $B8_{19-26}$ response when the epitopes were separated on BMDCs. This partial rescue may be due to peptide exchange between BMDCs that were pulsed separately and adoptively transferred as a mix, which would

subsequently result in epitope co-presentation and $K3_{6\text{-}15}$-specific memory $CD8^+$ T cell immunodomination. However, additional factors that we did not test such as cross-competition for growth factors, antigen-specific T cell precursor frequencies, or TCR avidity [111] likely contribute to the memory T cell immunodomination as well.

Remarkably, immunodomination during the secondary response against CPXV was exerted by SDE-specific memory $CD8^+$ T cell. The capacity for SDE-specific memory $CD8^+$ T cells to inhibit the response to an IDE has been shown with influenza virus [54], but prior priming with SDE peptides did not result in memory $CD8^+$ T cell immunodomination using VACV, as shown by Wang et al [56]. Here in our study, memory $CD8^+$ T cell immunodomination was clearly evident when SDE-primed mice were challenged with WT CPXV, whereby the naïve $B8_{19\text{-}26}$-specific $CD8^+$ T cell response was suppressed. Moreover, memory $CD8^+$ T cell immunodomination was not affected by MHCI inhibition. However, mice were primed by CPXV infection (in this study) as opposed to individual SDE peptides (as done by Wang et al). These experimental differences suggest that the priming stimulus and the breadth of the primary response influences immunodomination during secondary responses against poxviruses.

Taken together, our findings highlight the need to consider the effects of pre-existing immunity on the outcome of secondary responses and vaccinations. An advantage to using VACV-based vaccines is that in addition to providing protection against heterologous pathogens, the native vector epitopes (both IDEs and SDEs) can provide cross-protection against related orthopoxviruses, as supported by our findings here and previous reports [112–115]. However, as a consequence of pre-existing immunity, memory $CD8^+$ T cell immunodomination may limit the target antigen response following immunization with VACV-based vaccines, in turn resulting in non-efficacious vaccinations. For example, native VACV epitopes can mask responses against

target antigens expressed by VACV vaccine vectors [74]. Nevertheless, our results support the ongoing evaluation for poxviruses as promising vaccine vectors, and stress the necessity to develop novel vaccination strategies.

Materials and Methods

Cell lines, mice and viruses.

Cell lines HeLa, Vero, and P815 were obtained from the American Type Culture Collection (ATCC). DC2.4 cells were a kind gift from Dr. Kenneth Rock, University of Massachusetts Medical School. HeLa, Vero, DC2.4, and P815 cells were cultured respectively in Dulbecco's Modified Eagle Medium (DMEM), Minimum Essential Medium (MEM) or RPMI supplemented with 10% FBS (Mediatech), 100 U/ml penicillin, 100 g/ml streptomycin, 1mM sodium pyruvate, and non-essential amino acids (Gibco). VACV-WR was obtained from the ATCC. MCMV Smith strain was a gift from Dr. Herbert Virgin, Washington University. CPXV BAC pBR mini-F construct was kindly provided by Dr. Karsten Tischer, Free University of Berlin. Mutant viruses were generated by *en passant* mutagenesis [116] using primers listed in S2.1 Table. Gene fragments were synthesized (Integrated DNA Technologies) and assembled using Gibson Assembly (New England BioLabs) for cloning of the B8-mCherry fusion contructs (S2.2 Table). Infectious BAC-derived viruses (S2.3 Table) were reconstituted using a slightly modified method previously described by Xu *et al* [117]. In brief, ~$8x10^5$ Vero cells seeded in 6-well plates were infected with fowlpox virus (FWPV) at an MOI of 1. Transfection of FWPV-infected Vero cells was carried out 1 hour post-infection (hpi) with 4 μg of BAC DNA and 5 μL of Lipofectamine 2000 transfection reagent (ThermoFisher Scientific) according to the

manufacturer's instruction. Serial dilutions of reconstituted infectious virus were passaged up to four times on Vero cells in order to remove the mini-F vector sequence. Wells harbouring single GFP-negative plaque were isolated and used for preparing virus stocks as previously described [53]. C57BL/6Ncr mice were purchased from the National Cancer Institute. B6.129S2-Ighm^{tm1Cgn}/J mice were purchased from the Jackson Laboratory. *Batf3*$^{-/-}$ mice crossed to the C57BL/6 and BALB/c background were kindly provided by Dr. Kenneth Murphy, Washington University. Growth curves were performed on Vero cells. Supernatant and cells were harvested at 12, 24, 28, and 72 hpi and viral titers were determined by plaque assay using Vero cells.

Peptide binding Assay

TAP2-deficient RMA-S (H-2^b) cells were cultured overnight at 28°C in 5% CO_2 to accumulate peptide-receptive MHCI molecules at the cell surface. Peptides were then added at various concentrations and the cells were transferred to 37°C. After 6 h of incubation at 37°C, cells were harvested and washed twice in PBS. H-2K^b cell surface expression was then measured by flow cytometry.

Western blot

1 x 10^6 HeLa cells were infected at a MOI of 5. Cells and supernant were collected at 4 hpi and were lysed on ice for 5 min in RIPA lysis buffer supplemented with 1x Halt protease and phosphatase inhibitor cocktail. Cells were further processed for subcellular fractionation using a Subcellular Protein Fractionation Kit (ThermoFisher). Samples were mixed with Laemmli sample buffer (Bio-Rad), incubated at 95°C for 5 minutes, separated by SDS-PAGE, and transferred to PVDF membranes. Immunoblotting was performed using rabbit polyclonal anti-

mCherry and rabbit monoclonal anti-EGFR (Abcam) followed by horseradish peroxidase (HRP)-conjugated goat anti-rabbit IgG (Cell Signalling).

Generation of bone marrow chimeras

6 weeks of age *Batf3*$^{-/-}$-F_1 ($H2^b$x$H2^d$) mice were depleted of NK cells by i.p. administration of 100 μg of PK136 antibody. Two days later, the mice were lethally irradiated with 950 rads and were reconstituted with 1x10^7 T cell depleted C57BL/6, BALB/c, or a 1:1 mixture of BALB/c-Thy1.1 and *Batf3*$^{-/-}$-F_1 bone marrow cells. Bone marrow chimeras were treated with antibiotics for 4 weeks and were allowed to reconstitute for 8 weeks before use.

Generation of bone marrow-derived DCs and immunization

BM-derived dendritic cells (BMDCs) were generated by culturing BM cells in the presence of 20 ng/mL GM-CSF and IL-4 (PeproTech) for 8 days, as previously described [118]. LPS (150ng/nL) was then added and the cells were allowed to mature overnight. The cells were then pulsed with peptide (1g/mL, 45 min). Cells were washed extensively in PBS and a total of 2.5 x 10^5 DCs was injected intravenously (i.v.) into recipient mice.

Mouse infection and $CD8^+$ T cell adoptive transfer

Mice were age- and sex-matched for each experiment and used at 8-10 weeks of age. Mice were infected as previously described for i.n. and s.s. infections [31]. For s.s. infections, fur was trimmed with clippers, then a thin layer of Vaseline was applied over the trimmed region and the remaining fur was shaved over with a double-edge razor blade one day before infection. Mice infected by i.p. or s.c. administration were injected with a volume of 100μL or 200μL of virus

inoculum per mouse, respectively. For co-infection experiments, splenocytes isolated from B6 mice were infected at an MOI of 5, harvested 1 hpi, and washed three times with PBS. 1 x 10^5 infected cells in 200 μL of PBS were transferred intravenously into naïve B6 mice. For the CPXV SDE protection experiment, $CD8^+$ T cells from splenocytes of infected B6 mice that had been infected 7 days earlier with WT CPXV or MCMV were isolated by positive selection using anti CD8a MicroBeads (Miltenyi Biotec). 3 x 10^6 $CD8^+$ T cells were transferred intravenously into naïve B6 mice. Mice were infected approximately 24 h after transfer.

Flow cytometry, IFN-γ production assays, and antibodies

Single-cell suspensions from the lungs and spleens were prepared at the indicated days post-infection as previously described [31]. 1x10^6 cells were seeded in 96-well plates and were re-stimulated with peptides or with 1x10^5 DC2.4 cells that had been infected for 4 h with ΔMHCI-i or ΔMHCI-iΔB8 CPXV (MOI 5). Cells were incubated at 37°C, 5% CO_2. After 1 h at 37°C, GolgiPlug (BD Biosciences) was added to each well. Three hours later, cells were stained on ice with Fixable Viability Dye eFlour 506 (eBioscience) before staining of cell surfaces for the indicated surface markers. Cells were then fixed/permeabilized and stained for IFN-γ. Background levels were determined using cells from uninfected mice, which usually ranged between 0.01-0.05%, and were subtracted from the values presented. For intracellular staining of GzmB and tetramer staining, cells were stained *ex vivo* without stimulation and without incubation with GolgiPlug. H-$2K^b$-TSYKFESV tetramers were produced in the Immunomonitoring Laboratory within the Center for Human Immunology and Immunotherapy Programs (Washington University). The following monoclonal antibodies were obtained from ThermoFisher, BD Biosciences or eBioscience: CD3 (145-2C11), CD8α (53-6.7), CD8β

(eBioH35-17.2), CD4 (RM4-5), CD44 (IM7), CD62L (MEL-14), GzmB (GB12), KLRG1 (2F1), CD127 (A7R34) and IFN-γ (XMG1.2).

Statistics

The data are shown as mean ± SEM and were analysed with an unpaired Student *t* test or one-way ANOVA followed by Tukey posttest comparison using Prism GraphPad software, asterisks indicate statistical significance and the *p* values are denoted as $*p<0.05$, $**p<0.01$, $***p<0.001$.

Figures and Tables

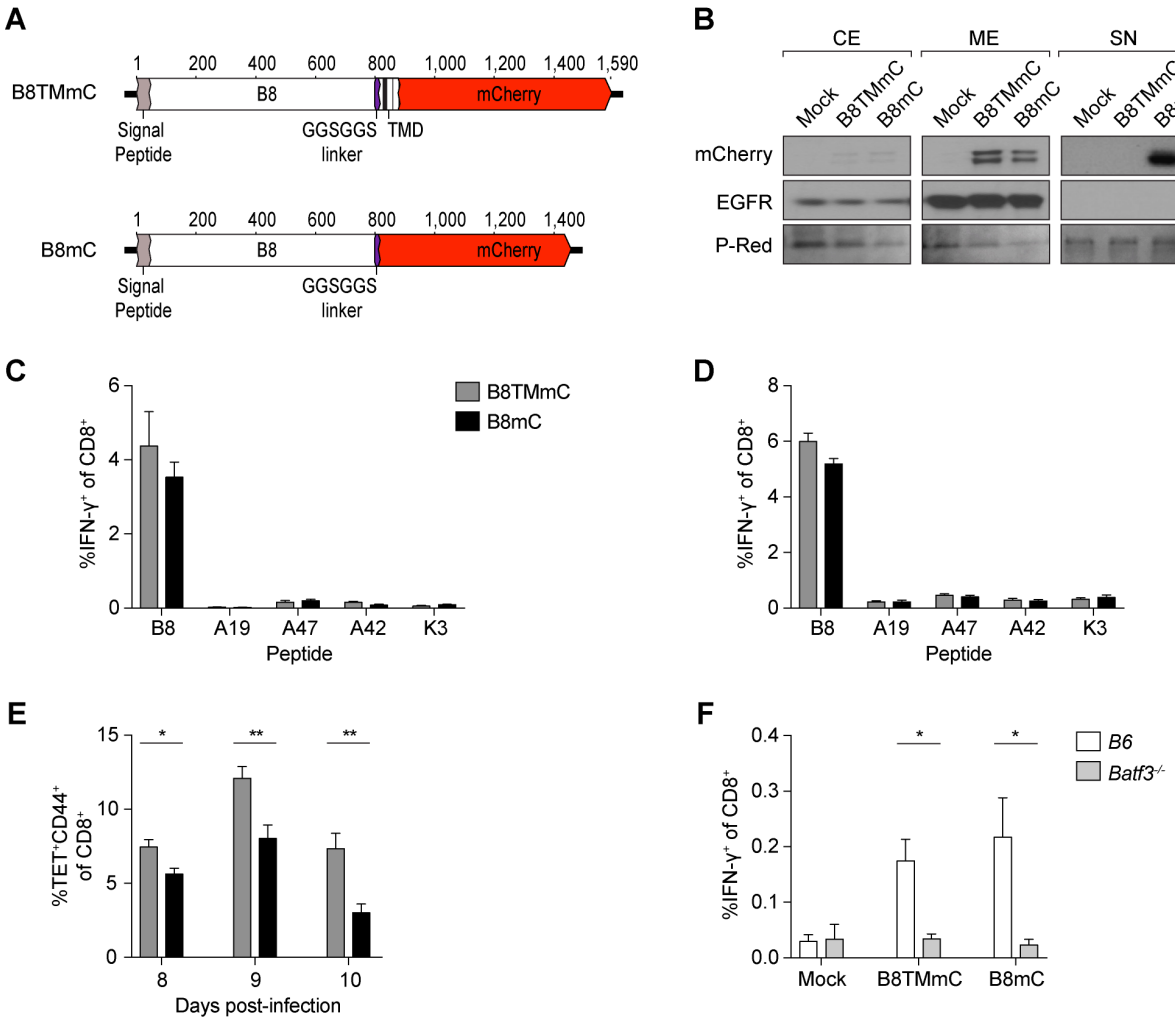

Fig 2.1 Secretion of the immunodominant antigen is not required for immunodominance

(A) Schematic representation of the B8-mCherry fusion proteins; the location of the signal peptide, GGSGGS linker, TMD, and mCherry are depicted. (B) B8TMmC is not secreted. HeLa cells were infected at an MOI of 5 with B8TMmC or B8MC. Cells and supernatant were harvested at 4 hpi for subcellular fractionation and mCherry and EGFR expression was determined by western blot; equal loading and transfer of samples was confirmed with ponceau S

red (P-Red) staining. CE = cytoplasmic extract; ME = membrane extract; SN = supernatant. Data are representative of two independent experiments. (C, D) Comparable CTL priming by B8TMmC and B8mC. $CD8^+$ T cell responses in the spleen of B6 (n = 5) i.n. infected with 5 x 10^3 pfu (C) and 1.5 x 10^4 pfu (D) B8TMmC or B8mC were determined by *ex vivo* restimulation with CPXV peptides and ICS at 8 dpi. Data are representative of two independent experiments. (E) Cell-associated antigen is cross-presented more efficiently than soluble antigen. B8-specific $CD8^+$ T cell responses in the spleen of B6 (n = 5) i.n. infected with 1.5 x 10^5 pfu B8TMmC or B8mC were determined by tetramer staining at 8, 9, and 10 dpi. Data are representative of two independent experiments. (F) $CD8^+$ T cell responses require $BATF3^+$ DCs. B6 and *Batf3*$^{-/-}$ mice (n = 7-10) were i.n. infected with 5 x 10^3 pfu B8TMmC or B8mC and the B8-specific $CD8^+$ T cell responses in the spleen were determined at 6 dpi. n = 3 mock-infected mice. Data are the combined results of three independent experiments.

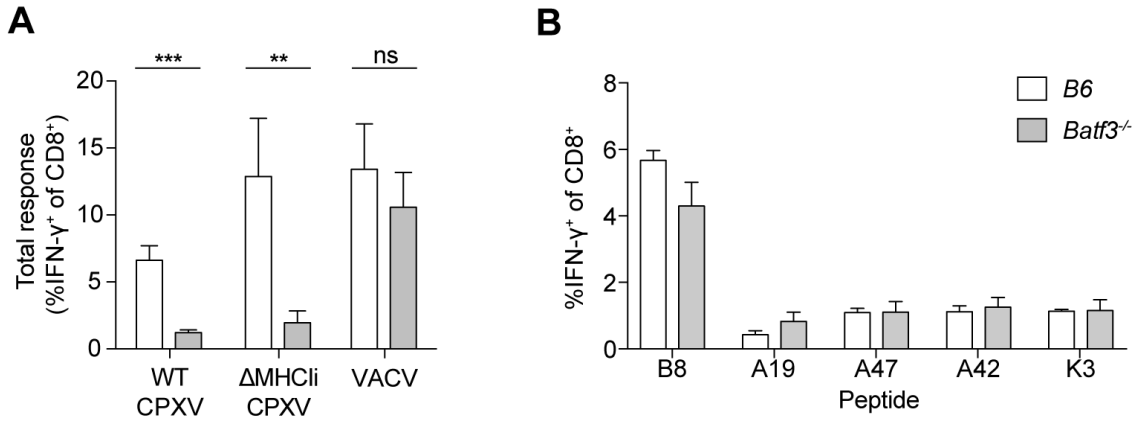

Fig 2.2 Cross-priming induces CTL responses during CPXV infection. (A) BATF3^{+} DCs cross-prime CPXV-specific CTL precursors. B6 or *Batf3*$^{-/-}$ mice (n = 6) were infected i.p. with 1 x 10^5 pfu WT CPXV, ΔMHCIi, or VACV-WR, and CD8^{+} T cell responses were measured by *ex vivo* restimulation with infected DC2.4 cells and ICS at 8 dpi. The data are the combined results of three independent experiments. (B) Induction of VACV-specific CTLs is not dependent BATF3^{+} DCs. B6 or *Batf3*$^{-/-}$ mice (n = 6-7) were infected i.p. with 1 x 10^5 pfu VACV-WR and CD8^{+} T cell responses in the spleen were measured at 6 dpi. The data are the combined results of two independent experiments.

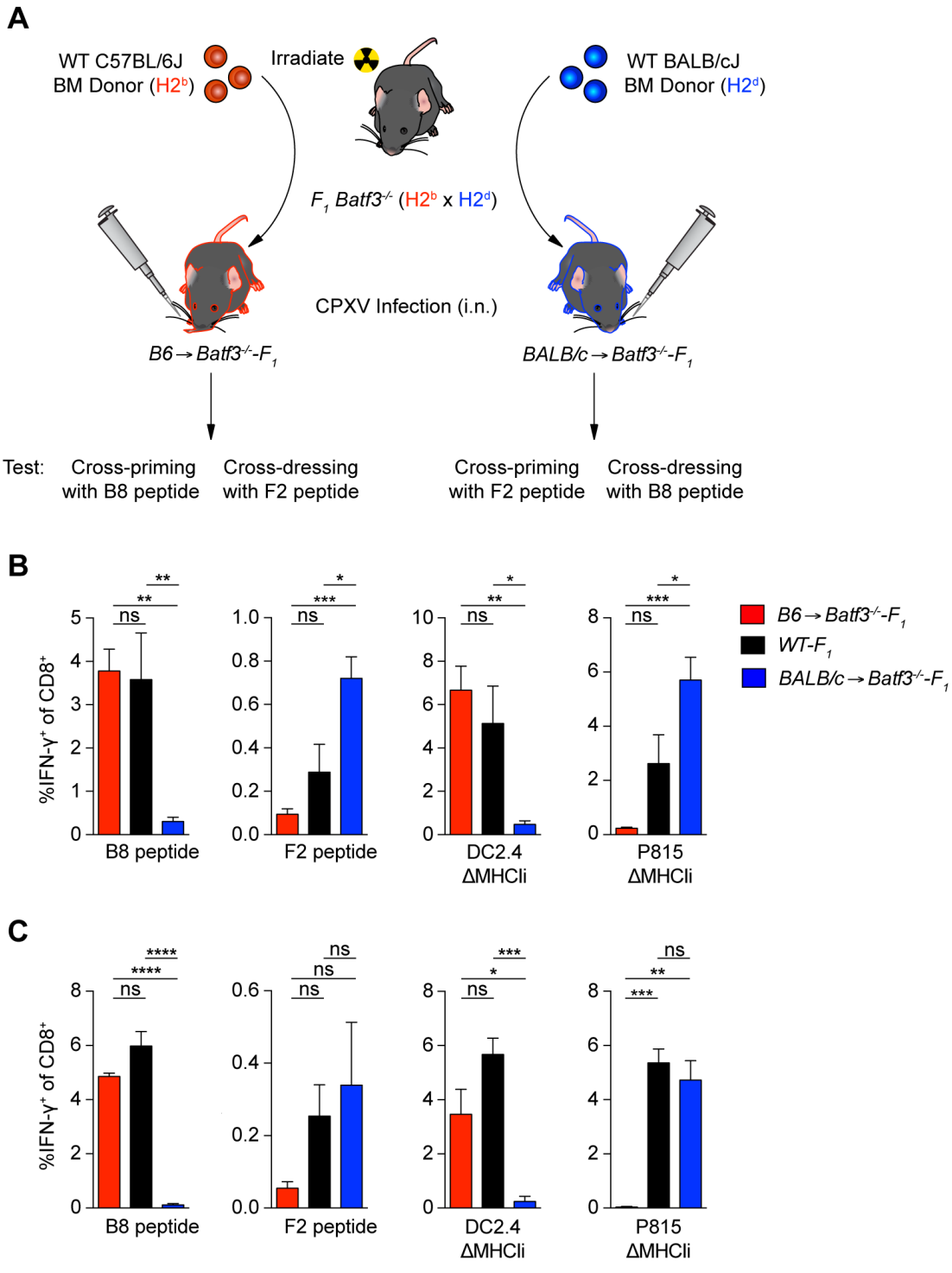
A
WT C57BL/6J
BM Donor (H2b)
Irradiate
WT BALB/cJ
BM Donor (H2d)
F1 Batf3-/- (H2b x H2d)
CPXV Infection (i.n.)
B6→Batf3-/-F1
BALB/c→Batf3-/-F1
Test:
Cross-priming with B8 peptide
Cross-dressing with F2 peptide
Cross-priming with F2 peptide
Cross-dressing with B8 peptide
B
%IFN-γ+ of CD8+
B8 peptide
F2 peptide
DC2.4 ΔMHCIi
P815 ΔMHCIi
B6→Batf3-/-F1
WT-F1
BALB/c→Batf3-/-F1
C
%IFN-γ+ of CD8+
B8 peptide
F2 peptide
DC2.4 ΔMHCIi
P815 ΔMHCIi

Fig 2.3 Conventional cross-priming, but not cross-dressing, is the main mechanism driving CTL responses during CPXV infection. (A) Schematic of BMC cross-dressing experiment. B) CTLs are not activated by cross-dressed APCs. *Batf3*$^{-/-}$-F_1 mice (n = 5-6) were depleted of NK cells, lethally irradiated 2 days after NK cell depletion, and reconstituted with 1 x 10^7 T cell depleted BM cells from B6 or BALB/c mice. 8 weeks later, chimeric mice were infected i.n. with 5 x 10^3 pfu WT CPXV and $CD8^+$ T cell responses in the lungs were determined by ICS at 8 dpi. (C) Memory CTLs are not activated by cross-dressed APCs. Chimeric mice (n = 3-5) previously infected for 25 days were challenged with 5 x 10^4 pfu WT CPXV and $CD8^+$ T cell responses in the lungs were determined by ICS at 8 days after challenge. The data are the combined results of three independent experiments.

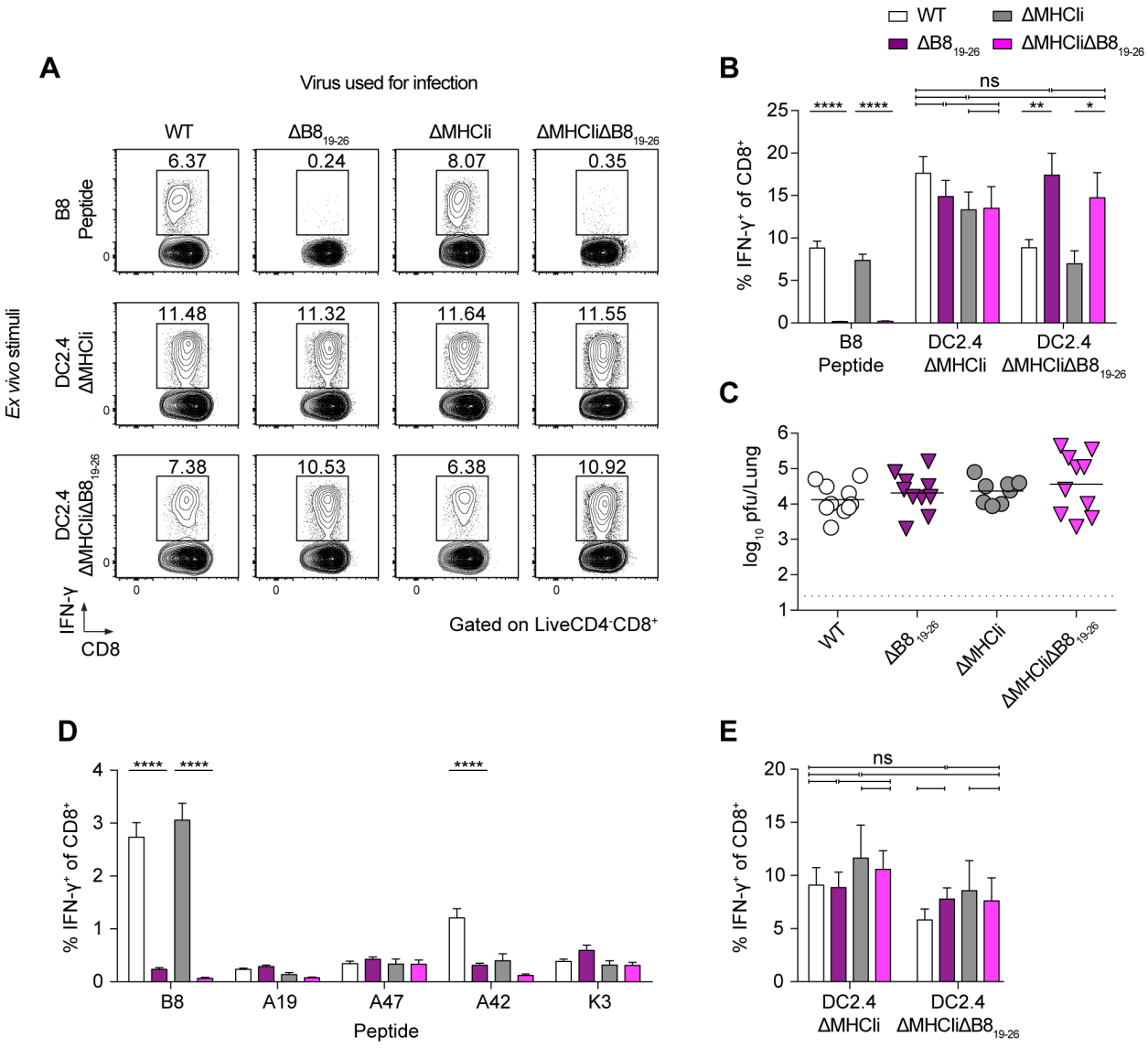

Fig 2.4 Cryptic subdominant epitopes can compensate for the loss of the CPXV immunodominant epitope-specific CTL response, revealing immunodomination. CTL immunodomination occurs during primary responses against CPXV. (A and B) B6 mice (n = 11-13) were infected i.n with 5 x 10^3 pfu of WT, $\Delta B8_{19\text{-}26}$, ΔMHCIi, or $\Delta MHCIi\Delta B8_{19\text{-}26}$ and were sacrificed at 8dpi. $CD8^+$ T cells in the lungs were restimulated with $B8_{19\text{-}26}$ peptide or DC2.4 cells infected with ΔMHCIi or $\Delta MHCIi\Delta B8_{19\text{-}26}$. The legend to B indicates the viruses used for infections and the X-axis indicates the stimuli used for *ex vivo* restimulation and ICS. Data are

the combined results of five independent experiments. (C) WT and mutant viral strains replicate to similar titers. Viral titers in the lungs of infected B6 mice were determined at 8 dpi by plaque assay. (D) Comparable CTL responses against all viral strains tested. B6 mice (n = 6) were infected by i.p. and splenic $CD8^+$ T cells were restimulated with peptides or (E) with DC2.4 cells infected with ΔMHCIi or ΔMHCIiΔ$B8_{19\text{-}26}$. Data are the combined results of four independent experiments.

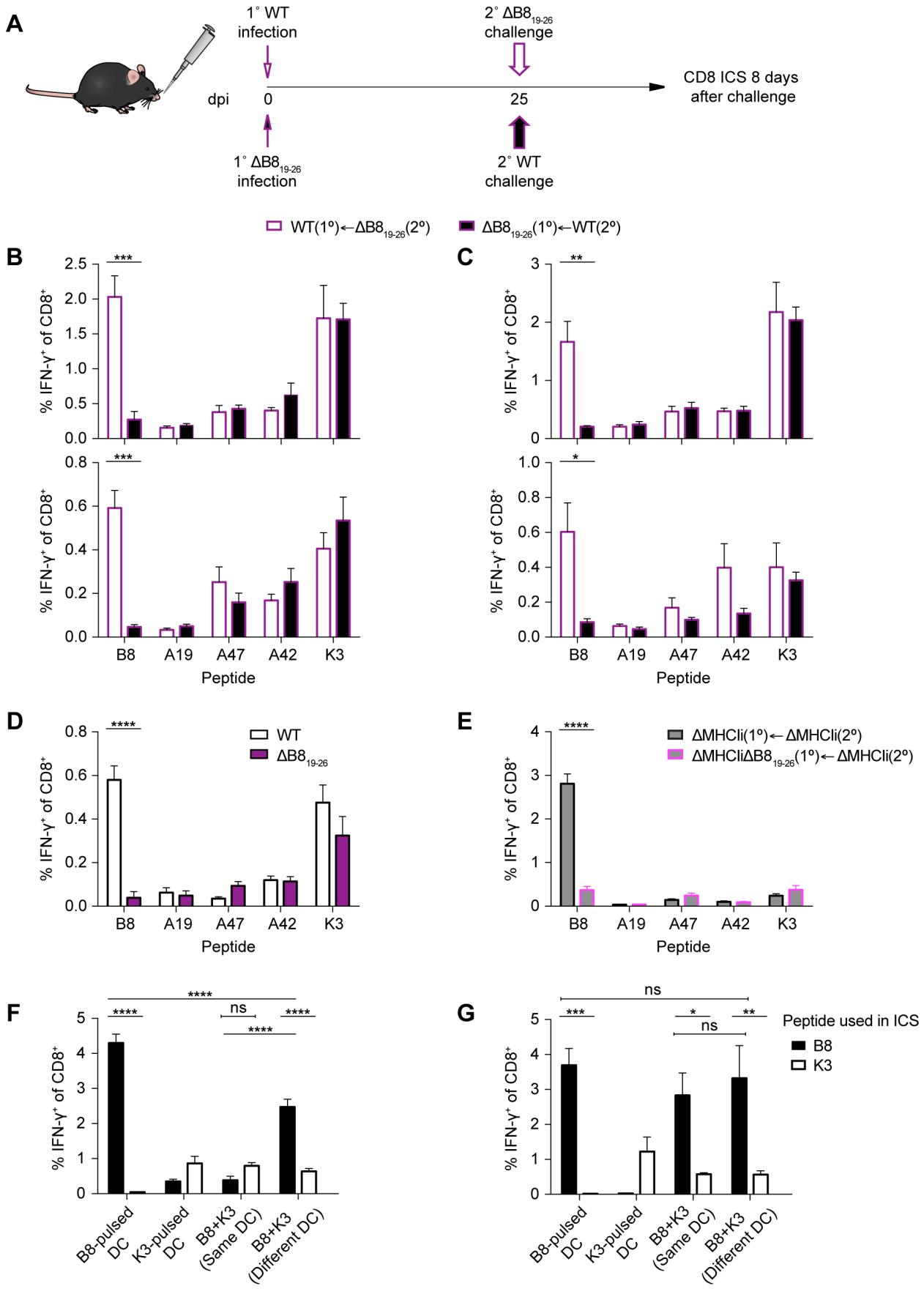
A
1° WT infection
2° ΔB8 19-26 challenge
dpi
0
25
CD8 ICS 8 days after challenge
1° ΔB8 19-26 infection
2° WT challenge
WT(1°)←ΔB8 19-26(2°)
ΔB8 19-26(1°)←WT(2°)
B
C
% IFN-γ+ of CD8+
B8
A19
A47
A42
K3
Peptide
D
WT
ΔB8 19-26
E
ΔMHCIi(1°)←ΔMHCIi(2°)
ΔMHCIiΔB8 19-26(1°)←ΔMHCIi(2°)
F
G
ns
Peptide used in ICS
B8
K3
B8-pulsed DC
K3-pulsed DC
B8+K3 (Same DC)
B8+K3 (Different DC)

Fig 2.5 CPXV subdominant epitope-specific memory CTLs immunodominate responses by naïve CD8$^+$ T cells. (A) Schematic of i.n. prime/boost experiment. (B and C) Immunodomination of naïve CD8$^+$ T cells. B6 mice (n = 5-6) were primed i.n. with 5 x 10^3 pfu, i.n. boosted at 25 dpi with 5 x 10^3 pfu (B) or 5 x 10^4 pfu (C), and sacrificed 8 days after boosting. CD8$^+$ T cell responses in the lungs (top) and spleens (bottom) were determined by ICS. Data are the combined results from two independent experiments. (D) Generation of memory CD8$^+$ T cells. i.n. primed mice were sacrificed at 25 dpi and memory CD8$^+$ T cells were measured in the spleen by ICS. (E) Antibody-independent memory CTL immunodomination. μmT mice were primed by s.s. with 1 x 10^5 and i.n. boosted with 1 x 10^5 pfu at 25 dpi. CD8$^+$ T cell responses in the spleens were determined 7 days after boost. Data are the combined results from two independent experiments. (F) Memory CTLs cross-compete for peptide-MHCI complexes on APCs. Peptide-pulsed DCs were adoptively transferred by tail vein injection into $\Delta B8_{19\text{-}26}$-primed B6 mice (n = 4) and CD8$^+$ T cell responses in the spleen were evaluated by ICS 6 days after transfer. (G) Naïve CD8$^+$ T cells do not cross-compete for peptide-MHCI complexes on APCs. Peptide-pulsed BMDCs were transferred into naïve B6 mice and CD8$^+$ T cell responses were evaluated by ICS as in the experimental setup of F. Data are representative of two independent experiments.

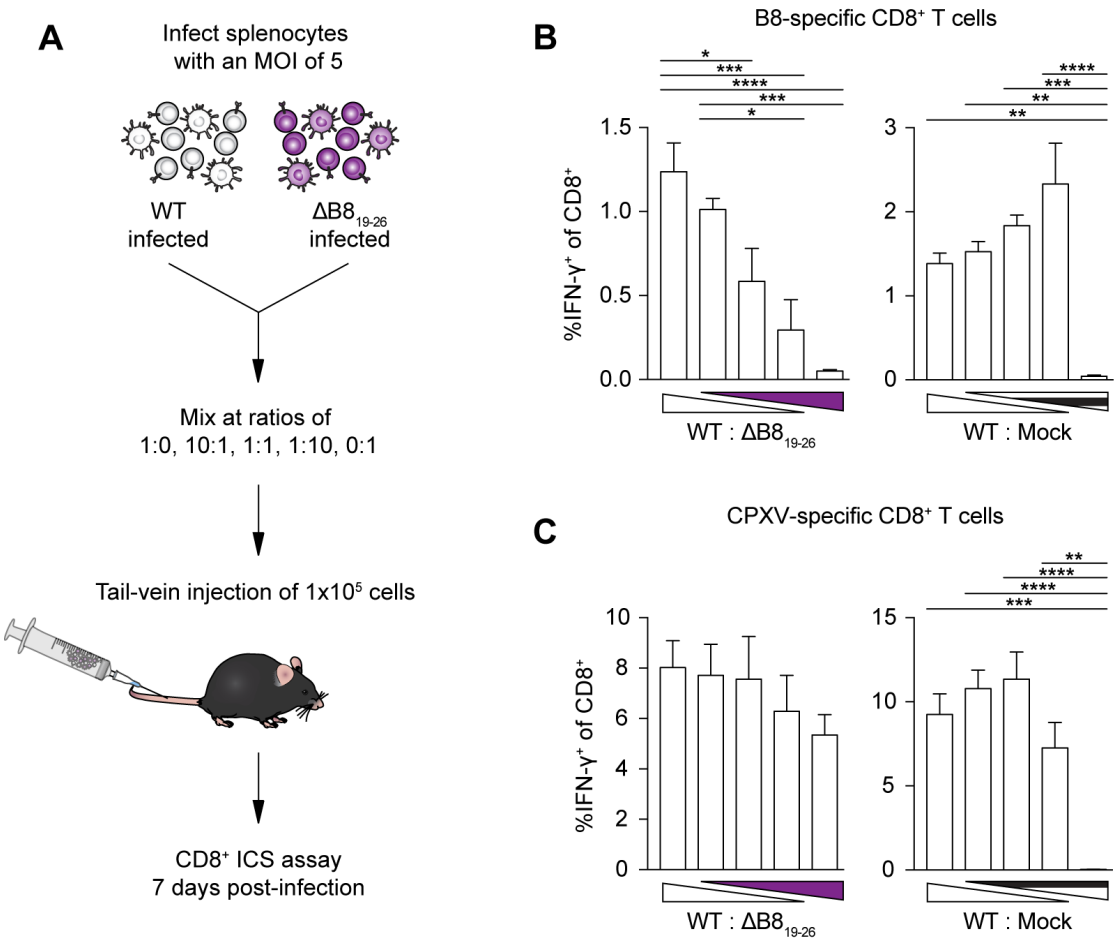

Fig 2.6 CPXV subdominant epitopes gain dominance when the relative abundance of subdominant antigens is increased during primary responses. (A) Schematic of co-infection experiment. Splenocytes were harvested from B6 mice and infected at an MOI of 5 with WT CPXV and $\Delta B8_{19\text{-}26}$ separately or mock-infected. At 1 hpi, infected cells were mixed at different ratios and a total of 1 x 10^5 infected cells were administered into naïve B6 mice (n = 5-6) by tail vein injection. (B) A role for antigen levels in CTL immunodomination. Mice were sacrificed at 7 dpi and splenic $CD8^+$ T cells were restimulated with B8 peptide or (C) with DC2.4 cells infected with ΔMHCIi. Data are the combined results from two independent experiments.

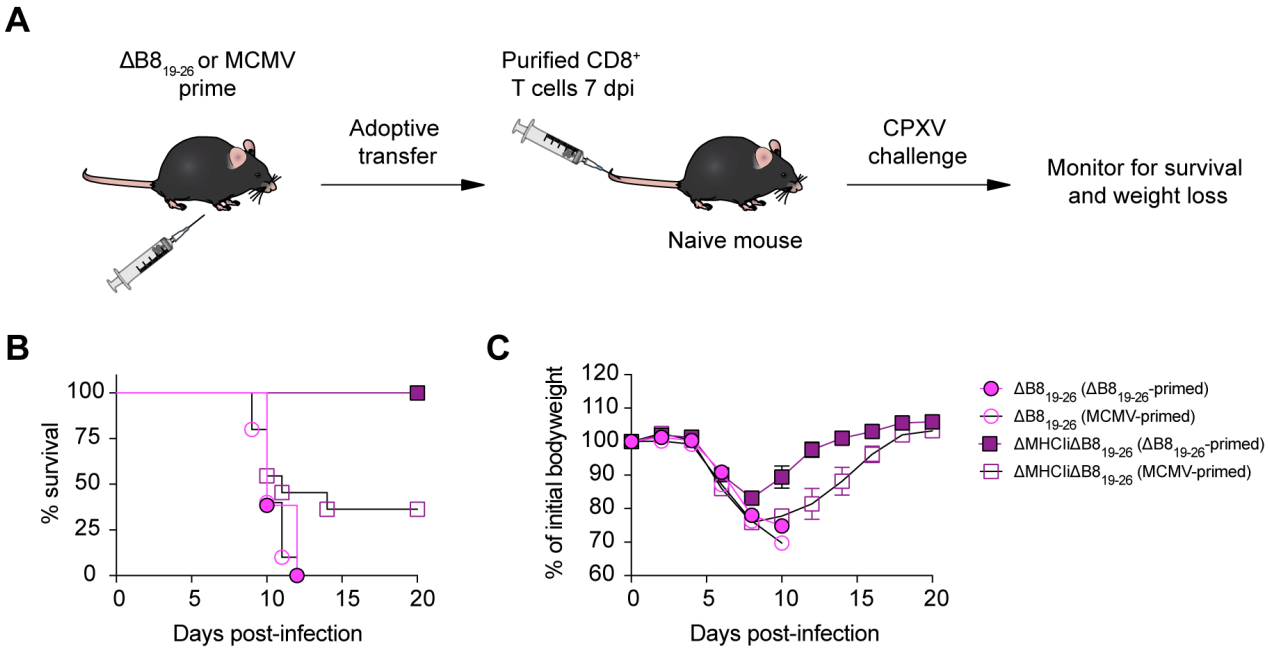

Fig 2.7 Subdominant epitope-specific CTL responses protect against CPXV infection. (A) Schematic of adoptive transfer experiment. B6 mice were primed with $\Delta B8_{19\text{-}26}$ or MCMV by s.c. and i.p. routes, respectively. At 7 dpi, splenic $CD8^+$ T cells were isolated by positive selection and adoptively transferred into naive B6 mice (n = 11-13) by tail vein injection. After ~1 day, mice were infected by i.n. inoculation with $\Delta B8_{19\text{-}26}$ or $\Delta MHCIi\Delta B8_{19\text{-}26}$ and monitored for survival (B) and weight loss (C). Data are the combined results from two independent experiments.

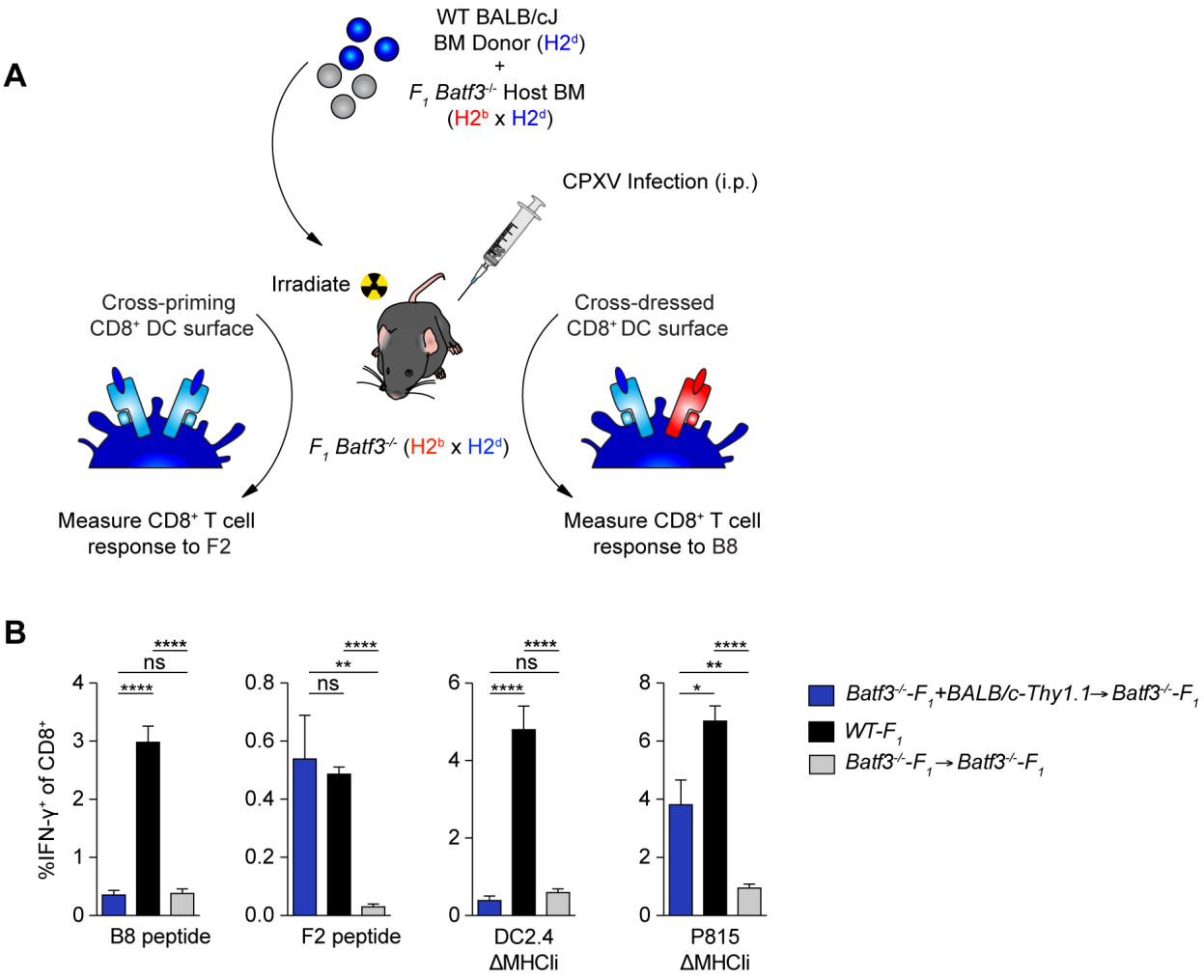

S2.1 Fig. Cross-dressing by hematopoietic cells does not induce CTL responses during CPXV infection. (A) Schematic of BMC cross-dressing experiment.

(B) Hematopoietic cells do not contribute to CTL-priming *via* cross-dressing of APCs. Lethally irradiated *Batf3*$^{-/-}$ -F_1 mice (n = 8) reconstituted with a 1:1 mixture of BALB/c-Thy1.1 and *Batf3*$^{-/-}$-*F_1* bone BM cells were infected i.p. with 1 x 10^5 pfu WT CPXV and assessed as in the experimental setup in Fig 3. n = 4 WT-F_1 CPXV-infected mice. The data are the combined results of three independent experiments.

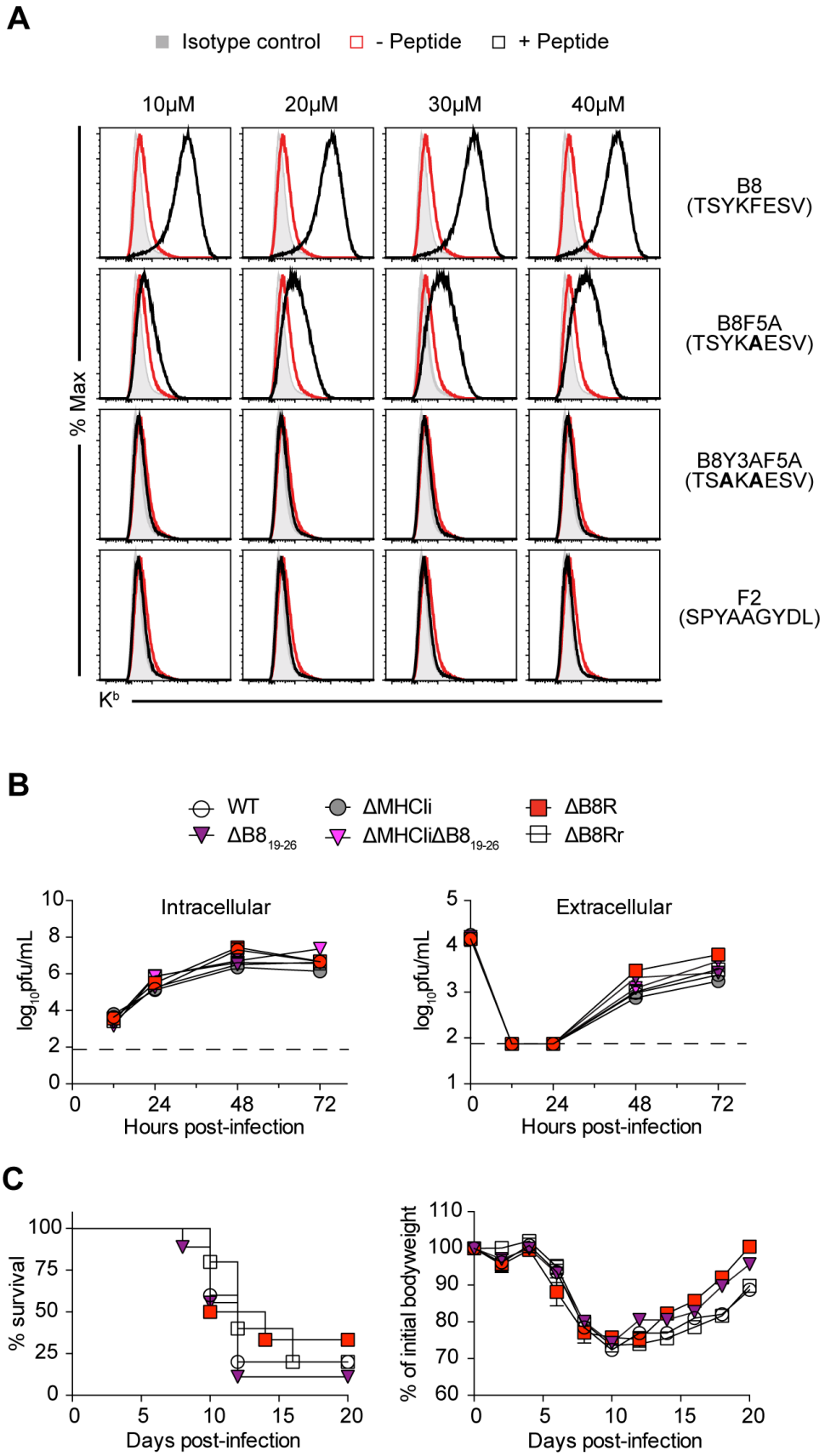
A
Isotype control
- Peptide
+ Peptide
10μM
20μM
30μM
40μM
B8
(TSYKFESV)
B8F5A
(TSYKAESV)
B8Y3AF5A
(TSAKAESV)
F2
(SPYAAGYDL)
% Max
Kb
B
WT
ΔMHCIi
ΔB8R
ΔB8 19-26
ΔMHCIiΔB8 19-26
ΔB8Rr
Intracellular
Extracellular
log10pfu/mL
Hours post-infection
C
% survival
Days post-infection
% of initial bodyweight

S2.2 Fig. Mutating the CPXV immunodominant CD8$^+$ T cell epitope anchor residues alters peptide binding affinity to MHCI H-2K^b, but does not affect CPXV replication and virulence. Peptide binding assays were performed using RMA-S cells. (A) Peptide anchor residues are critical for H-2K^b binding. Cell surface staining of H-2K^b after incubation with peptide (black) or without peptide (red) are shown; isotype control staining is shown in grey. Data are representative of three independent experiments. (B) B8 mutations do not affect viral kinetics *in vitro*. Vero cells were infected at an MOI of 0.01 for multi-step growth curves. Data are the combined results of three independent experiments performed in duplicates. (C) B8 mutations do not affect viral pathogenesis *in vivo*. B6 mice (n = 5-9) were infected i.n. with 4 x 10^4 pfu of the indicated viruses and monitored for survival and weight loss.

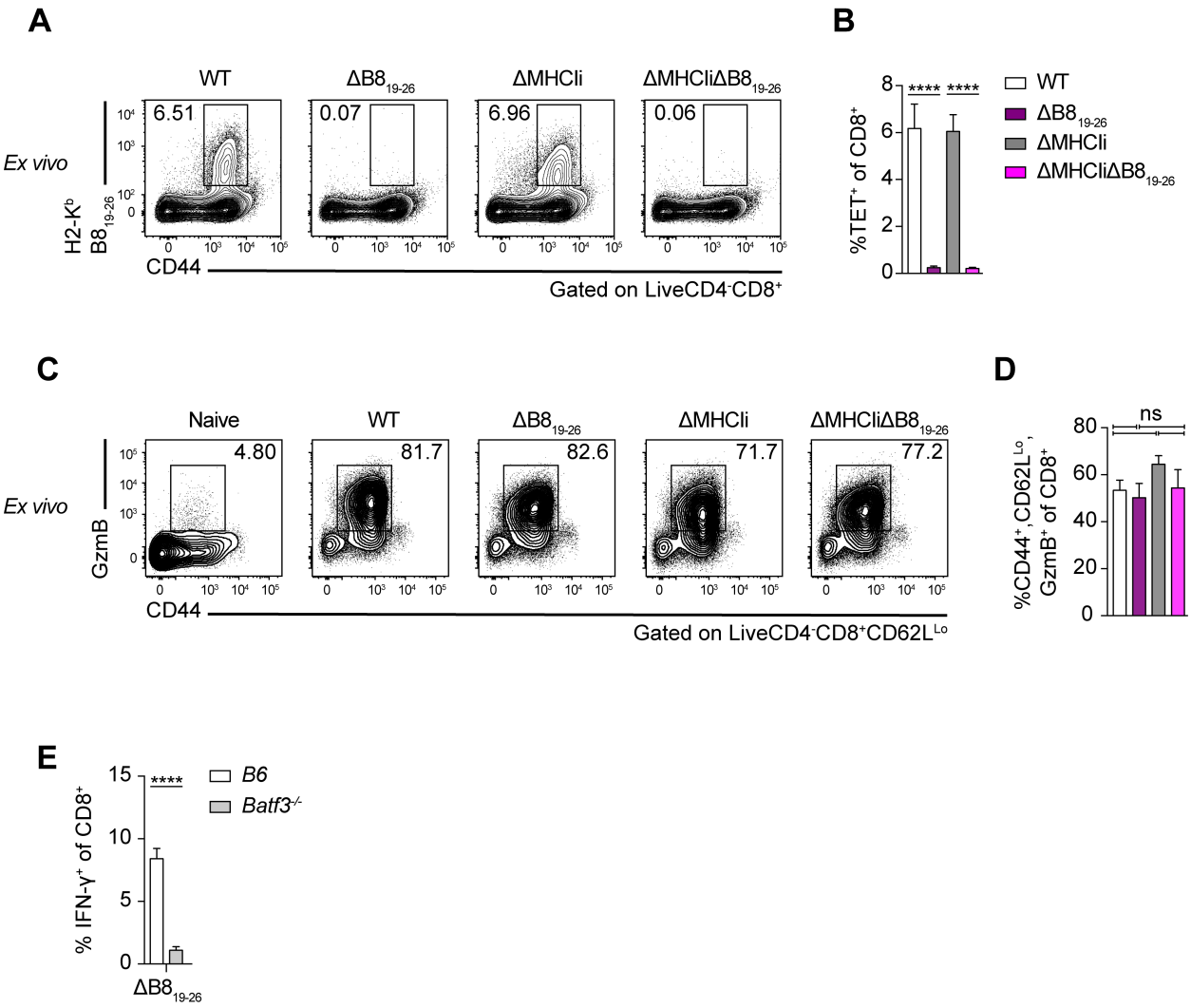

S2.3 Fig. Cross-priming of cryptic subdominant epitopes can compensate for the loss of the CPXV immunodominant epitope-specific CTL response.

Peptide anchor residues are critical for inducing B8-specific CTL responses. (A and B) B6 mice (n = 10) were infected i.n with 5 x 10^3 pfu WT, $\Delta B8_{19\text{-}26}$, ΔMHCIi, or ΔMHCIi$\Delta B8_{19\text{-}26}$ and were sacrificed at 8dpi. The B8-specific CTL response was evaluated by tetramer staining. Data are the combined results from two independent experiments. (C and D) Comparable CTL responses against all viral strains. B6 mice (n = 5) were infected and sacrificed at 8 dpi as in experimental setup of A and B. Cell surface expression of CD62L, CD44 and intracellular GzmB was

determined for $CD8^+$ T cells in the lungs. Data are representative of three independent experiments. (E) $BATF3^+$ DCs cross-prime SDE-specific CTL precursors. B6 or *Batf3*$^{-/-}$ mice (n = 7) were infected i.p. with 1 x 10^5 pfu $\Delta B8_{19\text{-}26}$ and $CD8^+$ T cell responses were measured by *ex vivo* restimulation with ΔMHCIi$\Delta B8_{19\text{-}26}$-infected DC2.4 cells and ICS at 8 dpi. Data are the combined results from two independent experiments.

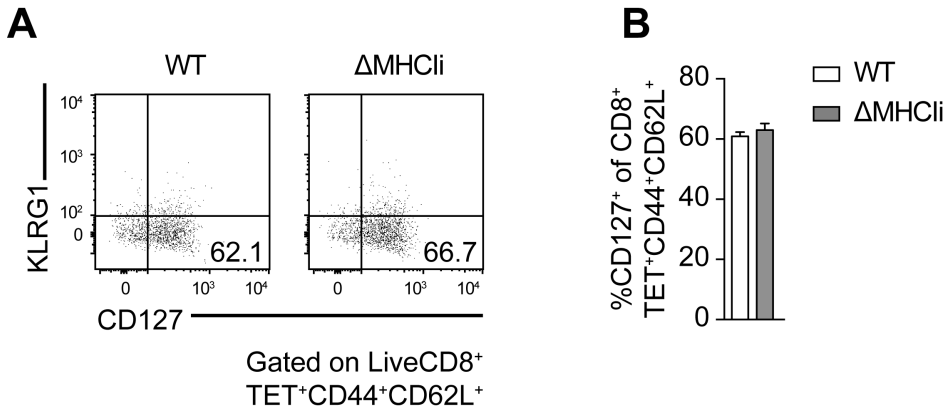

S2.4 Fig. Viral MHCI inhibition does not affect the generation of memory CD8$^+$ T cells

(A and B) Generation of memory CD8$^+$ T cells following CPXV infection. B6 mice (n = 7) were primed i.n. with 5 x 10^3 pfu WT or ΔMHCIi and were sacrificed at 25 dpi. Cell surface expression of memory T cell markers (CD62L, CD44, KLRG1, and CD127) was determined for TET$^+$ CD8 T cells in the spleen. Data are the combined results from two independent experiments.

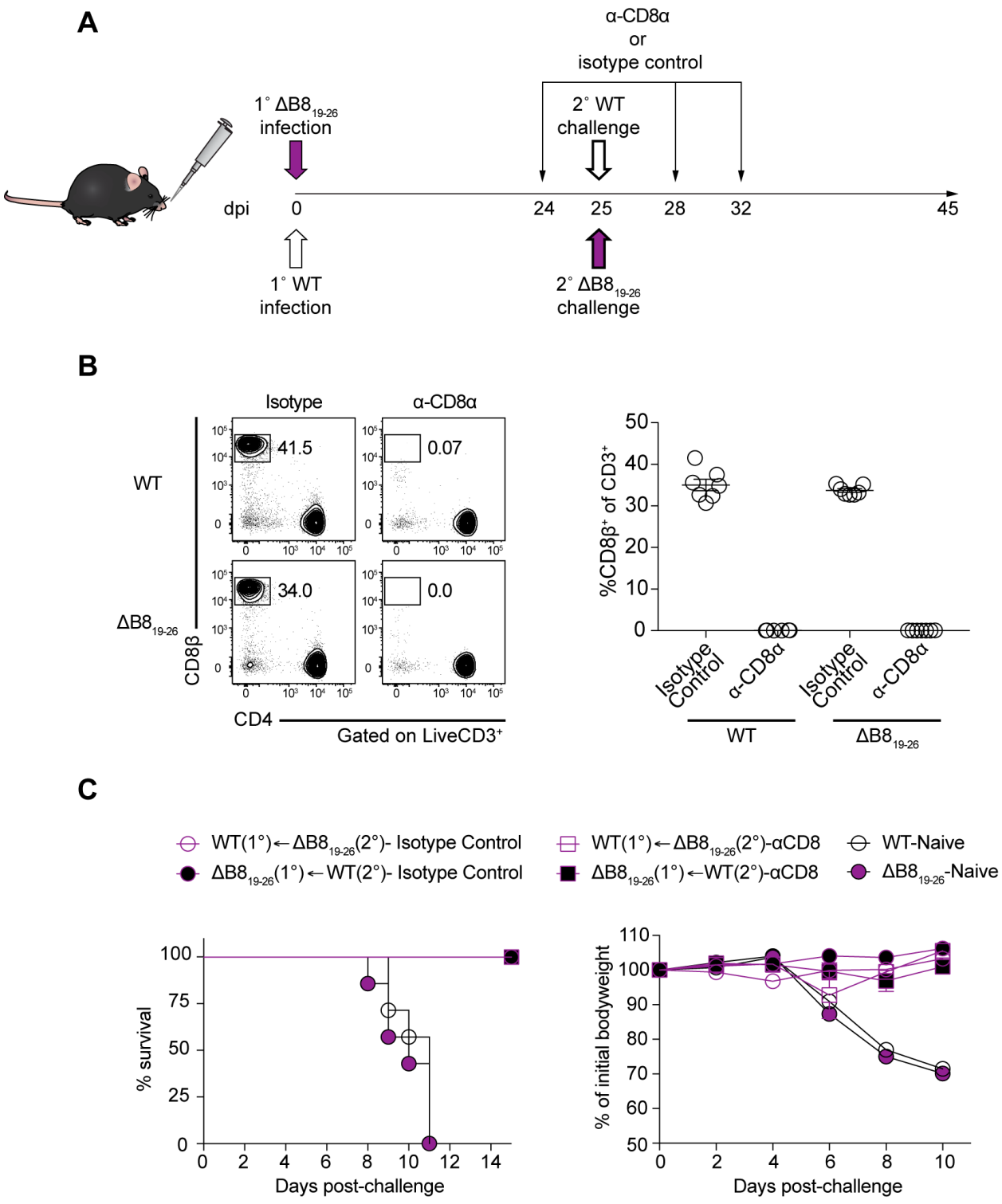
A
α-CD8α
or
isotype control
1˚ ΔB8 19-26
infection
2˚ WT
challenge
dpi
0
24
25
28
32
45
1˚ WT
infection
2˚ ΔB8 19-26
challenge
B
Isotype
α-CD8α
WT
ΔB8 19-26
41.5
0.07
34.0
0.0
CD8β
CD4
Gated on LiveCD3+
%CD8β+ of CD3+
Isotype Control
α-CD8α
WT
ΔB8 19-26
C
WT(1°)←ΔB8 19-26(2°)- Isotype Control
ΔB8 19-26(1°)←WT(2°)- Isotype Control
WT(1°)←ΔB8 19-26(2°)-αCD8
ΔB8 19-26(1°)←WT(2°)-αCD8
WT-Naive
ΔB8 19-26-Naive
% survival
Days post-challenge
% of initial bodyweight
Days post-challenge

S2.5 Fig. CPXV-immunized mice survive lethal challenge in the absence of memory $CD8^+$ T cells

(A) Schematic of immunization and challenge experiment. B6 mice (n= 6-7) were primed i.n. with 5 x 10^3 pfu of CPXV and lethally challenged at 25 dpi. Anti-CD8α or isotype control antibodies were administered at the indicated times. (B) Complete depletion of $CD8^+$ T cells. The efficiency of antibody-mediated CD8 depletion was determined one day after the first administration of antibodies. (C) CPXV immunized mice generate protective antibody responses. Challenged mice were monitored for survival and weight loss.

Primer Name	Primer Sequence
CPXV202	
I-SceI-KAN_202_fwd	ATATTATCACTTCAACGACAATAGTCAAATAACAGCCAACTTTTTATCAATAATACAAAATAGGGATAACAGGGTAATCGATTT
I-SceI-KAN_202_rev	TAGACGGTTTTATTTCATTTTTTTGTATTATTGATAAAAAGTTGGCTGTTATTTGACTATGCCAGTGTTACAACCAATTAACC
B8RY3AF5A	
B8RY3AF5A_I-SceI-KAN_fwd	AATAATAGCATAAATGCTACAATAACTAGTGCTAAGGCTGAATCCGTCAATTTTGATTCCTAGGGATAACAGGGTAATCGATTT
B8RY3AF5A_I-SceI-KAN_rev	TCTCCAGTCCATTCAATTTTGGAATCAAAATTGACGGATTCAGCCTTAGCACTAGTTATTGCCAGTGTTACAACCAATTAACC
CPXV203	
I-SceI-KAN_203_fwd	ACGCTGGTTACCGCTATTAGCTCTAACCATTTTCAGGATGCATGTTAAAACAGAATTGTATAGGGATAACAGGGTAATCGATTT
I-SceI-KAN_203_rev	TTCCTGATTGATTAGCCA ATTACA ATTCTGTTTTAACATGCATCCTGAAAATGGTTAGAGGCCAGTGTTACAACCAATTAACC
CPXV012	
I-SceI-KAN_012_fwd	TAATACATGCTAAAGGGCCCGTATATTTTTACAATATTCACATGATAAACATGATTATATTAGGGATAACAGGGTAATCGATTT
I-SceI-KAN_012_rev	AACTAATTAGCGATGATATAATATAATCATGTTTATCATGTGAATATTGTAAAAATATACGCCAGTGTTACAACCAATTAACC
B8-mC	
202-KAN-202-mC_fwd	AAT TTA AAA TAT ATT ATC ACT TCA ACG ACA ATA G
202-KAN-202-mC_rev	CAG CGT ATA ATA GAC GGT TTT ATT TC

S2.1 Table. Primer sequences.

Gene block	Sequence
B8mC_N-terminal	AATTTAAAATATATTATCACTTCAACGACAATAGTCAAATAACAGCCAACATGAGATCTGTAATTCTAACAGTTTTGCTAATTAATAGCATAA ATGCTACAATAACTAGTTATAAGTTTGAATCCGTCAATTTTGATTCCAAAATTGAATGGACTGGAGATGGTCTATACAATATATCCCTTAAA AATTATGGGATCAAGACGTGGCAGCATATGTATACAAATGTACCAGAAGGAACATACGACGTATCCGGATTTCCAAAGAATGATTTCGTA TCTTTCTGGGTTAAATTCGAACAAGGCGACTATAAAGTGGAAGAGTATTGTACAGGACTATGTGTCGAAGTAAAAATTGGACCACCGAC TGTAACATTGACTGAATACGAAGACCATATCAATTTGTACATCGAGCATCCGTATGCCACTAGAGGTAGCAAGAAGATTCCTATTTACAA ACGCAATGACATGTGTGATATCTACTTGTTGTATACTGCTAACTTCACATTCGGAGATTCTGAAGAACCAGTAACGTATGATATTGATGAC TACGATTGCACATCTACAGGTTGCAGCATAGACTTTGCCACAACAGAAAAAGTGTGTGTGACGGCACAGGGAGCCACAGAAGGGTTT CTAGAAAAAATTACTCCATGGAGTTCGGAAGTATGTCTGACACCTAAAAAGAATGTATATACATGCGCAATTAGATCCAAAGAAGATGTT CCCAATTTCAAGGACAAAATGGCCAGAGTTATCAAGAGAAAATTTAATAAACAGTCTCAATCTTATTTGACTAAATTTCTCGATAGCACAT CGAATGACGTCATGACCGTGCTTAGCATGCTTGACGGTGGTTCTGGTGGTTCTTAGGGATAACAGGGTAATCG
B8TMmC_TMD_C-terminal	TGGGTGTCCTTGGAGCTATGGCCATCATTGGAGCTGTGGTGGCTTTTGTGGTTTCAAAAGGTGAAGAAGATAATATGGCTATTATTAAA GAATTTATGAGATTTAAAGTTCATATGGAAGGTTCAGTTAATGGTCATGAATTTGAAATTGAAGGTGAAGGTGAAGGTAGACCATATGAA GGTACTCAAACTGCTAAATTGAAAGTTACTAAAGGTGGTCCATTACCATTTGCTTGGGATATTTTGTCACCACAATTTATGTATGGTTCAA AAGCTTATGTTAAACATCCAGCTGATATTCCAGATTATTTAAAATTGTCATTTCCAGAAGGTTTTAAATGGGAAAGAGTTATGAATTTTGAA GATGGTGGTGTTGTTACTGTTACTCAAGATTCATCATTACAAGATGGTGAATTTATTTATAAAGTTAAATTGAGAGGTACTAATTTTCCATC AGATGGTCCAGTTATGCAAAAAAAAACTATGGGTTGGGAAGCTTCATCAGAAAGAATGTATCCAGAAGATGGTGCTTTAAAAGGTGAAA TTAAACAAAGATTGAAATTAAAAGATGGTGGTCATTATGATGCTGAAGTTAAAACTACTTATAAAGCTAAAAAACCAGTTCAATTACCAGG TGCTTATAATGTTAATATTAAATTGGATATTACTTCACATAATGAAGATTATACTATTGTTGAACAATATGAAAGAGCTGAAGGTAGACATTC AACTGGTGGTATGGATGAATTATATAAATAA

S2.2 Table. Synthesized gene fragments.

Virus name	Clone ID	Mutation
ΔB8R	pBR-Δ202	Complete B8R (CPXV202) deletion
ΔB8Rr	pBR-Δ202rev	B8R revertant
$\Delta B8_{19\text{-}26}$	pBR-B8Y3AF5A	Alanine substitions in the $B8_{19\text{-}26}$ epitope amino acid sequence at position 3 (tyrosine) and position 5 (phenylalanine)
ΔMHCIi	pBR-Δ12Δ203	Complete deletion of CPXV012 and CPXV203
$\Delta MHCIi\Delta B8_{19\text{-}26}$	pBR-Δ12Δ203B8Y3AF5A	$B8_{19\text{-}26}$ epitope mutant (B8Y3AF5A) in the Δ12Δ203 background
B8TMmC	pBR-202mC	B8-mCherry fusion protein containing a transmembrane domain
B8mC	pBR-202mC_con	B8-mCherry fusion protein
VACV	VACV-WR	Vaccinia Virus strain Western Reserve
WT	pBR-CPXV-BR	Cowpox Virus strain Brighton Red

S2.3 Table. Viruses used in this study.

Chapter 3:

Viral MHCI inhibition evades tissue-resident memory $CD8^+$ T cell (T_{RM}) responses, but not local antigen-driven T_{RM} formation

This chapter has been submitted as a manuscript that is currently under review for publication at the *Journal of Experimental Medicine*.

Authors: Elvin J. Lauron[1], Liping Yang[1], Dorothy K. Sojka[1], Graham D. Williams[2], Ian B. Harvey[1], Michael D. Bern[1], Eugene Park[1], Francisco Victorino[4], Adrianus C. M. Boon[1,2,3], Wayne M. Yokoyama[1,3,4]

[1]Department of Medicine. Washington University School of Medicine, St. Louis, MO 63110, USA

[2]Department of Molecular Microbiology. Washington University School of Medicine, St. Louis, MO 63110, USA

[3]Department of Pathology and Immunology. Washington University School of Medicine, St. Louis, MO 63110, USA

[4]Division of Rheumatology. Washington University School of Medicine, St. Louis, MO 63110, USA

Abstract

Tissue-resident memory $CD8^+$ T cells (T_{RM}) confer rapid protection and immunity against viral infections. Many viruses have evolved mechanisms to inhibit MHCI presentation in order to evade cytotoxic $CD8^+$ T cells (CTLs), suggesting that these mechanisms may also apply to T_{RM}-mediated protection. However, the effects of viral MHCI inhibition on the function and generation of T_{RM} is unclear. We show that viral MHCI inhibition dampens immunodominance within the lung T_{RM} pool, indicating an effect on the T_{RM} repertoire, but this effect is not elicited in the skin. Unexpectedly, local cognate antigen enhances $CD8^+$ T_{RM} development even in the occurrence of viral MHCI inhibition and CTL evasion. However, local cognate antigen is not required for $CD8^+$ T_{RM} maintenance. We also show that viral MHCI inhibition efficiently evades $CD8^+$ T_{RM} effector functions. Our findings suggest that the T cell receptor (TCR) signaling threshold for CTL-mediated cytotoxicity and T_{RM} activation may be higher than the threshold for antigen-driven differentiation of CTLs to T_{RM}.

Introduction

Cytotoxic $CD8^+$ T cells (CTLs) mediate potent immunity against viral infections and respond to foreign antigens presented by major histocompatibility complex I (MHCI) molecules [59–61]. The importance of MHCI antigen presentation is underscored by the fact that viruses have evolved strategies to obstruct MHCI presentation. For instance MHCI inhibition by cowpox virus (CPXV) evades CTL responses during primary infections, and the absence of the endogenous MHCI inhibitors CPXV012 and CPXV203 significantly attenuates CPXV in a CTL-dependent manner [31,36,52]. Moreover, the ability to inhibit MHCI presentation appears to be an evolutionarily conserved feature among cytomegaloviruses (CMVs) and other viruses. Viral MHCI inhibition evades CTL responses against murine CMV (MCMV) infection in the salivary glands (SGs) of naïve hosts and is critical in allowing for rhesus CMV (RhCMV) superinfection of hosts harboring memory $CD8^+$ T cells [72,119]. However, tissue-resident memory $CD8^+$ T cells (T_{RM}) are able to protect against local infection when MCMV is directly introduced into the SGs, likely due to an early viral tropism for cells refractory to viral MHCI inhibition [120]. Therefore, the affects of viral MHCI inhibition on $CD8^+$ T_{RM} responses remain unclear.

$CD8^+$ T_{RM} typically form in non-lymphoid tissues following viral infection and are a non-circulating subset of memory T cells, whereas the effector memory T cell (T_{EM}) and central memory T cell (T_{CM}) subsets continuously recirculate [121]. Because $CD8^+$ T_{RM} primarily develop and remain at common sites of pathogen entry, they are considered a front-line defense against secondary or recurrent peripheral infections; both $CD8^+$ and $CD4^+$ T_{RM} promote viral control and survival against lethal infection, mediate cross-strain protection, and can even provide better protection than the circulating T_{RM} counterparts [122–127].

The factors driving T_{RM} development have implications for tissue-specific vaccine strategies. For example, the 'prime and pull' strategy demonstrates that CTLs can be recruited to the skin or vagina in an antigen-independent manner and drive T_{RM} formation, resulting in long-term immunity against local challenge [124,128]. Conversely, recruitment or inflammation alone does not generate T_{RM} in the lungs unless local cognate antigen is present [129,130], indicating tissue-specific requirements for local cognate antigen during T_{RM} differentiation. Depots of persisting viral antigens in the lung may also affect the maintenance of memory T cells [131,132]. However, it is unknown whether persistent antigen presentation occurs in the skin or if MHCI complexes are important for the maintenance of endogenous skin $CD8^+$ T_{RM}. In the context of viral infections, local cognate antigen recognition promotes the formation of $CD8^+$ T_{RM} in the skin, and is required for $CD8^+$ T_{RM} formation in the central nervous system, peripheral nervous system, and the lungs [124,133–136].

These findings on the potential role of local antigen during viral infection raise an interesting question: can viral MHCI inhibition affect local antigen recognition and reduce $CD8^+$ T_{RM} formation? To investigate this issue, here we compared $CD8^+$ T_{RM} formation and protection following local infection with CPXV, which effectively downregulates MHCI and evades CTLs *in vivo* [31,36,52,53], and a CPXV mutant lacking the capacity to inhibit MHCI presentation. Surprisingly, viral MHCI inhibition affected $CD4^+$ T_{RM} formation, but not $CD8^+$ T_{RM} formation, in the skin. We found that local secondary antigenic stimulation promoted $CD8^+$ T_{RM} formation, despite CPXV-mediated MHCI inhibition and CTL evasion. After T_{RM} differentiation, local cognate antigen presentation was dispensable for T_{RM} maintenance, but was critical by infected cells to induce protective $CD8^+$ T_{RM} responses.

Results

Viral MHCI inhibition affects the formation of $CD4^+$ T_{RM}, but not $CD8^+$ T_{RM}

CPXV mediates MHCI inhibition, which likely results in lower levels of local antigenic stimulation of virus-specific CTLs by infected cells. Because local antigenic stimulation enhances $CD8^+$ T_{RM} formation during vaccinia virus (VACV) skin infection [133], we hypothesized that $CD8^+$ T_{RM} formation would be diminished in CPXV-infected skin. To test this, we infected mice by skin scarification (s.s.) with WT or Δ12Δ203-CPXV and performed kinetic analyses of $CD8^+$ T cells that recognize the immunodominant H-$2K^b$-restricted epitope $B8_{19\text{-}26}$. Infection with both viruses resulted in robust expansion and recruitment of $B8_{19\text{-}26}$-specific $CD8^+$ T cells to the skin at 1 week post-infection, which reduced in numbers approximately ~12 fold by 3 weeks post-infection (Fig 3.1A). Nonetheless, $B8_{19\text{-}26}$-specific $CD8^+$ T cells were still detectable in the skin and the spleens of previously infected mice long after clearance of the infection (Fig 3.1, A to D); CPXV skin infections are highly localized and are cleared within 1-2 weeks post-infection [31]. Mice infected with WT CPXV had a higher relative abundance of $B8_{19\text{-}26}$-specific $CD8^+$ T cells in the skin at 7 days post-infection (dpi) in comparison to Δ12Δ203-infected mice (Fig 3.1, C and D), but there were no significant differences in absolute numbers in the skin for all assessed time points.

Analysis of $B8_{19\text{-}26}$-specific $CD8^+$ T cells during the memory phase showed that they were predominantly located in the previously infected skin flank relative to the uninfected contralateral flank (Fig 3.1B). These findings are consistent with previous reports [122,133,134]. We show that these cells expressed high levels of the T_{RM} markers CD103 and CD69 than the $B8_{19\text{-}26}$-specific $CD8^+$ T cells in the spleen (Fig 3.1, E and F), suggesting that CPXV s.s. infection

generates authentic $CD8^+$ T_{RM}. To verify tissue-residency of $CD103^+CD69^+CD8^+$ cells, we performed parabiosis between $CD45.1^+$ naïve mice and $CD45.2^+$ mice previously infected with CPXV, referred to as naïve and memory mice respectively (Fig 3.1G). Comparison of the $CD103^+CD69^+CD8^+$ T_{RM} in the skin of naïve and memory parabionts revealed the presence of these cells in only the memory parabionts, showing that they are unable to circulate and are indeed a resident population (Fig 3.1, H and I). Furthermore, $B8_{19\text{-}26}$-tetramer$^+$ cells in the spleens equilibrated between memory and naïve parabionts, but $B8_{19\text{-}26}$-tetramer$^+$ T_{RM} in the skin were only present in memory parabionts (Fig 3.1, J to K). Regarding $CD4^+$ T_{RM}, CPXV s.s. generated $CD103^+CD69^+CD4^+$ T cells in the skin in comparable numbers to $CD8^+$ T_{RM}, and parabiosis revealed that these cells were *bona fide* skin-resident $CD4^+$ T cells (Fig S3.1, A to C). Interestingly, we found that viral MHCI inhibition significantly reduced the abundance of these $CD103^+CD69^+CD4^+$ T cells in the skin (Fig S3.1, A and B). Taken together, these results reveal that viral MHCI inhibition does not affect the overall development of $CD8^+$ T_{RM}, but does impair the formation of $CD4^+$ T_{RM} in the skin.

$CD4^+$ T cell help is critical for the local development of lung $CD8^+$ T_{RM} [137], but is dispensable for the formation of $CD8^+$ T_{RM} in the female reproductive tract [138]. To test the role of $CD4^+$ T cell help in the development of $CD8^+$ T_{RM} in the skin, we depleted $CD4^+$ T cells by injecting depleting antibodies 1 day before infection, and 2 and 5 dpi. This approach eliminates $CD4^+$ T cells during acute infection, but allows for their recovery by 30 dpi. $CD4^+$ T cell help was not required for priming of $CD8^+$ T cells in the presence or absence of viral MHCI inhibition (Fig S3.1, D and E). In accordance with our previous findings [31,52], we found that mice infected with WT CPXV by s.s. succumbed to infection in the absence of $CD4^+$ T cell help (Fig S3.1F), despite the mounting an anti-CPXV $CD8^+$ T cell response (Fig S3.1, E and F). These results

underline the capacity of CPXV to efficiently evade $CD8^+$ T cells and suggest that $CD4^+$ T cell help is required to control localized CPXV infection. In contrast, all mice infected with Δ12Δ203 CPXV survived in the absence of $CD4^+$ T cell help (Fig S3.1F), which is also consistent with our previous findings that $CD8^+$ T cells alone are sufficient to control CPXV infection only in the absence of viral MHCI inhibition [31,52]. Given that Δ12Δ203 did not cause mortality, this provided a setting to assess the role of $CD4^+$ T cells in skin $CD8^+$ T_{RM} development. As expected, depleting $CD4^+$ T cells during the primary response reduced the overall number of $CD4^+$ T cells in the skin of mice previously infected with Δ12Δ203, but did not affect the overall development of $CD4^+$ T_{RM} cells since the percentage of $CD103^+CD4^+$ T cells in the skin was similar in isotype-control treated mice (Fig S3.1, G and H). However, it is possible that these cells are not tissue-resident and that they may represent a different subset of $CD4^+$ T cells. Surprisingly, the formation of $CD8^+$ T_{RM} cells was augmented in the absence of $CD4^+$ T cell help (Fig S3.1, G to I), indicating that $CD4^+$ T cell help is not required for the generation of skin $CD8^+$ T_{RM} and may even hinder their development.

Viral MHCI inhibition dampens immunodominance within the lung $CD8^+$ T_{RM} population

We next assessed the effects of CPXV-mediated MHCI inhibition on lung $CD8^+$ T_{RM} since the developmental requirements can differ substantially between certain tissue microenvironments [135]. In order to distinguish circulating memory $CD8^+$ T cells from T_{RM} we performed *in vivo* intravascular (IV) staining [139]. This method exclusively labels circulating and intravascular lymphocytes (IV^+ cells), but not tissue-associated lymphocytes (IV^-). Within the lung tissue, the overall proportions of IV^-CD8^+ T cells were equal in mice infected intranasally (i.n.) with WT CPXV or Δ12Δ203 at 12 and 30 dpi, suggesting that viral MHCI inhibition also

does not affect lung $CD8^+$ T_{RM} formation (Fig 3.2, A and B). However, higher proportions of IV^- $B8_{19\text{-}26}$-specific $CD8^+$ T cells were found in the lungs following Δ12Δ203 infection compared to WT CPXV infection (Fig 3.2C). This difference was also reflected in the spleen and blood at 30 dpi, despite equal proportions of $B8_{19\text{-}26}$-specific $CD8^+$ T cells in the spleen and blood at 12 dpi (Fig 3.2, D and E). Viral MHCI inhibition also significantly reduced the expression of CD103 on IV^- $B8_{19\text{-}26}$-specific $CD8^+$ T cells at 12 dpi, but not CD69 expression (Fig 3.2, F and G). The reduced expression of CD103 did not appear to affect $CD8^+$ T_{RM} development since IV^- $B8_{19\text{-}26}$-specific $CD8^+$ T cells in the lungs of WT CPXV- and Δ12Δ203-infected mice expressed comparable levels of CD69 and CD103 by 30 dpi (Fig 3.2, F and G). These data indicate that viral MHCI inhibition reduces the immunodominance of the $B8_{19\text{-}26}$-specific cells within the $CD8^+$ T_{RM} pool.

Local cognate antigen enhances $CD8^+$ T_{RM} cell formation, despite effective viral MHCI inhibition and CTL evasion

Thus far, our results suggest that $CD8^+$ T_{RM} development is independent of local antigen stimulation during CPXV infection. However, infection with WT CPXV is prolonged in comparison to Δ12Δ203 infection [31], and it is therefore possible that during WT CPXV infection continuous recruitment of CTLs may compensate for the decreased secondary antigenic stimulation on T_{RM} formation. To test if continuous recruitment of CTLs to the skin augments $CD8^+$ T_{RM} formation in the presence of viral MHCI inhibition, we utilized the sphingosine 1-phosphate receptor-1 (S1PR) agonist FTY720, which prevents lymphocyte egress from lymphoid tissues. FTY720 treatment early during infection (1, 3, and 5 dpi) significantly reduced the presence of circulating $CD8^+$ T cells in the blood and the recruitment of $CD8^+$ T cells to infected

skin, but not priming of $B8_{19\text{-}26}$-specific $CD8^+$ T cells in the inguinal lymph node (Fig S3.2, A to C). We next performed co-infections of mice with WT CPXV and Δ12Δ203 on opposite flanks, then blocked recruitment of CTLs starting at 7 days post-infection (dpi) with FTY720 treatment (Fig S3.2D). If continuous recruitment of CTLs compensates for reduced secondary antigenic stimulation, we expect that FTY720 treatment would reduce the abundance of $CD8^+$ T_{RM} in WT CPXV-infected skin relative to Δ12Δ203-infected skin. While FTY720 significantly reduced the presence of $CD4^+$ and $CD8^+$ T cells in the blood of co-infected mice, the relative abundance of $B8_{19\text{-}26}$-specific $CD8^+$ T cells at 9 dpi and $CD8^+$ T_{RM} cells at 40 dpi was not significantly different in the WT CPXV and Δ12Δ203 infected skin, with or without FTY720 treatment (Fig S3.2, E and F). These results indicate that $CD8^+$ T_{RM} develop without continuous recruitment of CTLs.

Since $CD8^+$ T_{RM} development occurred despite viral MHCI inhibition, we tested if $CD8^+$ T_{RM} formation is independent of local antigen by performing co-infections, on opposite flanks, with CPXV viruses that express either a WT (WT and Δ12Δ203-CPXV) or a variant of the immunodominant $B8_{19\text{-}26}$ epitope (B8Y3AF5A and Δ12Δ203B8Y3AF5A) that is not presented on MHCI [36] (Fig 3.3A). During the acute phase of infection, $B8_{19\text{-}26}$-specific $CD8^+$ T cells had modestly higher frequencies of CD69 expression in the skin where $B8_{19\text{-}26}$ was expressed in comparison to the skin where the $B8_{19\text{-}26}$ epitope was absent, whereas CD103 expression was unaffected (Fig S3.3, A and B). Nonetheless, a similar percentage and number of $B8_{19\text{-}26}$-specific $CD8^+$ T cells were recruited to both infected skin flanks in a local antigen-independent manner (Fig 3.3B). This was also the case when co-infections were performed with Δ12Δ203 and Δ12Δ203B8Y3AF5A. At 35 dpi, however, $B8_{19\text{-}26}$-specific $CD8^+$ T cells were significantly enriched in the skin where $B8_{19\text{-}26}$ was locally expressed as compared to infection where $B8_{19\text{-}26}$

was locally absent (Fig 3.3C), even in the presence of CPXV-mediated MHCI inhibition. Furthermore, the abundance of total $CD8^+$ T_{RM} was equal on both flanks of co-infected mice (Fig 3.3D), suggesting that T_{RM} formation was only affected for $B8_{19\text{-}26}$-specific $CD8^+$ T cells. Taken together, these data indicate that local antigen does promote $CD8^+$ T_{RM} formation during CPXV infection, regardless of viral MHCI inhibition.

Viral MHCI inhibition decreases CTL effector function, but not recognition of local cognate antigen

We previously demonstrated that CPXV-mediated MHCI inhibition prevents CPXV-specific CTLs from recognizing infected cells [31,36,53]. Consistent with our previous findings, CTLs from CPXV-infected mice did not produce IFN-γ when co-cultured with WT CPXV-infected DC2.4 cells (Fig 3.4A). This effect was dependent on CPXV012 and CPXV203 as CTLs co-cultured with Δ12Δ203-infected DC2.4 cells produced significantly higher levels of IFN-γ and upregulated expression of Nur77 (Fig 3.4A), a transcription factor that is specifically induced upon TCR engagement [140], as compared to WT CPXV-infected cells. However, our results suggest that CPXV-specific CTLs can receive antigenic stimulation at the site of infection *in vivo* (Fig 3.3).

To test if our *in vitro* findings extend to *in vivo* infection, we co-infected IFN-γ.Thy1.1 knockin reporter mice with WT and Δ12Δ203 CPXV on opposite flanks. Similar to our previous findings [31], CPXV s.s. resulted in significantly higher frequencies of IFN-γ-producing $CD8^+$ T cells in Δ12Δ203-infected skin in comparison to WT CPXV-infected skin (Fig 3.4B). Conversely, the frequency of $Nur77^+CD8^+$ T cells was not significantly different. We also found similar results following co-infection of Nur77 GFP reporter mice (Fig S3.3C). In accordance

with our findings that local cognate antigen promotes T_{RM} formation (Fig 3.3C), these findings suggest that CTLs recruited to CPXV-infected skin receive local cognate antigen stimulation, despite viral MHCI inhibition and efficient CTL evasion by CPXV.

To identify the cells that could display local cognate antigen, we assessed CPXV tropism in the skin of mice infected by CPXV s.s. There was significant recruitment of leukocytes in the skin at 6 dpi (Fig 3.4C). The majority of infected cells were MHCII/CD45 double positive and comprised of mainly $CD11b^+$ dendritic cells (DCs) and monocyte-derived DCs (moDCs) (Fig 3.4, D and E). Moreover, $CPXV^+$ and $MHCII^+$ cells were found in close proximity to $CD8^+$ cells (Fig 3.4F), suggesting that CTLs may likely engage infected $CD11b^+$ DCs or moDCs at the site of infection; though viral MHCI inhibition should prevent virus-specific T cell stimulation. Strikingly, $CD103^+$ DCs were largely uninfected (Fig 3.4E), but were also found in close proximity to $CD8^+$ cells at the site of infection (Fig 3.4F), suggesting CTLs in the skin may be engaging cross-presenting cells that are also involved in priming of naïve CPXV-specific CTL precursors [31,36]

$CD8^+$ T_{RM} in the skin persist in the absence of cognate antigen stimulation

Having established the importance of local cognate antigen in $CD8^+$ T_{RM} formation against CPXV, we questioned whether local cognate antigen plays a role after $CD8^+$ T_{RM} populations are established. To address this, we generated *B2m*$^{fl/fl}$RS26-Cre-ER^{T2} mice in which tamoxifen treatment ablates MHCI expression. *B2m*$^{fl/fl}$RS26-Cre-ER^{T2} mice infected by s.s. were treated with tamoxifen at 49 dpi and $CD8^+$ T_{RM} were analyzed in the skin approximately one month after treatment (Fig 3.5A). Tamoxifen treatment eliminated expression of MHCI on $CD45^+$ cells from the skin and spleen of *B2m*$^{fl/fl}$RS26-Cre-ER^{T2} mice (Fig 3.5B), but not from

tamoxifen treated *B2m*$^{fl/fl}$ littermate controls. We detected $B8_{19\text{-}26}$-specific T_{RM} at comparable levels in the skin of tamoxifen-treated *B2m*$^{fl/fl}$RS26-Cre-ER^{T2} and *B2m*$^{fl/fl}$ mice (Fig 3.5C), indicating that persistent antigen presentation is not required for $CD8^+$ T_{RM} maintenance. This was also observed for total $CD8^+$ T_{RM} in the skin (Fig 3.5D). Furthermore, we assessed TCR engagement on $CD8^+$ T_{RM} using the Nur77 GFP reporter mice and found that $CD8^+$ T_{RM} are Nur77-negative (Fig 3.5E). Therefore, $CD8^+$ T_{RM} do not receive cognate antigen stimulation in the skin and are maintained in an antigen-independent manner.

Viral MHCI inhibition evades local $CD8^+$ T_{RM} responses

Since viral MHCI inhibition evades CTL responses during primary CPXV infection, we next sought to investigate the effects of viral MHCI inhibition on $CD8^+$ T_{RM} effector function in the absence of other anti-CPXV immune responses. To do so we generated a recombinant influenza virus that expresses the CPXV $B8_{19\text{-}26}$ epitope (Flu-B8) and infected mice by the i.n route. This resulted in the formation of $B8_{19\text{-}26}$ -specific T_{RM} in the lungs of infected mice at 30 dpi (Fig S3.4). We next challenged the mice with CPXV at 30 dpi (Fig 3.6A). To prevent circulating memory $CD8^+$ T cells from contributing to viral control upon CPXV challenge, we treated Flu-B8-infected mice with FTY720 throughout the course of the CPXV challenge. Viral titers in the lungs of mice challenged with Δ12Δ203 were significantly lower than in mice challenged with WT CPXV (Fig 3.6B), demonstrating that viral MHCI inhibition reduces protective $CD8^+$ T_{RM} responses in the lungs. $CD8^+$ T_{RM}-mediated protection was antigen-dependent since challenge with B8 deficient viruses resulted in titers comparable to challenge with WT CPXV.

To test if these findings also hold true during CPXV skin infection, we used μMT mice, which lack mature B cells, in order to avoid humoral responses against CPXV challenge. μMT mice previously infected by s.s. with Δ12Δ203 harbored few $B8_{19\text{-}26}$-specific $CD8^+$ T_{RM} in the skin (Fig S3.5), which is consistent with the findings that infection of μMT mice generates significantly lower numbers of memory $CD8^+$ T cells in comparison to infection of WT C57BL/6 mice [141,142]. We next tested whether depleting $CD4^+$ T cells during acute infection of μMT mice would increase $CD8^+$ T_{RM} formation. Similar to what we observed in WT C57BL/6 mice (Fig S3.1, G to I), depleting $CD4^+$ T cells significantly increased $CD8^+$ T_{RM} formation in the skin of μMT mice infected by s.s., but not i.n. infection (Fig S3.5). In contrast, depleting $CD4^+$ T cells did not significantly increase the number of $B8_{19\text{-}26}$-specific $CD8^+$ T cells in the spleen of μMT mice previously infected by s.s. at 30 dpi.

Based on these findings, we induced $CD8^+$ T_{RM} formation in $CD4^+$ T cell-depleted μMT mice by s.s. with Δ12Δ203 and subsequently challenged the skin with WT CPXV and Δ12Δ203 at 30dpi (Fig 3.6C). Viral titers in the skin of naïve mice were not significantly different in WT CPXV and Δ12Δ203-infected lesions 4 days after challenge (Fig 3.6D). Similarly, viral titers were not significantly different in previously infected μMT mice lacking skin $CD8^+$ T_{RM} (i.n. infected). Conversely, viral titers and scab formation in the Δ12Δ203 lesions of μMT mice harboring skin $CD8^+$ T_{RM} (s.s. infected) were significantly reduced (Fig 3.6D). WT CPXV titers were also reduced in mice immunized by s.s., although the difference was not statistically significant. It is possible that $CD8^+$ T_{RM} activation by Δ12Δ203-infected cells provoked an antiviral state in surrounding areas, as previously demonstrated for skin $CD8^+$ T_{RM} [143], and thereby protected against WT CPXV infection at adjacent sites. These data indicate that $CD8^+$ T_{RM} are protective against CPXV, but more so in the absence of viral MHCI inhibition.

Interestingly, similar results were obtained in μMT mice treated with isotype control antibodies (Fig 3.6E).

Discussion

In this study, we assessed the effects of viral MHCI inhibition on the generation and function of T_{RM}. While viral MHCI inhibition prevents CTL-mediated viral clearance, curiously it does not appear to obstruct local antigenic stimulation of CTLs and subsequent $CD8^+$ T_{RM} formation. Consistent with what was previously reported for VACV skin infection [133,134], local antigenic stimulation promoted $CD8^+$ T_{RM} formation in CPXV-infected skin. Our findings suggest that local antigenic stimulation of CTLs may promote $CD8^+$ T_{RM} development without eliciting T cell-mediated cytotoxicity or cytokine production directed against infected cells.

Our findings also raise the possibility that T_{RM} precursors receive local antigenic stimulation from cross-presenting cells in situ [144,145]. This possibility would explain why local antigen stimulation enhances T_{RM} formation that is not significantly affected by the presence of viral MHCI inhibition. Since cross-presentation by $BATF3^+$ DCs imprints T_{RM} precursors in the lymph nodes [146] and is required for CPXV-specific T cell priming [31,36], these cells are candidates for being involved in local cross-presentation; further investigation will be needed to determine their relative contribution to in situ cross-presentation on T_{RM} development. Intriguingly, these data also raise the possibility that local cross-presentation may be involved in the activation of skin $CD8^+$ T_{RM}.

Local antigen presentation by APCs is critical for the activation of $CD8^+$ T_{RM} in the female genital tract and CNS [136,147], but whether direct contact with infected target cells is

required for $CD8^+$ T_{RM} functions is uncertain. For instance, in situ peptide stimulation of $CD8^+$ T_{RM} is sufficient to induce a tissue-wide antiviral state and protects against antigenically distinct viruses [143,148]. Therefore, $CD8^+$ T_{RM} activation and protection can ensue independently of direct cell-cell contact with infected target cells. Conversely, we found that $CD8^+$ T_{RM} protection during viral infection is abrogated by viral MHCI inhibition, suggesting that TCR/peptide-MHCI (pMHCI) stimulation via engagement of infected target cells is needed for optimal $CD8^+$ T_{RM} functions. Based on the *in vivo* effect of viral MHCI inhibition, we postulate that the level of TCR stimulation needed to trigger $CD8^+$ T_{RM} and CTL effector functions is higher than the level needed to promote local antigen-dependent T_{RM} formation.

Additionally, T_{RM} development and formation in the lungs of CPXV-infected mice remained largely unaffected by viral MHCI inhibition, but viral MHCI inhibition dampened immunodominance within the lung T_{RM} pool. Immunodominance is not affected by CPXV012 and CPXV203 during primary CPXV infection [31,36], but the breadth and the levels of viral epitopes presented in the context of viral MHCI inhibition can differ from the epitopes presented in the absence of viral MHCI inhibition [57,85]. As a consequence, increased antigen presentation and antigen abundance during respiratory infection with Δ12Δ203 potentially promotes CTL cross-competition for pMHCI complexes, which can affect the T_{RM} repertoire [134,135]. These findings were not found following CPXV skin infection, suggesting that differences in the microenvironment also contribute to the effects on T_{RM} immunodominance. Moreover, respiratory viral infections results in persistent antigen presentation [131,149,150], and can contribute to the locality of memory T cells [151]. Persistent antigen presentation was therefore an appealing explanation for the long-term maintenance of T_{RM} in peripheral tissues.

Here we used inducible deletion of *B2m* to test if persistent stimulation is required for maintaining T_{RM}. We found that deletion of *B2m* after T_{RM} formation did not affect the number of T_{RM} cells, suggesting that local cognate antigen, or even low-level stimulation from cross-reactive pMHCI complexes is not required for T_{RM} maintenance. However, since our studies focused on the $CD45^+$ compartment, it is possible that low-level expression of MHCI on non-hematopoietic cells could contribute to T_{RM} maintenance. Nonetheless, our results add to previous reports [124,128,152–154] by suggesting that T_{RM} maintenance is also apparently independent of cross-reactive pMHCI complexes.

Ultimately, our findings shed light on the maintenance, generation, and activation of T_{RM}, and highlight the effects of viral MHCI inhibition on local $CD8^+$ T_{RM} responses, which should be seriously considered in regards to vaccine design against viruses that target the MHCI pathway.

Materials and methods

Mice, cell lines, and viruses

C57BL/6 mice were purchased from the National Cancer Institute. Transgenic and knockout mice were purchased from the Jackson Laboratory, with the exception of $B2m^{fl/fl}$ and IFNγ KI Thy1.1 mice. IFNγ KI Thy1.1 mice were kindly provided by Dr. Casey Weaver, University of Alabama School of Medicine. $B2m^{fl/fl}$ mice were generated as described by Bern et al., 2018 (submitted). DC2.4 cells were cultured in RPMI supplemented with 10% FBS (Mediatech), 100 U/ml Penicillin, 100 g/ml streptomycin, 1mM sodium pyruvate, L-glutamine, and non-essential amino acids (Gibco). Madin–Darby Canine Kidney (MDCK) cells were maintained in MEM with 5% FBS, MEM-vitamins (Gibco), L-glutamine, 100 U/ml Penicillin, and 100 g/ml streptomycin. Human embryonic kidney cells (293T) were maintained in Opti-MEM (Life

Technologies) with 10% FBS, L-glutamine, 100 U/ml Penicillin, and 100 g/ml streptomycin. DC2.4 cells were gifted from Dr. Kenneth Rock, University of Massachusetts Medical School. MDCK and 293T cells were a kind gift from Dr. Richard Webby at St. Jude Children's Research Hospital.

For the generation of IAV-B8$_{19\text{-}26}$ (Flu-B8), the CPXV B8$_{19\text{-}26}$ epitope was inserted into the stalk region of neuraminidase (NA), in-frame, between nucleotides 148 and 170 using inverse PCR (Phusion-HF, ThermoFisher) and the restriction enzyme AarI (ThermoFisher) to ligate the mutant plasmid. Co-cultures of 293T and MDCK cells were transfected with eight bidirectional pHW2000 plasmids containing cDNA for A/Puerto Rico/08/1934 (H1N1) (1 µg per plasmid) with polyethylenimine (8 µg total). Rescue of the reverse genetic virus was performed as previously described [155]. BAC-derived CPXV viruses were generated as previously described [36].

Mouse infection and parabiosis surgery

Mice 8-10 weeks of age were sex- and age-matched for each experiment. i.n. and s.s. infections were performed as previously described [31]. In brief, mice were anesthetized and 30 µl of virus inoculum diluted in PBS was administered i.n. For s.s., fur from the flank of mice was depilated using Nair™. The following day, mice were anesthetized and the flanks were infected by s.s. at three adjacent sites, 1 x 10^5 pfu/site. Parabiosis surgery was performed as previously described [156,157]. Parabiosed mice were rested for two weeks before sacrificing and harvesting tissues.

Immunofluorescence.

2 x 3 cm^2 piece of skin was harvested from infected mice and were prepared as previously described [158]. Sections were blocked using 10% goat serum in PBS for 1h before incubating with primary antibodies for 1h. Cells were then washed with 0.5% triton in PBS, incubated with Streptavidin-AF555 (ThermoFisher), washed with 0.5% triton in PBS, and mounted with DAPI (Vectashield). Stained sections were analysed with laser scanning confocal microscope LSM880 (Zeiss). Primary antibodies were obtained from BD Pharmingen and include CD103-Biotin (M290), IA/IE-AF647 (M5/114.15.2), and CD8α-AF488 (53-6.7).

***In vivo* antibody, FTY720, and tamoxifen treatment.**

To induce TCR ligation *in vivo*, 50 μg of anti-CD3e monoclonal antibody (145-2C11; ThermoFisher) was administered into mice by i.v. injection 16 hours prior to harvesting tissues. FTY720 (Cayman Chemical) was administered by i.p. injection (10 mg/kg) in aqueous solution. To deplete $CD4^+$ T cells, 200 μg anti-CD4 (GK1.5) or isotype control (anti-rat IgG2b; Bio X Cell) were injected i.p. To deplete NK cells, 100 μg anti-NK1.1 (PK136) was injected i.p. weekly. For intravascular staining, fluorochrome-conjugated anti-CD45.2 (104; BioLegend) was administered by i.v. injection. Three minutes after injection, mice were sacrificed and tissues were harvested. Mice were treated topically with 1 mg 4-hydroxytamoxifen (Sigma-Aldrich) dissolved in ethanol and were fed with tamoxifen diet (Envigo) during the indicated times shown.

Flow cytometry, intracellular cytokine staining, and antibodies

Single-cell suspensions from the spleens, lymph nodes, lungs, and ~2 x 3 cm^2 piece of skin were prepared at the indicated days post-infection as previously described [31,123]. Skin and lung tissues

were minced and incubated in with Hanks balanced salt solution (HBSS) containing 1 mg/mL collagenase A (Roche) and 22.4 g/mL Dnase I (Roch) at 37° C for 30 minutes. Samples were then filtered through a 70 μm mesh strainer prior to staining. Samples for flow cytometric analyses were stained on ice with Fixable Viability Dye eFlour 506 (eBioscience) before tetramer and cell surface staining. For tetramer staining, cells were incubated with H-2K^{b}-TSYFESV tetramers for 45 minutes at room temperature prior to cell surface staining of the indicated surface markers. Tetramers were produced in the Immunomonitoring Laboratory within the Center for Human Immunology and Immunotherapy Programs (Washington University). *Ex vivo* restimulation and intracellular cytokine staining for IFN-γ was performed as previously described [36]. For staining of Nur77, the Foxp3/Transcription Factor Staining Buffer Set was used according to the manufacturer's protocol (eBioscience). The following antibodies were purchased from Abcam, BD Biosciences, eBioscience, BioLegend, or ThermoFisher: CD3 (145-2C11), NK1.1 (PK136), CD19 (eBio1D3), CD64 (X54-5/7.1), CD8α (53-6.7), CD4 (RM4-5), VACV (Ab19970), CD4 (RM4-4), CD44 (IM7), CD103 (2E7), CD69 (H1.2F3), H-2K^{b} (AF-88.5), CD11c (N418), CD45.1 (A20), CD45.2 (104), CD24 (M1/69), IA/IE (M5/114.15.2), SIRPα (P84), CD11b (M1/70), Ly6C (HK1.4), Nur77 (12.14).

Statistic analysis

The data were analysed with an unpaired Student *t* test or one-way ANOVA followed by Tukey posttest comparison using Prism GraphPad software. Asterisks indicate statistical significance and *p* values are denoted as *p<0.05, **p<0.01, ***p<0.001, ****p<0.0001.

Figures and Tables

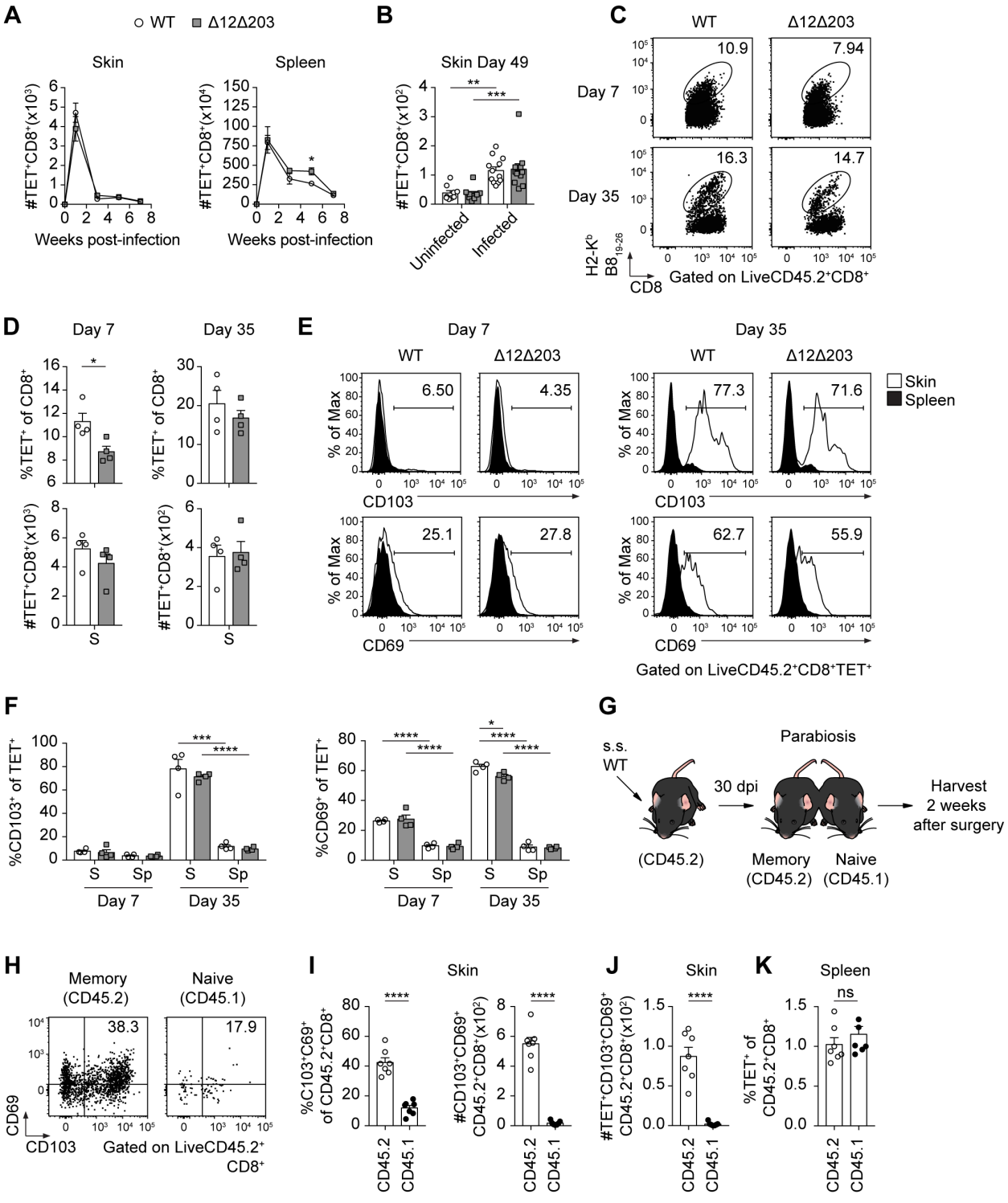

Fig 3.1 Viral MHCI inhibition does not affect the overall development of $CD8^+$ T_{RM}. C57BL/6 mice were infected by s.s. with WT CPXV or Δ12Δ203 (**A** to **F**). (**A**) The absolute number of $B8_{19\text{-}26}$-$tetramer^+$ cells in the skin (S) and spleen (SP) of infected mice over time. n = 4 mice per time point. Representative of three independent experiments. (**B**) The absolute number of $B8_{19\text{-}26}$-$tetramer^+$ cells in previously infected skin flank and the contralateral uninfected skin flank at 49 dpi. (**C**) Representative flow plots of $B8_{19\text{-}26}$-$tetramer^+$ cells in the skin at the indicated time points. (**D**) Percentage (top) and absolute number (bottom) of $B8_{19\text{-}26}$-$tetramer^+$ cells in the skin on 7 dpi and 35 dpi. (**E**) Representative flow plots of CD103 and CD69 expression on $B8_{19\text{-}26}$-$tetramer^+$ cells are shown for the indicated time points. (**F**) Percentage of CD103 (Left) and CD69 (Right) expression on $B8_{19\text{-}26}$-$tetramer^+$ cells are shown for the indicated time points. (**G**) Schematic of parabiosis experiment. (**H**) Representative flow plots of $CD103^+CD69^+$ skin $CD8^+$ T cells in parabiosed mice. (**I**) Percentage and absolute numbers of $CD103^+CD69^+$ skin $CD8^+$ T cells in parabiosed mice. (**J**) The absolute number of $B8_{19\text{-}26}$-$tetramer^+$ T_{RM} in the skin of parabiosed mice. (**K**) Percentage of $B8_{19\text{-}26}$-$tetramer^+$ cells in the spleen of parabiosed mice. Representative of three independent experiments (for panel A to F). Data were pooled from two independent experiments (for panel H to K). Symbols represent individual mice. Error bars represent means ± SEM.

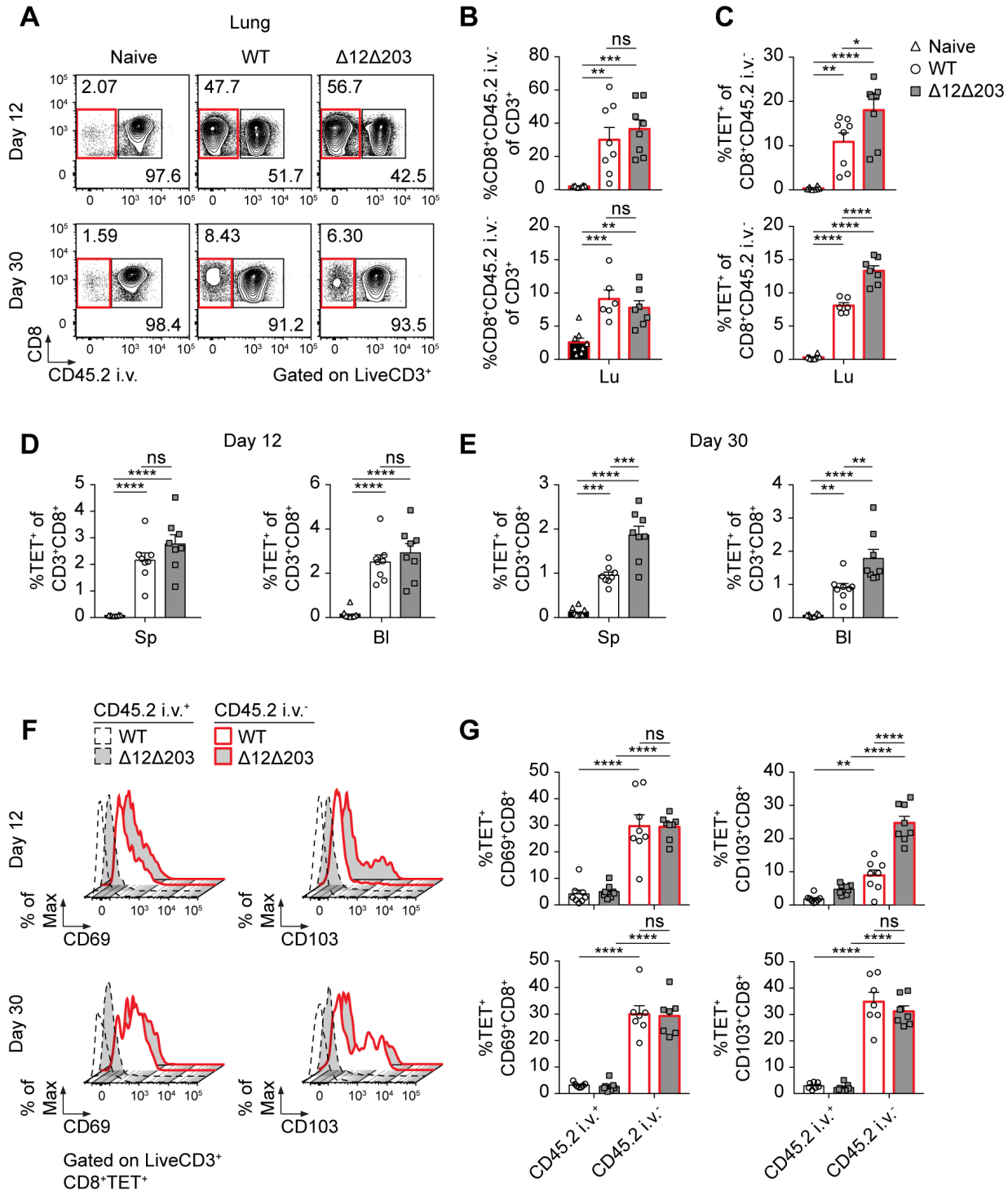
A
Lung
Naive
WT
Δ12Δ203
Day 12
Day 30
2.07
47.7
56.7
97.6
51.7
42.5
1.59
8.43
6.30
98.4
91.2
93.5
CD8
CD45.2 i.v.
Gated on LiveCD3+
B
%CD8+CD45.2 i.v.- of CD3+
Lu
C
%TET+ of CD8+CD45.2 i.v.-
Naive
WT
Δ12Δ203
Lu
D
Day 12
%TET+ of CD3+CD8+
Sp
Bl
E
Day 30
F
CD45.2 i.v.+
CD45.2 i.v.-
WT
Δ12Δ203
% of Max
CD69
CD103
Gated on LiveCD3+
CD8+TET+
G
%TET+ CD69+CD8+
%TET+ CD103+CD8+
CD45.2 i.v.+
CD45.2 i.v.-
ns

Fig 3.2 Viral MHCI inhibition affects immunodominance within the lung $CD8^+$ T_{RM} population.

C57BL/6 mice were infected i.n. with WT CPXV or Δ12Δ203. Intravascular staining with an anti-CD45 antibody was performed before euthanizing mice at 12 and 30 dpi. (**A**) Representative flow plots of CD45 expression on $CD8^+$ cells in the lungs (Lu). Data are representative of two independent experiments. (**B**) Percentage of IV^-CD8^+ cells in the lungs at 12 (top row) and 30 (bottom) dpi. Data are pooled from two independent experiments. Symbols represent individual mice. Error bars represent means ± SEM. (**C**) Percentage of $IV^-CD8^+B8_{19\text{-}26}$-$tetramer^+$ cells in the lungs at 12 (top row) and 30 (bottom) dpi. (**D** and **E**) Percentage of $IV^-CD8^+B8_{19\text{-}26}$-$tetramer^+$ cells in the blood (Bl) and spleen (SP) are shown at 12 and 30 dpi. Data are pooled from two independent experiments. Symbols represent individual mice. Error bars represent means ± SEM. (**F**) Representative flow plots of CD69 or CD103 expression on IV^+/IV^- $B8_{19\text{-}26}$-$tetramer^+$ cells at 12 and 30 dpi. (**G**) Percentage of CD69 and CD103 expression on IV^-/IV^- $B8_{19\text{-}26}$-$tetramer^+$ cells at 12 (top) and 30 (bottom) dpi. Data are pooled from two independent experiments. Symbols represent individual mice. Error bars represent means ± SEM.

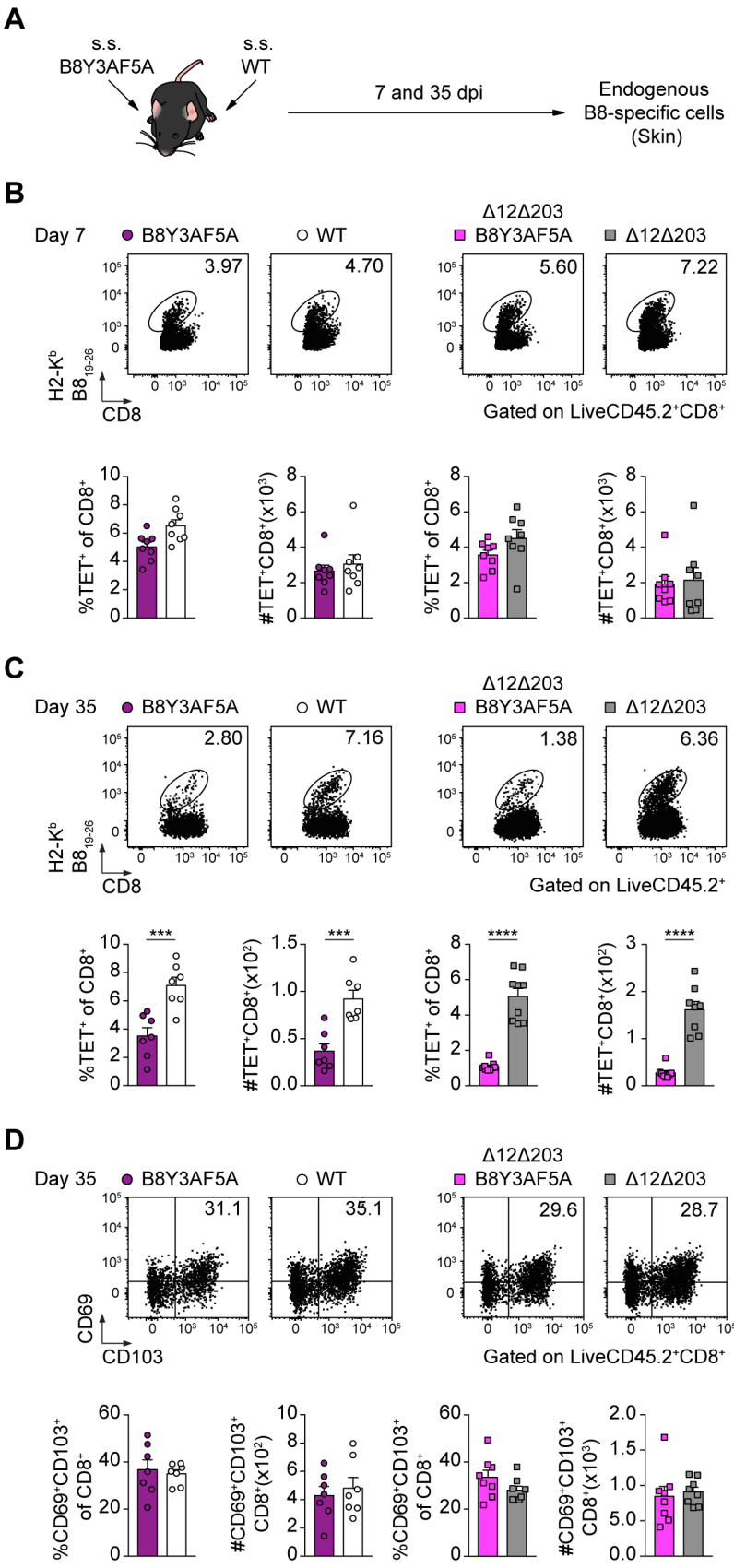
A
s.s.
B8Y3AF5A
s.s.
WT
7 and 35 dpi
Endogenous
B8-specific cells
(Skin)
B
Day 7
B8Y3AF5A
WT
Δ12Δ203
B8Y3AF5A
Δ12Δ203
3.97
4.70
5.60
7.22
H2-Kb
B8 19-26
CD8
Gated on LiveCD45.2+CD8+
%TET+ of CD8+
#TET+CD8+(x10³)
%TET+ of CD8+
#TET+CD8+(x10³)
C
Day 35
B8Y3AF5A
WT
Δ12Δ203
B8Y3AF5A
Δ12Δ203
2.80
7.16
1.38
6.36
H2-Kb
B8 19-26
CD8
Gated on LiveCD45.2+
***
***
****
****
%TET+ of CD8+
#TET+CD8+(x10²)
%TET+ of CD8+
#TET+CD8+(x10²)
D
Day 35
B8Y3AF5A
WT
Δ12Δ203
B8Y3AF5A
Δ12Δ203
31.1
35.1
29.6
28.7
CD69
CD103
Gated on LiveCD45.2+CD8+
%CD69+CD103+ of CD8+
#CD69+CD103+ CD8+(x10²)
%CD69+CD103+ of CD8+
#CD69+CD103+ CD8+(x10³)

Fig 3.3 Local cognate antigen enhances CD8$^+$ T_{RM} formation, even in the context of viral MHCI inhibition and CTL evasion.

(**A**) C57BL/6 mice were co-infected by s.s. with $B8_{19\text{-}26}$ sufficient CPXV (WT or Δ12Δ203) and $B8_{19\text{-}26}$ deficient (B8Y3AF5A or Δ12Δ203B8Y3AF5A). (**B**) Representative flow plots of $B8_{19\text{-}26}$-tetramer$^+$ cells in the skin at 7 dpi are shown above the percentage and absolute number of $B8_{19\text{-}26}$-tetramer$^+$ cells. (**C**) Representative flow plots of $B8_{19\text{-}26}$-tetramer$^+$ cells in the skin at 35 dpi are shown above the percentage and absolute number of $B8_{19\text{-}26}$-tetramer$^+$ cells. (**D**) Representative flow plots CD69 and CD103 expression on CD8$^+$ cells in the skin at 35 dpi are shown above the percentage and absolute number of CD69$^+$CD103$^+$ CD8$^+$ cells. Data are pooled from two independent experiments. Symbols represent individual mice. Error bars represent means ± SEM.

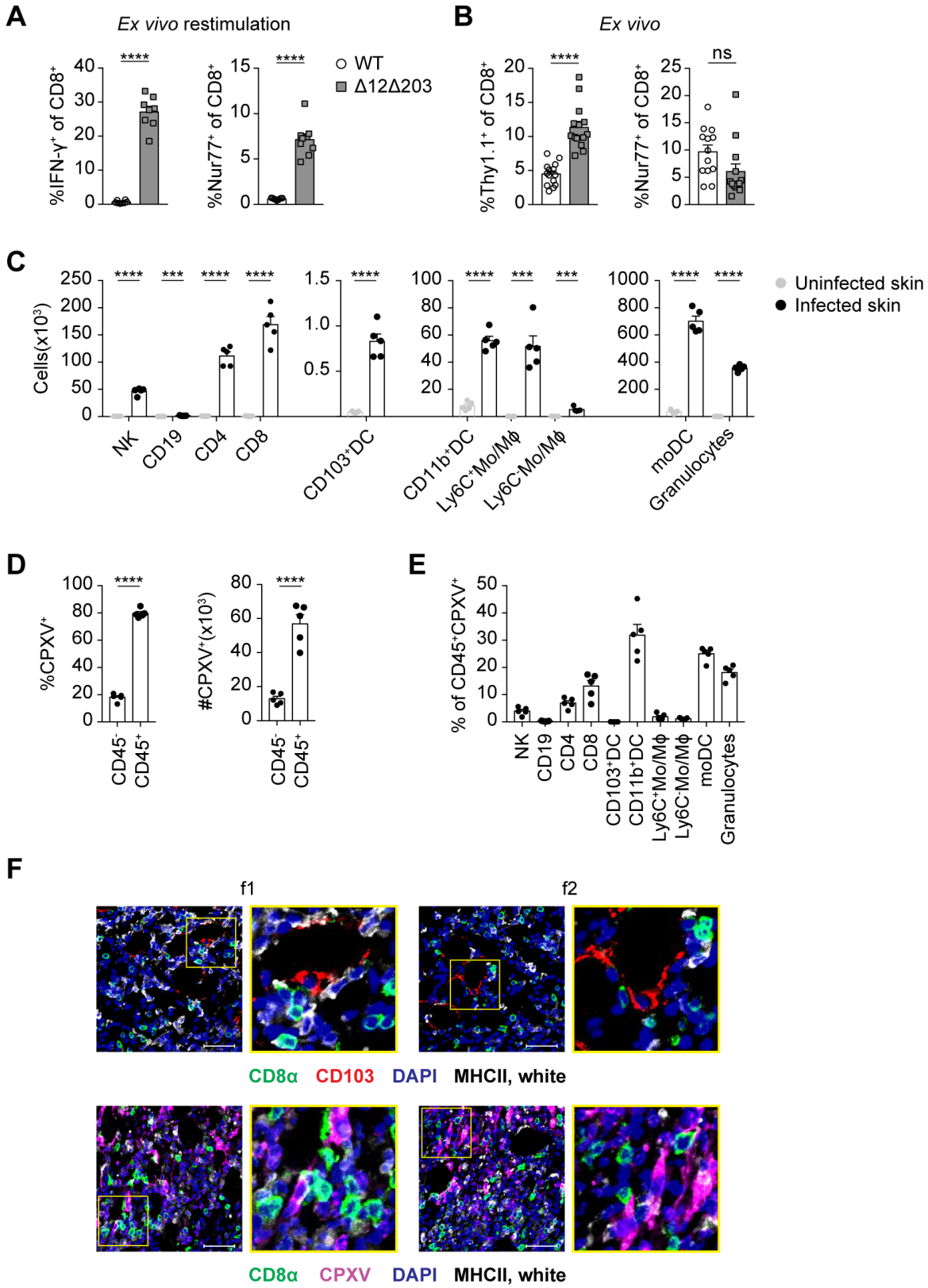
A
Ex vivo restimulation
%IFN-γ+ of CD8+
%Nur77+ of CD8+
WT
Δ12Δ203
B
Ex vivo
%Thy1.1+ of CD8+
%Nur77+ of CD8+
ns
C
Cells(x10³)
Uninfected skin
Infected skin
NK
CD19
CD4
CD8
CD103+DC
CD11b+DC
Ly6C+Mo/Mϕ
Ly6C-Mo/Mϕ
moDC
Granulocytes
D
%CPXV+
#CPXV+(x10³)
CD45-
CD45+
E
% of CD45+CPXV+
F
f1
f2
CD8α CD103 DAPI MHCII, white
CD8α CPXV DAPI MHCII, white

Fig 3.4 Viral MHCI inhibition evades CTL responses, but does not affect TCR engagement with cognate antigen/MHC complexes on infected target cells *in vivo*.

C57BL/6 mice or Thy1.1 KI IFN-γ reporter mice were co-infected with WT CPXV and Δ12Δ203. The spleens of infected C57BL/6 mice and skin of infected Thy1.1 KI IFN-γ reporter mice were harvested for *ex vivo* restimulation and direct *ex vivo* analyses respectively on 7 dpi. (**A**) Percentage of endogenous IFN-γ and Nur77 expression on $CD8^+$ cells stimulated with WT CPXV or Δ12Δ203-infected DC2.4 cells. Data are pooled from two independent experiments. (**B**) Percentage of IFN-γ (Thy1.1) and endogenous Nur77 expression on $CD8^+$ cells from WT CPXV or Δ12Δ203-infected skin. Data are pooled from three independent experiments. Symbols represent individual mice. Error bars represent means ± SEM. (**C** to **F**) C57BL/6 mice were infected by s.s. with WT CPXV and sacrificed on 6 dpi. (**C**) Absolute number of leukocytes recruited to WT CPXV-infected skin. Cells from the skin were gated on $CD45^+$ and defined as follows: NK ($CD3^-CD19^-NK1.1^+$), CD19 ($CD3^-CD19^+$; CD4, $CD19^-CD3^+CD4^+$), CD8 ($CD19^-CD3^+CD8^+$), $CD103^+$ DC ($MHCII^+CD11c^+CD24^+SIRP\alpha^-CD103^+$), $CD11b^+$ DC ($MHCII^+CD24^+CD64^-CD11b^+$), $Ly6C^+$ Mo/Mϕ ($MHCII^-CD64^+CD11b^+Ly6C^+$), $Ly6C^-$ Mo/Mϕ ($MHCII^-CD64^+CD11b^+Ly6C^-$), moDC ($MHCII^+CD11b^+CD64^+CD24^+$), granulocytes ($MHCII^-CD24^+CD11b^+$) (**D**) Percentage of $CPXV^+$ cells, as determined by staining with α-VACV antibodies and flow cytometric analysis. (**E**) Percentage of $CPXV^+$ cells within the $CD45^+$ population. Data are representative of two independent experiments. Symbols represent individual mice. Error bars represent means ± SEM. (**F**) Immunofluorescence staining of $CD8^+$, $CD103^+$, $CPXV^+$ and $MHCII^+$ cells in the skin at 6 dpi. Scale bars, 50 μm.

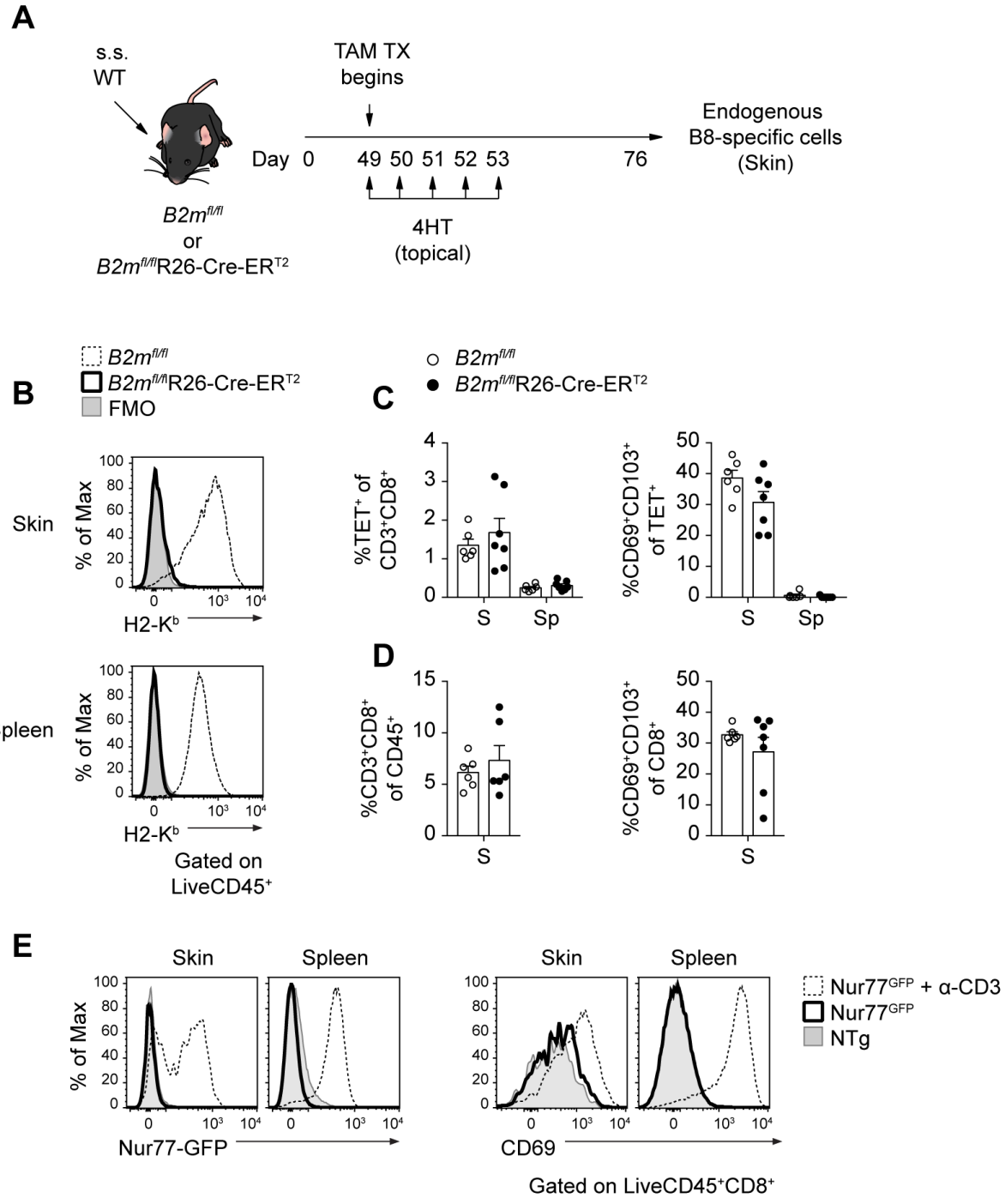
A
s.s.
WT
TAM TX
begins
Day 0
49 50 51 52 53
76
Endogenous
B8-specific cells
(Skin)
B2m^fl/fl
or
B2m^fl/flR26-Cre-ER^T2
4HT
(topical)
B
B2m^fl/fl
B2m^fl/flR26-Cre-ER^T2
FMO
Skin
Spleen
% of Max
H2-K^b
Gated on
LiveCD45^+
C
B2m^fl/fl
B2m^fl/flR26-Cre-ER^T2
%TET^+ of
CD3^+CD8^+
%CD69^+CD103^+
of TET^+
S
Sp
D
%CD3^+CD8^+
of CD45^+
%CD69^+CD103^+
of CD8^+
E
Skin
Spleen
% of Max
Nur77-GFP
CD69
Gated on LiveCD45^+CD8^+
Nur77^GFP + α-CD3
Nur77^GFP
NTg

Fig 3.5 $CD8^+$ T_{RM} are maintained in the absence of cognate antigen stimulation.

*$B2m^{fl/fl}$*RS26-Cre-ERT^{T2} mice and *$B2m^{fl/fl}$* litter mate controls were infected by s.s. with WT CPXV. On 49 dpi, mice were started on a tamoxifen chow diet and treated topically with 4HT daily for 5 days. Additionally, mice were treated with α-NK1.1 (100 μg/mouse) once weekly starting on 49 dpi to deplete NK cells. (**A** to **D**) Mice were euthanized at 76 dpi and $CD8^+$ T cells were analyzed in the skin (S) and spleen (SP). (**B**) Representative flow plots of H-$2K^b$ expression on $CD45^+$ cells from the skin and spleen on 76 dpi. (**C**) Percentage of $B8_{19\text{-}26}$-$tetramer^+$ and $CD69^+CD103^+$ cells in the skin and spleen at 76 dpi. (**D**) Percentage of total $CD8^+$ and $CD69^+CD103^+$ cells in the skin at 76 dpi. Data are pooled from two independent experiments. Symbols represent individual mice. Error bars represent means ± SEM. (**E**) $Nur77^{GFP}$ reporter mice and nontransgenic (NTg) littermate controls were infected by s.s. with WT CPXV and euthanized at 30 dpi. $CD8^+$ T cells were analyzed in the skin and spleen. As a positive control, B8 peptide was administered intradermally (i.d.) and an α-CD3 antibody was administered intravenously (i.v.) into $Nur77^{GFP}$ mice previously infected for 30 days. Representative flow plots of Nur77 (GFP) and CD69 expression on skin and splenic $CD8^+$ T cells is shown. Data are representative of three independent experiments; total n = 3 positive control mice, total n = 5 $Nur77^{GFP}$ mice, and total n = 6 Ntg mice.

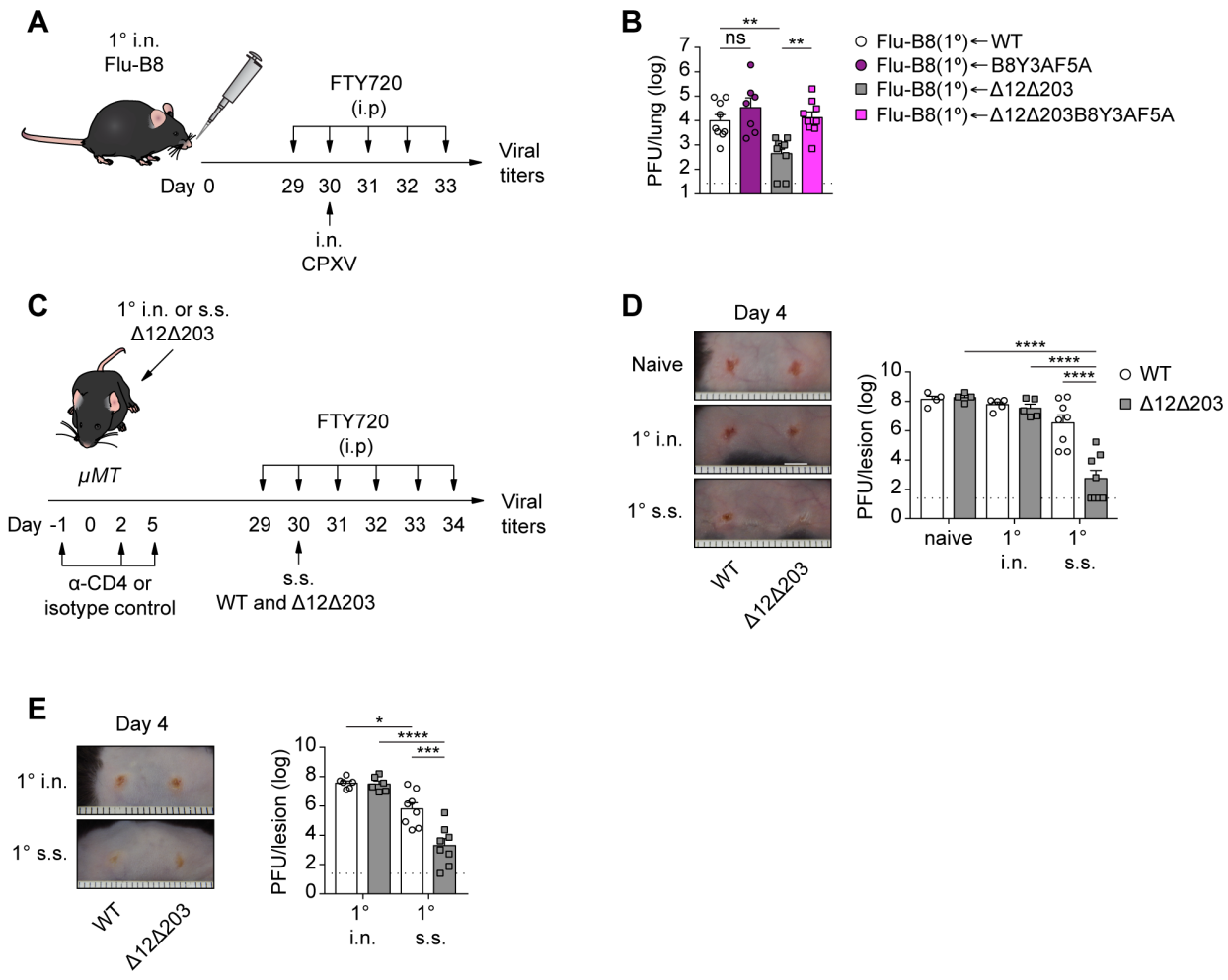

Fig 3.6 Viral MHCI inhibition evades protective CD8$^+$ T_{RM} responses.

(**A**) Schematic of heterologous prime/challenge experiment. (**B**) Viral titers in the lungs of Flu-B8-immunized mice challenged with CPXV. Data are pooled from two independent experiments. (**C**) Schematic of μmT mice skin challenge experiment. (**D**) Image of infected μmT flanks (left) and viral titers from skin lesions 4 days after s.s. challenge of α-CD4 treated naïve control and CPXV-immunized μmT mice. (**E**) Viral titers from skin lesions 4 days after s.s. challenge of isotype control treated CPXV-immunized μmT mice. Data are pooled from two or

three independent experiments. Symbols represent individual mice. Error bars represent means ± SEM.

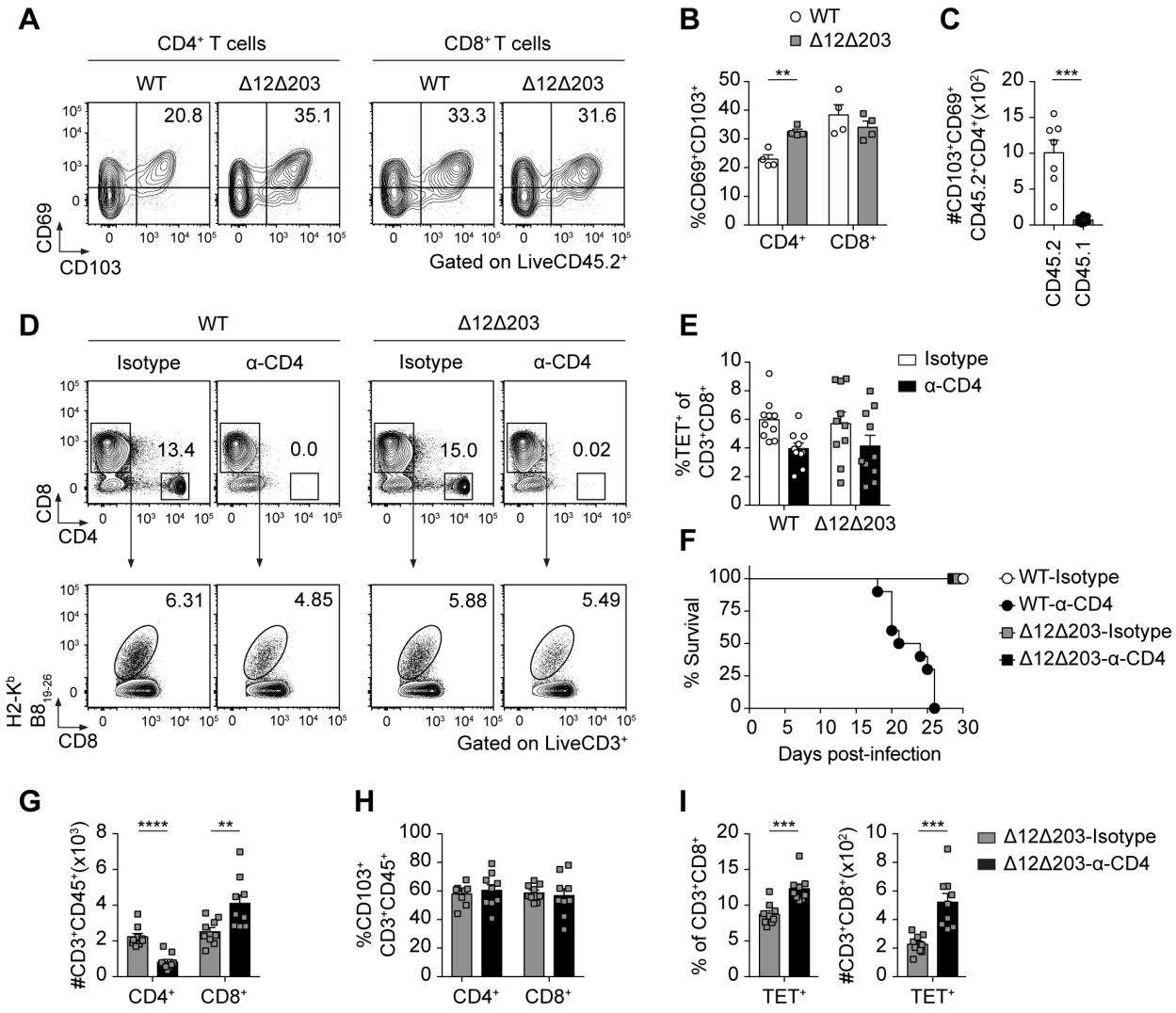

Fig S3.1 Viral MHCI inhibition affects the formation of CD4$^+$ T_{RM}.

C57BL/6 mice were infected by s.s. with WT CPXV or Δ12Δ203. (**A**) Representative flow plots of CD103 and CD69 expression on CD4$^+$ and CD8$^+$ cells in the skin at 35 dpi. (**B**) Percentage of CD69$^+$CD103$^+$ T cells in the skin at 35 dpi. Representative of three independent experiments. Symbols represent individual mice. Error bars represent means ± SEM. (**C**) The absolute number of CD4$^+$ T_{RM} in the skin of parabiosed mice. Parabiosis was performed as outlined in Figure 1G. (**D** to **I**) Mice infected by s.s. with WT CPXV or Δ12Δ203 were treated with α-CD4 or isotype control antibodies on day -1, 2, and 5 post-infection. (**D**) Representative flow plots of

peripheral blood T cells and $B8_{19\text{-}26}$-tetramer$^+$ cells at 7 dpi. (**E**) Percentage of $B8_{19\text{-}26}$-tetramer$^+$ cells from peripheral blood at 7 dpi. (**F**) Percent survival. n = 10 mice per group. Data are pooled from two independent experiments. (**G**) Absolute number of $CD4^+$ and $CD8^+$ T cells in the skin at 30 dpi. (**H**) Percentage of CD103 expression on T cells at 30 dpi. (**I**) Percentage (left) and absolute numbers (right) of $B8_{19\text{-}26}$-tetramer$^+$ cells in the skin at 30 dpi. Data are pooled from two independent experiments. Symbols represent individual mice. Error bars represent means ± SEM.

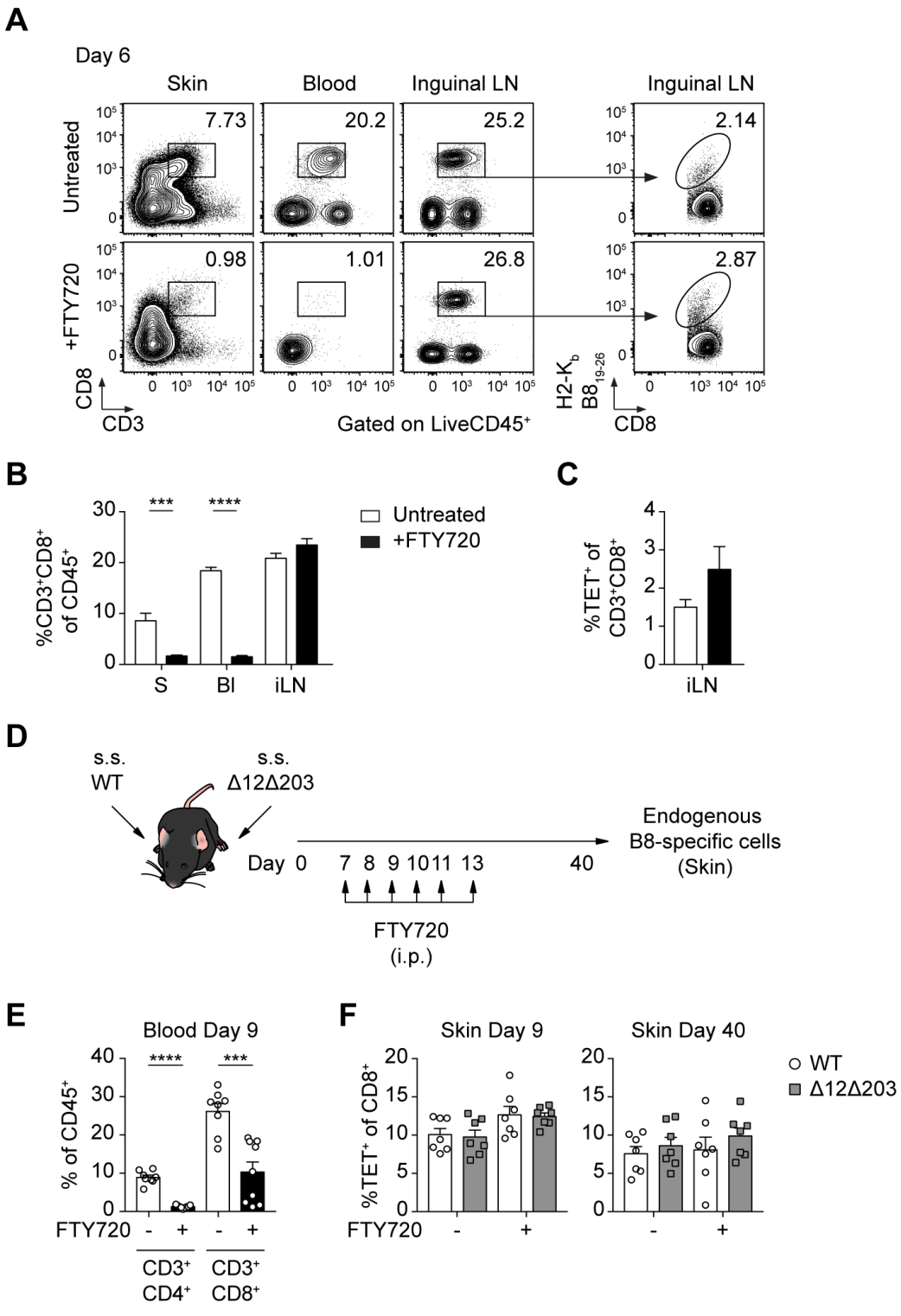
A
Day 6
Skin
Blood
Inguinal LN
Inguinal LN
Untreated
+FTY720
7.73
20.2
25.2
2.14
0.98
1.01
26.8
2.87
CD8
CD3
Gated on LiveCD45+
H2-Kb B8 19-26
CD8
B
%CD3+CD8+ of CD45+
***
****
Untreated
+FTY720
S
Bl
iLN
C
%TET+ of CD3+CD8+
iLN
D
s.s. WT
s.s. Δ12Δ203
Day 0 7 8 9 10 11 13 40
Endogenous B8-specific cells (Skin)
FTY720 (i.p.)
E
Blood Day 9
% of CD45+
****
***
FTY720 - + - +
CD3+ CD4+
CD3+ CD8+
F
Skin Day 9
Skin Day 40
%TET+ of CD8+
FTY720 - + - +
WT
Δ12Δ203

Fig S3.2 $CD8^+$ T_{RM} develop without continuous recruitment of CTLs during acute CPXV infection.

C57BL/6 mice were co-infected with WT CPXV and Δ12Δ203 and FTY720 was subsequently administered by intraperitoneal (i.p.) injection on 1, 3, and 5 dpi (**A** to **C**). $CD8^+$ T cells were analyzed in the skin (S), blood (Bl), and inguinal lymph node (iLN) at 6 dpi. (**A**) Representative flow plots. n = 9-15 mice per group. Data are representative of two independent experiments. (**B**) Percentage of $CD8^+$ cells. Data are pooled from two independent experiments. Error bars represent means ± SEM. (**C**) Percentage of $B8_{19\text{-}26}$-$tetramer^+$ cells in the iLN at 6 dpi. Data are pooled from two independent experiments. Error bars represent means ± SEM. (**D**) Schematic of co-infection experiment. T cells from peripheral blood (**E**) and $B8_{19\text{-}26}$-$tetramer^+$ cells in the skin (**F**) of mice infected as shown in (**D**) were analyzed at the indicated time points. Data are pooled from two independent experiments. Symbols represent individual mice. Error bars represent means ± SEM.

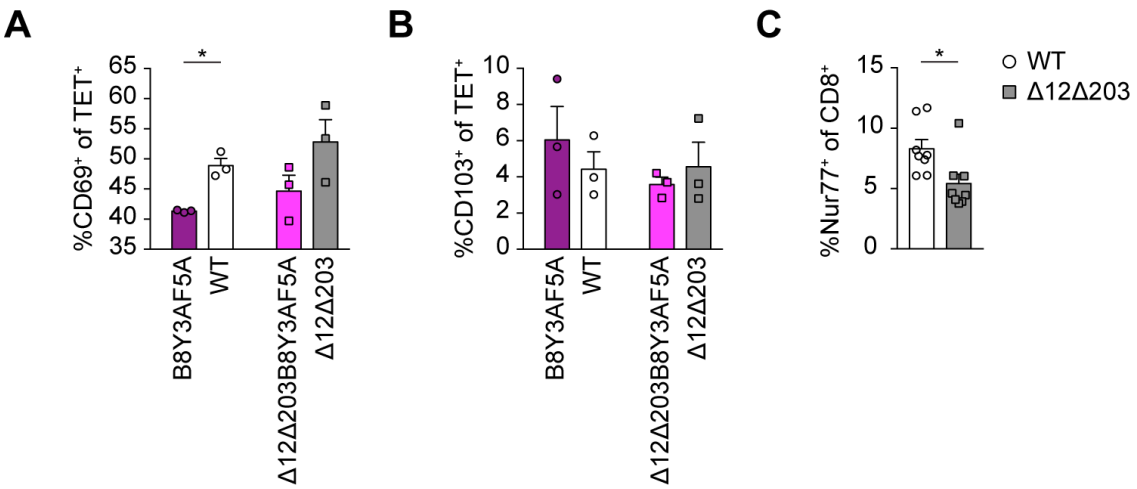

Fig S3.3 Local cognate antigen recognition upregulates CD69 and Nur77 expression by CTLs.

C57BL/6 mice were co-infected by s.s. with $B8_{19\text{-}26}$ sufficient CPXV (WT or Δ12Δ203) and $B8_{19\text{-}26}$ deficient (B8Y3AF5A or Δ12Δ203B8Y3AF5A) on opposite flanks. (**A**) Percentage of $B8_{19\text{-}26}$-tetramer$^+$ cells expressing CD69 at 7 dpi. (**B**) Percentage of $B8_{19\text{-}26}$-tetramer$^+$ cells expressing CD103 at 7 dpi. Data are representative of two independent experiments. Symbols represent individual mice. (**C**) Nur77^{GFP} mice were co-infected as outlined in Fig. 3A. Nur77 (GFP) expression by CD8$^+$ T cells from WT CPXV or Δ12Δ203-infected skin was analyzed at 7 dpi. Data are pooled from two independent experiments. Symbols represent individual mice. Error bars represent means ± SEM.

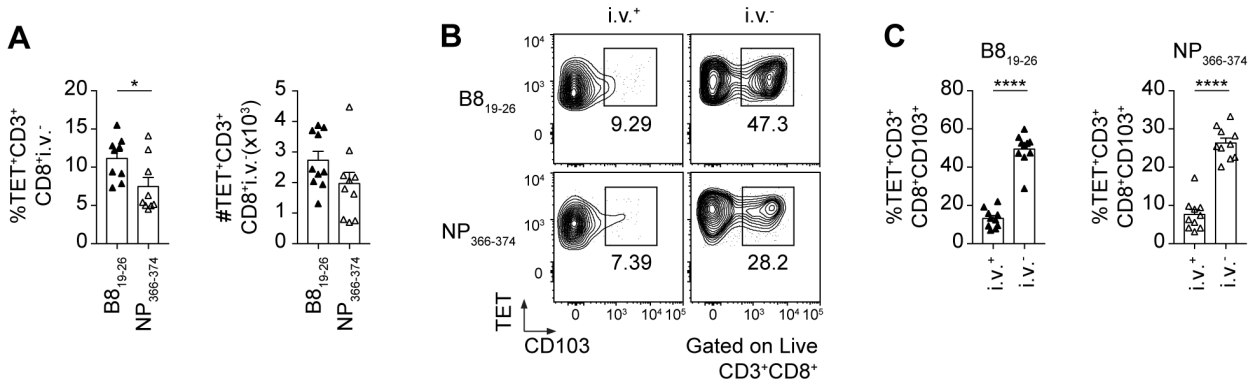

Fig S3.4 Flu-B8 respiratory infection generates $B8_{19\text{-}26}$ -specific $CD8^+$ T_{RM} in the lungs.

C57BL/6 mice were i.n. infected with recombinant Flu virus expressing the CPXV $B8_{19\text{-}26}$ epitope. Intravascular staining with an anti-CD45 antibody was performed before euthanizing mice at 30 dpi. (**A**) Percent of $B8_{19\text{-}26}$-tetramer$^+$ and $NP_{366\text{-}374}$-tetramer$^+$ IV^-cells in the lungs of Flu-B8-infected mice. Data are pooled from two independent experiments. Symbols represent individual mice. Error bars represent means ± SEM. (**B**) Representative flow plots of CD103 expression on tetramer$^+IV^-$ cells at 30 dpi. (**C**) Percentage of $CD103^+TET^+IV^-$ cells. Data are pooled from two independent experiments. Symbols represent individual mice. Error bars represent means ± SEM.

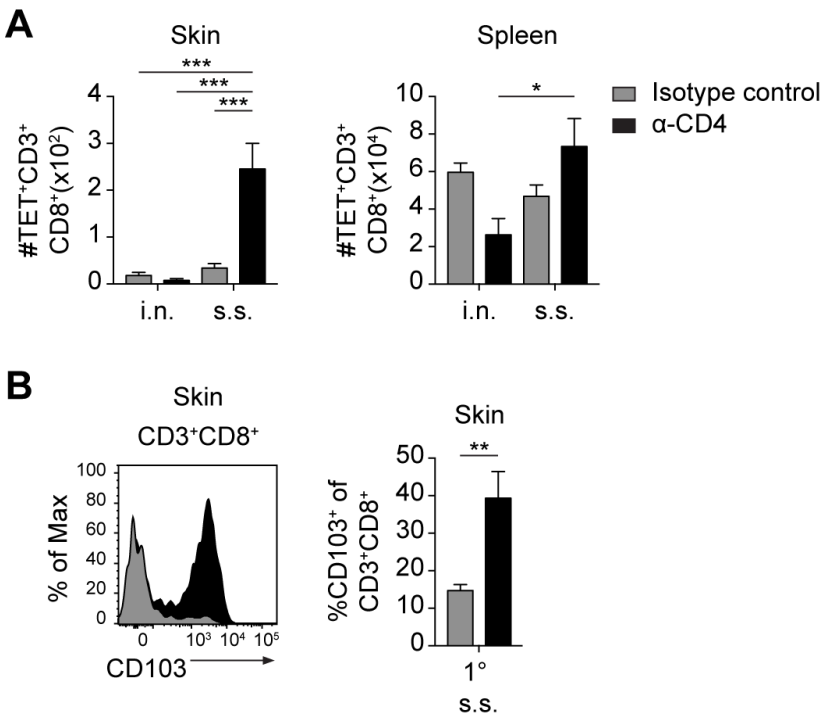

Fig S3.5 The number of CD8$^+$ T_{RM} is reduced in B cell-deficient mice.

μmT mice were infected by s.s. or i.n. with Δ12Δ203 and treated with α-CD4 or isotype control antibodies, as in Figure 2B. (**A**) Absolute number of $B8_{19\text{-}26}$-tetramer$^+$ cells in the skin and spleen of μmT mice previously infected for 30 days is shown. n = 4-5 mice per group. Data are pooled from two independent experiments. Error bars represent means ± SEM. (**B**) Representative flow plot of CD103 expression on CD8$^+$ T cells in the skin of μmT previously infected for 30 days is shown next to the percentage of CD103$^+$ cells. n = 5 mice per group. Data are pooled from two independent experiments. Error bars represent means ± SEM.

Chapter 4:

Discussion and Future Directions

Discussion

Over 200 years ago, Edward Jenner had a theory that prior exposure to CPXV could provide protection against smallpox. He tested his theory in 1796 by inoculating a child with CPXV taken from a cowpox pustule and showed that the child was indeed protected against smallpox. He also made an interesting observation that CPXV infection did not always protect against secondary infection with CPXV[159]. It is thus tempting to speculate that my findings on CPXV-mediated MHCI inhibition may explain this peculiar conundrum. The findings presented here should also be considered in regards to rationale vaccine design because many viruses possess the capacity to obstruct MHCI antigen presentation.

Major infectious diseases caused by viruses that target the MHCI pathway include hepatitis C, symptomatic congenital CMV disease, and acquired immune deficiency syndrome (AIDS) [160,161]. These viruses have propensities to evolve immune-escape mutations and mechanisms that can render antibody-based vaccines poorly effective[162–164]. Therefore, strategies aimed at eliciting strong $CD8^+$ T cell responses and memory $CD8^+$ T cell formation may be important for effective vaccine-induced immunity against such viruses. However, if these viruses effectively evade $CD8^+$ T cell responses *in vivo* by interfering with MHCI antigen presentation, it will be worthwhile to develop strategies for targeting viral MHCI inhibitors or for augmenting MHCI antigen presentation. These strategy may be particularly useful in providing cures against persistent and latent viral infections (e.g. CMV and HIV infection), in which memory $CD8^+$ T cells can potentially eliminate reactivated latent reservoirs but fail to do so because of viral MHCI inhibition[119,165–167].

The ability of viruses to inhibit MHCI presentation can however be exploited for vaccine vector development. For instance, viral MHCI inhibition by RhCMV allows the virus to

superinfect hosts that have established immunological memory to RhCMV[72], making CMV viruses appealing as vaccine vectors[168]. Using a vaccine vector capable of superinfecting hosts could circumvent the issue of rapid vaccine vector neutralization by pre-existing memory, which can diminish immune responses against targeted vaccine antigens. Successful superinfections could also permit repeated vaccinations against different target antigens while using the same vaccine vector backbone. Such a feat may be difficult to achieve with vaccine vectors that cannot reinfect hosts harboring immunological memory against the respective vector, including some poxvirus-based vaccines. Nevertheless, it would be interesting to explore CPXV as a vaccine vector since my studies suggest that viral MHCI inhibition may permit CPXV to reinfect CPXV-immunized hosts, although this has not been thoroughly tested.

Future directions

Memory $CD8^+$ T cells, including T_{RM}, may provide cross-protection against distinct viral strains [169–171]. For instance, vaccine-generated lung T_{RM} mediate heterosubtypic protection against respiratory infection with influenza virus [127]. T_{RM} have also been shown to provide protection in the skin and genital tract using a number of different viral infection models[123,124,128], demonstrating that T_{RM} can be excellent antiviral vaccine targets. An improved understanding of the processes that govern T_{RM} development and activation may thus aid in the design of efficacious T_{RM}-based vaccines. Others and myself have shown an important role for local cognate antigen in T_{RM} development and activation[133,134,136,172], yet the mode of local cognate antigen presentation (i.e. direct- or cross-presentation) used to prime or activate T_{RM} remain to be elucidated. Determining the relative contribution of direct/cross-presentation and how these

modes of antigen presentation affects these processes is challenging, but can likely be addressed using the CPXV murine infection model.

There are several advantages in using the CPXV infection model. One is that the priming of naïve CPXV-specific $CD8^+$ T cell precursors during CPXV infection is dependent on $BATF3^+$ DCs, the main cross-presenting DC subsets. Local $BATF3^+$ DCs also remain uninfected at the site of infection, suggesting that $BATF3^+$ DCs are actually cross-presenting antigen. Another important factor is that the contribution of direct presentation by CPXV-infected cells at the site of infection is likely minimized due to the effects of CPXV012 and CPXV203. These points strongly imply that cross-presenting $BATF3^+$ DCs provide local antigenic stimulation to CTLs, thereby promoting T_{RM} formation, but experiments to directly test this hypothesis need to be performed. Interestingly, the findings and points discussed here also raise the possibility that local cross-presentation may be involved in T_{RM} activation. However, additional experiments are also required to determine the role of local cross-presentation during secondary CPXV infection. The CPXV infection model therefore provides an exceptional opportunity to investigate the mechanisms of local antigen-driven $CD8^+$ T_{RM} differentiation and activation; further studies with CPXV may ultimately facilitate the development of improved tissue-specific vaccine design.

References

1. Rimoin, A. W. *et al.* Major increase in human monkeypox incidence 30 years after smallpox vaccination campaigns cease in the Democratic Republic of Congo. *Proc. Natl. Acad. Sci.* **107,** 16262–16267 (2010).

2. Liu, T., Zhang, L., Joo, D. & Sun, S.-C. NF-κB signaling in inflammation. *Signal Transduct. Target. Ther.* **2,** 17023 (2017).

3. Hutchens, M. A. *et al.* Protective Effect of Toll-like Receptor 4 in Pulmonary Vaccinia Infection. *PLoS Pathog* **4,** e1000153 (2008).

4. Hutchens, M. *et al.* TLR3 increases disease morbidity and mortality from vaccinia infection. *J. Immunol. Baltim. Md 1950* **180,** 483–491 (2008).

5. Cao, H. *et al.* Innate Immune Response of Human Plasmacytoid Dendritic Cells to Poxvirus Infection Is Subverted by Vaccinia E3 via Its Z-DNA/RNA Binding Domain. *PLoS ONE* **7,** e36823 (2012).

6. Martinez, J., Huang, X. & Yang, Y. Toll-like receptor 8-mediated activation of murine plasmacytoid dendritic cells by vaccinia viral DNA. *Proc. Natl. Acad. Sci. U. S. A.* **107,** 6442–6447 (2010).

7. Samuelsson, C. *et al.* Survival of lethal poxvirus infection in mice depends on TLR9, and therapeutic vaccination provides protection. *J. Clin. Invest.* **118,** 1776–1784 (2008).

8. Dai, P. *et al.* Myxoma virus induces type I interferon production in murine plasmacytoid dendritic cells via a TLR9/MyD88-, IRF5/IRF7-, and IFNAR-dependent pathway. *J. Virol.* **85,** 10814–10825 (2011).

9. Dai, P. *et al.* Modified Vaccinia Virus Ankara Triggers Type I IFN Production in Murine Conventional Dendritic Cells via a cGAS/STING-Mediated Cytosolic DNA-Sensing Pathway. *PLoS Pathog* **10,** e1003989 (2014).

10. Schoggins, J. W. *et al.* Pan-viral specificity of IFN-induced genes reveals new roles for cGAS in innate immunity. *Nature* **505,** 691–695 (2014).

11. Wang, F. *et al.* RIG-I mediates the co-induction of tumor necrosis factor and type I interferon elicited by myxoma virus in primary human macrophages. *PLoS Pathog.* **4,** e1000099 (2008).

12. Myskiw, C. *et al.* RNA species generated in vaccinia virus infected cells activate cell type-specific MDA5 or RIG-I dependent interferon gene transcription and PKR dependent apoptosis. *Virology* **413,** 183–193 (2011).

13. Pollpeter, D., Komuro, A., Barber, G. N. & Horvath, C. M. Impaired Cellular Responses to Cytosolic DNA or Infection with Listeria monocytogenes and Vaccinia Virus in the Absence of the Murine LGP2 Protein. *PLoS ONE* **6,** e18842 (2011).

14. Piao, W. *et al.* Tyrosine phosphorylation of MyD88 adapter-like (Mal) is critical for signal transduction and blocked in endotoxin tolerance. *J. Biol. Chem.* **283,** 3109–3119 (2008).

15. Wang, C. *et al.* TAK1 is a ubiquitin-dependent kinase of MKK and IKK. *Nature* **412,** 346–351 (2001).

16. DiPerna, G. *et al.* Poxvirus protein N1L targets the I-kappaB kinase complex, inhibits signaling to NF-kappaB by the tumor necrosis factor superfamily of receptors, and inhibits NF-kappaB and IRF3 signaling by toll-like receptors. *J. Biol. Chem.* **279,** 36570–36578 (2004).

17. Ember, S. W. J., Ren, H., Ferguson, B. J. & Smith, G. L. Vaccinia virus protein C4 inhibits NF-κB activation and promotes virus virulence. *J. Gen. Virol.* **93,** 2098–2108 (2012).

18. Stack, J. *et al.* Vaccinia virus protein A46R targets multiple Toll-like–interleukin-1 receptor adaptors and contributes to virulence. *J. Exp. Med.* **201,** 1007–1018 (2005).

19. Harte, M. T. *et al.* The Poxvirus Protein A52R Targets Toll-like Receptor Signaling Complexes to Suppress Host Defense. *J. Exp. Med.* **197,** 343–351 (2003).

20. Chen, R. A.-J., Jacobs, N. & Smith, G. L. Vaccinia virus strain Western Reserve protein B14 is an intracellular virulence factor. *J. Gen. Virol.* **87,** 1451–1458 (2006).

21. Fagan-Garcia, K. & Barry, M. A vaccinia virus deletion mutant reveals the presence of additional inhibitors of NF-kappaB. *J. Virol.* **85,** 883–894 (2011).

22. Smith, C. A. *et al.* T2 open reading frame from the Shope fibroma virus encodes a soluble form of the TNF receptor. *Biochem. Biophys. Res. Commun.* **176,** 335–342 (1991).

23. Upton, C., Macen, J. L., Schreiber, M. & McFadden, G. Myxoma virus expresses a secreted protein with homology to the tumor necrosis factor receptor gene family that contributes to viral virulence. *Virology* **184,** 370–382 (1991).

24. Hu, F. Q., Smith, C. A. & Pickup, D. J. Cowpox virus contains two copies of an early gene encoding a soluble secreted form of the type II TNF receptor. *Virology* **204,** 343–356 (1994).

25. Loparev, V. N. *et al.* A third distinct tumor necrosis factor receptor of orthopoxviruses. *Proc. Natl. Acad. Sci. U. S. A.* **95,** 3786–3791 (1998).

26. Smith, C. A. *et al.* Cowpox virus genome encodes a second soluble homologue of cellular TNF receptors, distinct from CrmB, that binds TNF but not LT alpha. *Virology* **223,** 132–147 (1996).

27. Palumbo, G. J., Buller, R. M. & Glasgow, W. C. Multigenic evasion of inflammation by poxviruses. *J. Virol.* **68,** 1737–1749 (1994).

28. Gileva, I. P. *et al.* Properties of the recombinant TNF-binding proteins from variola, monkeypox, and cowpox viruses are different. *Biochim. Biophys. Acta* **1764,** 1710–1718 (2006).

29. Cheshire, J. L. & Baldwin, A. S. Synergistic activation of NF-kappaB by tumor necrosis factor alpha and gamma interferon via enhanced I kappaB alpha degradation and de novo I kappaBbeta degradation. *Mol. Cell. Biol.* **17,** 6746–6754 (1997).

30. Liu, T., Khanna, K. M., Carriere, B. N. & Hendricks, R. L. Gamma interferon can prevent herpes simplex virus type 1 reactivation from latency in sensory neurons. *J. Virol.* **75,** 11178–11184 (2001).

31. Gainey, M. D., Rivenbark, J. G., Cho, H., Yang, L. & Yokoyama, W. M. Viral MHC class I inhibition evades CD8+ T-cell effector responses in vivo but not CD8+ T-cell priming. *Proc. Natl. Acad. Sci. U. S. A.* **109,** E3260–E3267 (2012).

32. Huang, S. *et al.* Immune response in mice that lack the interferon-gamma receptor. *Science* **259,** 1742–1745 (1993).

33. Symons, J. A., Tscharke, D. C., Price, N. & Smith, G. L. A study of the vaccinia virus interferon-gamma receptor and its contribution to virus virulence. *J. Gen. Virol.* **83,** 1953–1964 (2002).

34. Alcamí, A. & Smith, G. L. Vaccinia, cowpox, and camelpox viruses encode soluble gamma interferon receptors with novel broad species specificity. *J. Virol.* **69,** 4633–4639 (1995).

35. Sakala, I. G. *et al.* Poxvirus-Encoded Gamma Interferon Binding Protein Dampens the Host Immune Response to Infection. *J. Virol.* **81,** 3346–3353 (2007).

36. Lauron, E. J. *et al.* Cross-priming induces immunodomination in the presence of viral MHC class I inhibition. *PLoS Pathog.* **14,** e1006883 (2018).

37. Tscharke, D. C. *et al.* Identification of poxvirus CD8+ T cell determinants to enable rational design and characterization of smallpox vaccines. *J. Exp. Med.* **201,** 95–104 (2005).

38. Harty, J. T., Tvinnereim, A. R. & White, D. W. CD8+ T cell effector mechanisms in resistance to infection. *Annu. Rev. Immunol.* **18,** 275–308 (2000).

39. Karupiah, G., Buller, R. M., Van Rooijen, N., Duarte, C. J. & Chen, J. Different roles for CD4+ and CD8+ T lymphocytes and macrophage subsets in the control of a generalized virus infection. *J. Virol.* **70,** 8301–8309 (1996).

40. Xu, R., Johnson, A. J., Liggitt, D. & Bevan, M. J. Cellular and humoral immunity against vaccinia virus infection of mice. *J. Immunol. Baltim. Md 1950* **172,** 6265–6271 (2004).

41. Spriggs, M. K. *et al.* Beta 2-microglobulin-, CD8+ T-cell-deficient mice survive inoculation with high doses of vaccinia virus and exhibit altered IgG responses. *Proc. Natl. Acad. Sci. U. S. A.* **89,** 6070–6074 (1992).

42. Garside, P. *et al.* Visualization of specific B and T lymphocyte interactions in the lymph node. *Science* **281,** 96–99 (1998).

43. Crotty, S. A brief history of T cell help to B cells. *Nat. Rev. Immunol.* **15,** 185–189 (2015).

44. Benhnia, M. R.-E.-I. *et al.* Vaccinia virus extracellular enveloped virion neutralization in vitro and protection in vivo depend on complement. *J. Virol.* **83,** 1201–1215 (2009).

45. Fang, M. & Sigal, L. J. Antibodies and CD8+ T cells are complementary and essential for natural resistance to a highly lethal cytopathic virus. *J. Immunol. Baltim. Md 1950* **175,** 6829–6836 (2005).

46. Chaudhri, G., Panchanathan, V., Bluethmann, H. & Karupiah, G. Obligatory requirement for antibody in recovery from a primary poxvirus infection. *J. Virol.* **80,** 6339–6344 (2006).

47. McKenzie, R., Kotwal, G. J., Moss, B., Hammer, C. H. & Frank, M. M. Regulation of complement activity by vaccinia virus complement-control protein. *J. Infect. Dis.* **166,** 1245–1250 (1992).

48. Isaacs, S. N., Kotwal, G. J. & Moss, B. Vaccinia virus complement-control protein prevents antibody-dependent complement-enhanced neutralization of infectivity and contributes to virulence. *Proc. Natl. Acad. Sci. U. S. A.* **89,** 628–632 (1992).

49. Campbell, J. A. *et al.* Cutting edge: FcR-like 5 on innate B cells is targeted by a poxvirus MHC class I-like immunoevasin. *J. Immunol. Baltim. Md 1950* **185,** 28–32 (2010).

50. Rehm, K. E. *et al.* Vaccinia virus decreases major histocompatibility complex (MHC) class II antigen presentation, T-cell priming, and peptide association with MHC class II. *Immunology* **128,** 381–392 (2009).

51. Hammarlund, E. *et al.* Monkeypox virus evades antiviral CD4+ and CD8+ T cell responses by suppressing cognate T cell activation. *Proc. Natl. Acad. Sci. U. S. A.* **105,** 14567–14572 (2008).

52. Byun, M. *et al.* Two mechanistically distinct immune evasion proteins of cowpox virus combine to avoid antiviral CD8 T cells. *Cell Host Microbe* **6,** 422–432 (2009).

53. Byun, M., Wang, X., Pak, M., Hansen, T. H. & Yokoyama, W. M. Cowpox virus exploits the endoplasmic reticulum retention pathway to inhibit MHC class I transport to the cell surface. *Cell Host Microbe* **2,** 306–315 (2007).

54. Chen, W., Antón, L. C., Bennink, J. R. & Yewdell, J. W. Dissecting the multifactorial causes of immunodominance in class I-restricted T cell responses to viruses. *Immunity* **12,** 83–93 (2000).

55. Lin, L. C. W., Flesch, I. E. A. & Tscharke, D. C. Immunodomination during Peripheral Vaccinia Virus Infection. *PLOS Pathog* **9,** e1003329 (2013).

56. Wang, Y., Flesch, I. E. A. & Tscharke, D. C. Vaccinia virus CD8+ T-cell dominance hierarchies cannot be altered by prior immunization with individual peptides. *J. Virol.* **83,** 9008–9012 (2009).

57. Basta, S., Chen, W., Bennink, J. R. & Yewdell, J. W. Inhibitory effects of cytomegalovirus proteins US2 and US11 point to contributions from direct priming and cross-priming in induction of vaccinia virus-specific CD8(+) T cells. *J. Immunol. Baltim. Md 1950* **168,** 5403–5408 (2002).

58. Dasgupta, A., Hammarlund, E., Slifka, M. K. & Früh, K. Cowpox virus evades CTL recognition and inhibits the intracellular transport of MHC class I molecules. *J. Immunol. Baltim. Md 1950* **178,** 1654–1661 (2007).

59. Schmitz, J. E. *et al.* Control of viremia in simian immunodeficiency virus infection by CD8+ lymphocytes. *Science* **283,** 857–860 (1999).

60. Shoukry, N. H. *et al.* Memory CD8+ T cells are required for protection from persistent hepatitis C virus infection. *J. Exp. Med.* **197,** 1645–1655 (2003).

61. Simon, C. O. *et al.* CD8 T Cells Control Cytomegalovirus Latency by Epitope-Specific Sensing of Transcriptional Reactivation. *J. Virol.* **80,** 10436–10456 (2006).

62. Kim, T. S. & Braciale, T. J. Respiratory Dendritic Cell Subsets Differ in Their Capacity to Support the Induction of Virus-Specific Cytotoxic CD8+ T Cell Responses. *PLoS ONE* **4,** (2009).

63. Desch, A. N. *et al.* Dendritic cell subsets require cis-activation for cytotoxic CD8 T cell induction. *Nat. Commun.* **5,** 4674 (2014).

64. Desch, A. N. *et al.* CD103+ pulmonary dendritic cells preferentially acquire and present apoptotic cell–associated antigen. *J. Exp. Med.* **208,** 1789–1797 (2011).

65. Wakim, L. M. & Bevan, M. J. Cross-dressed dendritic cells drive memory CD8+ T-cell activation after viral infection. *Nature* **471,** 629–632 (2011).

66. Smyth, L. A. *et al.* Acquisition of MHC:peptide complexes by dendritic cells contributes to the generation of antiviral CD8+ T cell immunity in vivo. *J. Immunol. Baltim. Md 1950* **189,** 2274–2282 (2012).

67. Li, L. *et al.* Cross-dressed CD8α+/CD103+ dendritic cells prime CD8+ T cells following vaccination. *Proc. Natl. Acad. Sci. U. S. A.* **109,** 12716–12721 (2012).

68. Hansen, T. H. & Bouvier, M. MHC class I antigen presentation: learning from viral evasion strategies. *Nat. Rev. Immunol.* **9,** 503–513 (2009).

69. Pinto, A. K., Munks, M. W., Koszinowski, U. H. & Hill, A. B. Coordinated function of murine cytomegalovirus genes completely inhibits CTL lysis. *J. Immunol. Baltim. Md 1950* **177,** 3225–3234 (2006).

70. Stevenson, P. G. *et al.* K3-mediated evasion of CD8(+) T cells aids amplification of a latent gamma-herpesvirus. *Nat. Immunol.* **3,** 733–740 (2002).

71. Doom, C. M. & Hill, A. B. MHC class I immune evasion in MCMV infection. *Med. Microbiol. Immunol. (Berl.)* **197,** 191–204 (2008).

72. Hansen, S. G. *et al.* Evasion of CD8+ T cells is critical for superinfection by cytomegalovirus. *Science* **328,** 102–106 (2010).

73. Alzhanova, D. *et al.* Cowpox virus inhibits Transporter associated with Antigen Processing to evade T cell recognition. *Cell Host Microbe* **6,** 433–445 (2009).

74. Harrington, L. E., Most, R. van der, Whitton, J. L. & Ahmed, R. Recombinant Vaccinia Virus-Induced T-Cell Immunity: Quantitation of the Response to the Virus Vector and the Foreign Epitope. *J. Virol.* **76,** 3329–3337 (2002).

75. Stock, A. T., Jones, C. M., Heath, W. R. & Carbone, F. R. CTL response compensation for the loss of an immunodominant class I-restricted HSV-1 determinant. *Immunol. Cell Biol.* **84,** 543–550 (2006).

76. Nuara, A. A., Buller, R. M. L. & Bai, H. Identification of residues in the ectromelia virus gamma interferon-binding protein involved in expanded species specificity. *J. Gen. Virol.* **88,** 51–60 (2007).

77. McFadden, G. Poxvirus tropism. *Nat. Rev. Microbiol.* **3,** 201–213 (2005).

78. Crouch, A. C., Baxby, D., McCracken, C. M., Gaskell, R. M. & Bennett, M. Serological evidence for the reservoir hosts of cowpox virus in British wildlife. *Epidemiol. Infect.* **115,** 185–191 (1995).

79. Chantrey, J. *et al.* Cowpox: reservoir hosts and geographic range. *Epidemiol. Infect.* **122,** 455–460 (1999).

80. Hildner, K. *et al.* Batf3 Deficiency Reveals a Critical Role for CD8α+ Dendritic Cells in Cytotoxic T Cell Immunity. *Science* **322,** 1097–1100 (2008).

81. Woodworth, J. S., Fortune, S. M. & Behar, S. M. Bacterial protein secretion is required for priming of CD8+ T cells specific for the Mycobacterium tuberculosis antigen CFP10. *Infect. Immun.* **76,** 4199–4205 (2008).

82. Tavares, R. C. O. *et al.* Interferon gamma response to combinations 38 kDa/CFP-10, 38 kDa/MPT-64, ESAT-6/MPT-64 and ESAT-6/CFP-10, each related to a single recombinant protein of Mycobacterium tuberculosis in individuals from tuberculosis endemic areas. *Microbiol. Immunol.* **51,** 289–296 (2007).

83. Li, M. *et al.* Cell-associated ovalbumin is cross-presented much more efficiently than soluble ovalbumin in vivo. *J. Immunol. Baltim. Md 1950* **166,** 6099–6103 (2001).

84. Shen, L. & Rock, K. L. Cellular protein is the source of cross-priming antigen in vivo. *Proc. Natl. Acad. Sci. U. S. A.* **101,** 3035–3040 (2004).

85. Shen, X., Wong, S. B. J., Buck, C. B., Zhang, J. & Siliciano, R. F. Direct priming and cross-priming contribute differentially to the induction of CD8+ CTL following exposure to vaccinia virus via different routes. *J. Immunol. Baltim. Md 1950* **169,** 4222–4229 (2002).

86. Xu, R.-H., Remakus, S., Ma, X., Roscoe, F. & Sigal, L. J. Direct Presentation Is Sufficient for an Efficient Anti-Viral CD8+ T Cell Response. *PLoS Pathog.* **6,** (2010).

87. Eickhoff, S. *et al.* Robust Anti-viral Immunity Requires Multiple Distinct T Cell-Dendritic Cell Interactions. *Cell* **162,** 1322–1337 (2015).

88. Molano, A. *et al.* Peptide selection by an MHC H-2Kb class I molecule devoid of the central anchor ('C') pocket. *J. Immunol. Baltim. Md 1950* **160,** 2815–2823 (1998).

89. De Silva, A. D. *et al.* Thermolabile H-2Kb molecules expressed by transporter associated with antigen processing-deficient RMA-S cells are occupied by low-affinity peptides. *J. Immunol. Baltim. Md 1950* **163,** 4413–4420 (1999).

90. Kedl, R. M. *et al.* T Cells Compete for Access to Antigen-Bearing Antigen-Presenting Cells. *J. Exp. Med.* **192,** 1105–1114 (2000).

91. Rodriguez, F., Harkins, S., Slifka, M. K. & Whitton, J. L. Immunodominance in virus-induced CD8(+) T-cell responses is dramatically modified by DNA immunization and is regulated by gamma interferon. *J. Virol.* **76,** 4251–4259 (2002).

92. Kastenmuller, W. *et al.* Cross-competition of CD8+ T cells shapes the immunodominance hierarchy during boost vaccination. *J. Exp. Med.* **204,** 2187–2198 (2007).

93. Johnson, L. R., Weizman, O.-E., Rapp, M., Way, S. S. & Sun, J. C. Epitope-specific vaccination limits clonal expansion of heterologous naïve T cells during viral challenge. *Cell Rep.* **17,** 636–644 (2016).

94. Hansen, S. J. *et al.* Cowpox Virus Inhibits Human Dendritic Cell Immune Function By Nonlethal, Nonproductive Infection. *Virology* **412,** 411–425 (2011).

95. Spesock, A. H. *et al.* Cowpox virus induces interleukin-10 both in vitro and in vivo. *Virology* **417,** 87–97 (2011).

96. Smyth, L. A. *et al.* The relative efficiency of acquisition of MHC:peptide complexes and cross-presentation depends on dendritic cell type. *J. Immunol. Baltim. Md 1950* **181,** 3212–3220 (2008).

97. Huang, J. F. *et al.* TCR-Mediated internalization of peptide-MHC complexes acquired by T cells. *Science* **286,** 952–954 (1999).

98. Stinchcombe, J. C., Bossi, G., Booth, S. & Griffiths, G. M. The immunological synapse of CTL contains a secretory domain and membrane bridges. *Immunity* **15,** 751–761 (2001).

99. Hudrisier, D., Riond, J., Mazarguil, H., Gairin, J. E. & Joly, E. Cutting edge: CTLs rapidly capture membrane fragments from target cells in a TCR signaling-dependent manner. *J. Immunol. Baltim. Md 1950* **166,** 3645–3649 (2001).

100. Kedl, R. M., Schaefer, B. C., Kappler, J. W. & Marrack, P. T cells down-modulate peptide-MHC complexes on APCs in vivo. *Nat. Immunol.* **3,** 27–32 (2002).

101. Dinter, J. *et al.* Variable processing and cross-presentation of HIV by dendritic cells and macrophages shapes CTL immunodominance and immune escape. *PLoS Pathog.* **11,** e1004725 (2015).

102. Pavelic, V., Matter, M. S., Mumprecht, S., Breyer, I. & Ochsenbein, A. F. CTL induction by cross-priming is restricted to immunodominant epitopes. *Eur. J. Immunol.* **39,** 704–716 (2009).

103. Otahal, P. *et al.* Inefficient cross-presentation limits the CD8+ T cell response to a subdominant tumor antigen epitope. *J. Immunol. Baltim. Md 1950* **175,** 700–712 (2005).

104. Schaible, U. E. *et al.* Apoptosis facilitates antigen presentation to T lymphocytes through MHC-I and CD1 in tuberculosis. *Nat. Med.* **9,** 1039–1046 (2003).

105. Grotzke, J. E., Siler, A. C., Lewinsohn, D. A. & Lewinsohn, D. M. Secreted immunodominant Mycobacterium tuberculosis antigens are processed by the cytosolic pathway. *J. Immunol. Baltim. Md 1950* **185,** 4336–4343 (2010).

106. Hayball, J. D., Robinson, B. W. S. & Lake, R. A. CD4+ T cells cross-compete for MHC class II-restricted peptide antigen complexes on the surface of antigen presenting cells. *Immunol. Cell Biol.* **82,** 103–111 (2004).

107. Farrington, L. A., Smith, T. A., Grey, F., Hill, A. B. & Snyder, C. M. Competition for antigen at the level of the APC is a major determinant of immunodominance during memory inflation in murine cytomegalovirus infection. *J. Immunol. Baltim. Md 1950* **190,** 3410–3416 (2013).

108. Scherer, A., Salathé, M. & Bonhoeffer, S. High epitope expression levels increase competition between T cells. *PLoS Comput. Biol.* **2,** e109 (2006).

109. Wherry, E. J., Puorro, K. A., Porgador, A. & Eisenlohr, L. C. The induction of virus-specific CTL as a function of increasing epitope expression: responses rise steadily until excessively high levels of epitope are attained. *J. Immunol. Baltim. Md 1950* **163,** 3735–3745 (1999).

110. Probst, H. C., Dumrese, T. & van den Broek, M. F. Cutting edge: competition for APC by CTLs of different specificities is not functionally important during induction of antiviral responses. *J. Immunol. Baltim. Md 1950* **168,** 5387–5391 (2002).

111. Kotturi, M. F. *et al.* Naive Precursor Frequencies and MHC Binding Rather Than the Degree of Epitope Diversity Shape CD8+ T Cell Immunodominance. *J. Immunol. Baltim. Md 1950* **181,** 2124–2133 (2008).

112. Identification of poxvirus CD8+ T cell determinants to enable rational design and characterization of smallpox vaccines. - PubMed - NCBI. Available at: http://www.ncbi.nlm.nih.gov/pubmed/15623576. (Accessed: 17th March 2016)

113. Remakus, S., Rubio, D., Ma, X., Sette, A. & Sigal, L. J. Memory CD8+ T Cells Specific for a Single Immunodominant or Subdominant Determinant Induced by Peptide-Dendritic Cell Immunization Protect from an Acute Lethal Viral Disease. *J. Virol.* **86,** 9748–9759 (2012).

114. Paran, N. *et al.* Active vaccination with vaccinia virus A33 protects mice against lethal vaccinia and ectromelia viruses but not against cowpoxvirus; elucidation of the specific adaptive immune response. *Virol. J.* **10,** 229 (2013).

115. Gierynska, M., Szulc-Dabrowska, L., Dzieciatkowski, T., Golke, A. & Schollenberger, A. The generation of CD8+ T-cell population specific for vaccinia virus epitope involved in the antiviral protection against ectromelia virus challenge. *Pathog. Dis.* **73,** ftv088 (2015).

116. Tischer, B. K., von Einem, J., Kaufer, B. & Osterrieder, N. Two-step red-mediated recombination for versatile high-efficiency markerless DNA manipulation in Escherichia coli. *BioTechniques* **40,** 191–197 (2006).

117. Xu, Z., Zikos, D., Osterrieder, N. & Tischer, B. K. Generation of a complete single-gene knockout bacterial artificial chromosome library of cowpox virus and identification of its essential genes. *J. Virol.* **88,** 490–502 (2014).

118. Hamilton, S. E., Porter, B. B., Messingham, K. A. N., Badovinac, V. P. & Harty, J. T. MHC class Ia-restricted memory T cells inhibit expansion of a nonprotective MHC class Ib (H2-M3)-restricted memory response. *Nat. Immunol.* **5,** 159–168 (2004).

119. Lu, X., Pinto, A. K., Kelly, A. M., Cho, K. S. & Hill, A. B. Murine cytomegalovirus interference with antigen presentation contributes to the inability of CD8 T cells to control virus in the salivary gland. *J. Virol.* **80,** 4200–4202 (2006).

120. Thom, J. T., Weber, T. C., Walton, S. M., Torti, N. & Oxenius, A. The Salivary Gland Acts as a Sink for Tissue-Resident Memory CD8(+) T Cells, Facilitating Protection from Local Cytomegalovirus Infection. *Cell Rep.* **13,** 1125–1136 (2015).

121. Carbone, F. R. Tissue-Resident Memory T Cells and Fixed Immune Surveillance in Nonlymphoid Organs. *J. Immunol. Baltim. Md 1950* **195,** 17–22 (2015).

122. Gebhardt, T. *et al.* Memory T cells in nonlymphoid tissue that provide enhanced local immunity during infection with herpes simplex virus. *Nat. Immunol.* **10,** 524–530 (2009).

123. Jiang, X. *et al.* Skin infection generates non-migratory memory CD8+ T(RM) cells providing global skin immunity. *Nature* **483,** 227–231 (2012).

124. Mackay, L. K. *et al.* Long-lived epithelial immunity by tissue-resident memory T (TRM) cells in the absence of persisting local antigen presentation. *Proc. Natl. Acad. Sci. U. S. A.* **109,** 7037–7042 (2012).

125. Teijaro, J. R. *et al.* Cutting edge: Tissue-retentive lung memory CD4 T cells mediate optimal protection to respiratory virus infection. *J. Immunol. Baltim. Md 1950* **187,** 5510–5514 (2011).

126. Wu, T. *et al.* Lung-resident memory CD8 T cells (TRM) are indispensable for optimal cross-protection against pulmonary virus infection. *J. Leukoc. Biol.* **95,** 215–224 (2014).

127. Zens, K. D., Chen, J. K. & Farber, D. L. Vaccine-generated lung tissue-resident memory T cells provide heterosubtypic protection to influenza infection. *JCI Insight* **1,** (2016).

128. Shin, H. & Iwasaki, A. A vaccine strategy protects against genital herpes by establishing local memory T cells. *Nature* **491,** 463–467 (2012).

129. McMaster, S. R. *et al.* Pulmonary antigen encounter regulates the establishment of tissue-resident CD8 memory T cells in the lung airways and parenchyma. *Mucosal Immunol.* (2018). doi:10.1038/s41385-018-0003-x

130. Takamura, S. *et al.* Specific niches for lung-resident memory CD8+ T cells at the site of tissue regeneration enable CD69-independent maintenance. *J. Exp. Med.* **213,** 3057–3073 (2016).

131. Zammit, D. J., Turner, D. L., Klonowski, K. D., Lefrançois, L. & Cauley, L. S. Residual antigen presentation after influenza virus infection affects CD8 T cell activation and migration. *Immunity* **24,** 439–449 (2006).

132. Lee, Y.-T. *et al.* Environmental and antigen receptor-derived signals support sustained surveillance of the lungs by pathogen-specific cytotoxic T lymphocytes. *J. Virol.* **85,** 4085–4094 (2011).

133. Khan, T. N., Mooster, J. L., Kilgore, A. M., Osborn, J. F. & Nolz, J. C. Local antigen in nonlymphoid tissue promotes resident memory CD8+ T cell formation during viral infection. *J. Exp. Med.* **213,** 951–966 (2016).

134. Muschaweckh, A. *et al.* Antigen-dependent competition shapes the local repertoire of tissue-resident memory CD8+ T cells. *J. Exp. Med.* **213,** 3075–3086 (2016).

135. Pizzolla, A. *et al.* Resident memory CD8+ T cells in the upper respiratory tract prevent pulmonary influenza virus infection. *Sci. Immunol.* **2,** (2017).

136. Wakim, L. M., Woodward-Davis, A. & Bevan, M. J. Memory T cells persisting within the brain after local infection show functional adaptations to their tissue of residence. *Proc. Natl. Acad. Sci. U. S. A.* **107,** 17872–17879 (2010).

137. Laidlaw, B. J. *et al.* CD4+ T cell help guides formation of CD103+ lung-resident memory CD8+ T cells during influenza viral infection. *Immunity* **41,** 633–645 (2014).

138. Beura, L. K. *et al.* Intravital mucosal imaging of CD8+resident memory T cells shows tissue-autonomous recall responses that amplify secondary memory. *Nat. Immunol.* **19,** 173–182 (2018).

139. Anderson, K. G. *et al.* Cutting edge: intravascular staining redefines lung CD8 T cell responses. *J. Immunol. Baltim. Md 1950* **189,** 2702–2706 (2012).

140. Moran, A. E. *et al.* T cell receptor signal strength in Treg and iNKT cell development demonstrated by a novel fluorescent reporter mouse. *J. Exp. Med.* **208,** 1279–1289 (2011).

141. Asano, M. S. & Ahmed, R. CD8 T cell memory in B cell-deficient mice. *J. Exp. Med.* **183,** 2165–2174 (1996).

142. Shen, H. *et al.* A specific role for B cells in the generation of CD8 T cell memory by recombinant Listeria monocytogenes. *J. Immunol. Baltim. Md 1950* **170,** 1443–1451 (2003).

143. Ariotti, S. *et al.* T cell memory. Skin-resident memory $CD8^+$ T cells trigger a state of tissue-wide pathogen alert. *Science* **346,** 101–105 (2014).

144. Boissonnas, A. *et al.* CD8+ tumor-infiltrating T cells are trapped in the tumor-dendritic cell network. *Neoplasia N. Y. N* **15,** 85–94 (2013).

145. Broz, M. *et al.* Dissecting the Tumor Myeloid Compartment Reveals Rare Activating Antigen Presenting Cells, Critical for T cell Immunity. *Cancer Cell* **26,** 638–652 (2014).

146. Iborra, S. *et al.* Optimal Generation of Tissue-Resident but Not Circulating Memory T Cells during Viral Infection Requires Crosspriming by DNGR-1+ Dendritic Cells. *Immunity* **45,** 847–860 (2016).

147. Shin, H., Kumamoto, Y., Gopinath, S. & Iwasaki, A. CD301b+ dendritic cells stimulate tissue-resident memory CD8+ T cells to protect against genital HSV-2. *Nat. Commun.* **7,** (2016).

148. Schenkel, J. M. *et al.* Resident memory CD8 T cells trigger protective innate and adaptive immune responses. *Science* **346,** 98–101 (2014).

149. Jelley-Gibbs, D. M. *et al.* Persistent depots of influenza antigen fail to induce a cytotoxic CD8 T cell response. *J. Immunol. Baltim. Md 1950* **178,** 7563–7570 (2007).

150. Turner, D. L., Cauley, L. S., Khanna, K. M. & Lefrançois, L. Persistent Antigen Presentation after Acute Vesicular Stomatitis Virus Infection. *J. Virol.* **81,** 2039–2046 (2007).

151. Kim, T. S., Hufford, M. M., Sun, J., Fu, Y.-X. & Braciale, T. J. Antigen persistence and the control of local T cell memory by migrant respiratory dendritic cells after acute virus infection. *J. Exp. Med.* **207,** 1161–1172 (2010).

152. Casey, K. A. *et al.* Antigen independent differentiation and maintenance of effector-like resident memory T cells in tissues. *J. Immunol. Baltim. Md 1950* **188,** 4866–4875 (2012).

153. Davies, B. *et al.* Cutting Edge: Tissue-Resident Memory T Cells Generated by Multiple Immunizations or Localized Deposition Provide Enhanced Immunity. *J. Immunol.* **198,** 2233–2237 (2017).

154. Slütter, B. *et al.* Dynamics of influenza-induced lung-resident memory T cells underlie waning heterosubtypic immunity. *Sci. Immunol.* **2,** (2017).

155. Williams, G. D. *et al.* Nucleotide resolution mapping of influenza A virus nucleoprotein-RNA interactions reveals RNA features required for replication. *Nat. Commun.* **9,** 465 (2018).

156. Peng, H. *et al.* Liver-resident NK cells confer adaptive immunity in skin-contact inflammation. *J. Clin. Invest.* **123,** 1444–1456 (2013).

157. Sojka, D. K. *et al.* Tissue-resident natural killer (NK) cells are cell lineages distinct from thymic and conventional splenic NK cells. *eLife* **3,** e01659 (2014).

158. Hsu, K. M., Pratt, J. R., Akers, W. J., Achilefu, S. I. & Yokoyama, W. M. Murine Cytomegalovirus Displays Selective Infection of Cells within Hours after Systemic Administration. *J. Gen. Virol.* **90,** 33–43 (2009).

159. Jenner, E. *An Inquiry Into the Causes and Effects of the Variolae Vaccinae: A Disease Discovered in Some of the Western Counties of England, Particularly Gloucestershire, and Known by the Name of the Cow Pox*. ((Sampson Low, London) 42 pp., 1798).

160. Blagoveshchenskaya, A. D., Thomas, L., Feliciangeli, S. F., Hung, C. H. & Thomas, G. HIV-1 Nef downregulates MHC-I by a PACS-1- and PI3K-regulated ARF6 endocytic pathway. *Cell* **111,** 853–866 (2002).

161. Kang, W. *et al.* Hepatitis C Virus Attenuates Interferon-Induced MHC Class I Expression and Decreases CD8+ T-Cell Effector Functions. *Gastroenterology* **146,** 1351-60.e1–4 (2014).

162. Chung, A. W. *et al.* Immune escape from HIV-specific antibody-dependent cellular cytotoxicity (ADCC) pressure. *Proc. Natl. Acad. Sci. U. S. A.* **108,** 7505–7510 (2011).

163. Bailey, J. R. *et al.* Naturally selected hepatitis C virus polymorphisms confer broad neutralizing antibody resistance. *J. Clin. Invest.* **125,** 437–447 (2015).

164. Manley, K. *et al.* Human cytomegalovirus escapes a naturally occurring neutralizing antibody by incorporating it into assembling virions. *Cell Host Microbe* **10,** 197–209 (2011).

165. Tey, S.-K., Goodrum, F. & Khanna, R. CD8+ T-cell recognition of human cytomegalovirus latency-associated determinant pUL138. *J. Gen. Virol.* **91,** 2040–2048 (2010).

166. Walton, S. M. *et al.* Absence of cross-presenting cells in the salivary gland and viral immune evasion confine cytomegalovirus immune control to effector CD4 T cells. *PLoS Pathog.* **7,** e1002214 (2011).

167. Dekaban, G. A. & Dikeakos, J. D. HIV-I Nef inhibitors: a novel class of HIV-specific immune adjuvants in support of a cure. *AIDS Res. Ther.* **14,** (2017).

168. Hansen, S. G. *et al.* CYTOMEGALOVIRUS VECTORS VIOLATE CD8+ T CELL EPITOPE RECOGNITION PARADIGMS. *Science* **340,** (2013).

169. Boon, A. C. M. *et al.* Recognition of homo- and heterosubtypic variants of influenza A viruses by human CD8+ T lymphocytes. *J. Immunol. Baltim. Md 1950* **172,** 2453–2460 (2004).

170. Kreijtz, J. H. C. M. *et al.* Cross-recognition of avian H5N1 influenza virus by human cytotoxic T-lymphocyte populations directed to human influenza A virus. *J. Virol.* **82,** 5161–5166 (2008).

171. Tu, W. *et al.* Cytotoxic T lymphocytes established by seasonal human influenza cross-react against 2009 pandemic H1N1 influenza virus. *J. Virol.* **84,** 6527–6535 (2010).

172. Steinbach, K. *et al.* Brain-resident memory T cells represent an autonomous cytotoxic barrier to viral infection. *J. Exp. Med.* **213,** 1571–1587 (2016).